DISSERTATION

CHARACTERIZATION OF ZEBRAFISH MODELS OF FILAMIN C RELATED CARDIOMYOPATHY

Submitted by

Rasha M. Alnefaie

Graduate Degree Program in Cell and Molecular Biology

In partial fulfillment of the requirements

For the Degree of Doctor of Philosophy

Colorado State University

Fort Collins, Colorado

Spring 2019

Doctoral Committee:

Advisor: Deborah Garrity

ASN Reddy
Paul Lybourn
Racheal Muller

ABSTRACT

CHARACTERIZATION OF ZEBRAFISH MODELS OF FILAMIN C RELATED CARDIOMYOPATHY

Cardiomyopathies are a group of cardiac muscle diseases characterized by abnormal function and/or structure of the myocardium which cause arrhythmia, heart failure or sudden death. In many cases, cardiomyopathy is a genetic disease and the majority of inherited cases are caused by mutations in genes that encode cardiac costameric and sarcomeric proteins. Cardiomyopathies include different types, such as dilated cardiomyopathy (DCM), hypertrophic cardiomyopathy (HCM), restrictive cardiomyopathy (RCM), and arrythmogenic cardiomyopathy (ARCM). These groups of disorders can have common cellular phenotypes and mechanisms. To date, few studies have described the roles of filamin C in cardiac development or explained how mutations in filamin C cause cardiomyopathic disease. Due to the lack of a suitable animal model, the pathological mechanisms underlying this disease and the role of filaminC in cardiac development remain unclear. Here, we created a zebrafish loss-of-function model for two *flnc* paralogous genes. We investigated several genetic lines bearing mutations in filamin C that target different sites of the gene. As for humans, zebrafish mutants exhibited variable penetrance and variable expressivity. Double *flnca* and *flncb* mutant hearts exhibited more pronounced cardiac morphological defects compared to single mutants, leading to the conclusion that these paralogs play redundant roles in zebrafish heart development. The cardiac morphological phenotype of double *flnc* mutant embryos is characterized by a decrease in cardiac output and stroke volume as is also observed in patients who suffer from cardiomyopathies. Using a transgenic line expressing GFP in cardiac z-discs, we find that knockdown of *flnca* and *flncb* via morpholinos and double *flnca* and *flncb* mutant hearts

exhibited irregular z-discs. In support of this finding, ultrastructural analysis by transmission electronic microscopy for *flncb* morphant embryos and double *flnca* and *flncb* mutants indicated disorganized myofibrils with fewer consecutive sarcomeres. Particularly, z-discs were irregular or apparently absent, and numerous small vacuoles and potentially autophagous vesicles were observed. Additionally, through double *flnca* and *flncb* mutant, we demonstrated that filamin C is required for normal cardiomyocyte morphology and microfilament arrangement. In summary, the zebrafish model demonstrates an essential requirement for filamin C function during heart and skeletal muscle development. Depletion of filamin C impairs both sarcomerogenesis and alters the cytoskeletal architecture of cardiomyocytes.

ACKNOWLEDGMENTS

I would like to thank God for providing me with the ability to complete the PhD program. My special thanks to my advisor Dr. Deborah Garrity; without her guidance and mentoring this project would not have been completed. I benefitted a lot from her supervision. I'm grateful to my committee members for all their helpful suggestions to improve my project.

In addition, a thank you to Dr. David Bark for providing the high speed camera and all his professional guidance. I also wish to thank Alex Gendernalik for his help in using the high speed camera and Matlab. I would like to thank all the Garrity lab members (graduate and undergraduate students) for creating an awesome environment. Special thanks for my undergraduate student Max Hostetter for all his help to complete this project.

I would like to give thanks to Suzanne Royer for performing TEM. I would also like to thank Alissa Williams for helping in editing my dissertation.

I am extremely grateful for the opportunity granted by Albaha University for financial support for the PhD program. I'm also thankful to my family who have supported me as I accomplished my project.

Lastly, I would like to thank all those who helped me in any way in my PhD journey.

TABLE OF CONTENTS

Chapter1: Introduction

Summary

Cardiovascular diseases (CVDs) such as high blood pressure (also known as hypertension), stroke, coronary heart disease and heart failure have been categorized among the biggest threats to health of the American population (Roger, Go et al. 2011, Go, Mozaffarian et al. 2013). Cardiomyopathies can be defined as a heterogeneous class of diseases of the myocardium linked to medical and/or electrical dysfunction that normally exhibit inappropriate ventricular hypertrophy or dilation as a result of different etiologies, which are hereditary in most cases (Maron, Towbin et al. 2006). While cardiomyopathies can be restricted to the heart, they can also be part of generalized systemic disorders. Often, they result in cardiovascular death or a progressive heart failure-related disability (Maron, Towbin et al. 2006).

Mutations in different genes encoding cardiac proteins are responsible for familial cardiomyopathy disease. However, most of genetic alterations that cause inherited cardiomyopathies are still unknown (Dellefave and McNally 2010, Jefferies and Towbin 2010, Valdés-Mas, Gutiérrez-Fernández et al. 2014, McNally and Mestroni 2017). We reported recently a novel splicing variant of the filaminC (*FLNC*) gene in three unrelated families who suffer cardiomyopathy. This finding supports the hypothesis that mutations in the *FLNC* gene are linked to heritable cardiomyopathy in humans (Begay, Tharp et al. 2016). Developmental expression of *FLNC* occurs in skeletal muscles and in cardiac muscle. The FLNC protein interacts with many z-disc proteins and also links many cell membrane proteins to cortical actin fibers, which underlies its fundamental role in the organization of z-disc architecture and actin fibers network (van der Ven, Obermann et al.

2000). Moreover, filaminC links the costameric complexes with z-disc proteins. Thus, filaminC has a role in force transmission from the sarcomere to the sarcolemma (Peter, Cheng et al. 2011).

To date, few studies have investigated the relationship between cardiomyopathy and FLNC (Begay, Tharp et al. 2016, Begay, Graw et al. 2018, Nozari, Aghaei-Moghadam et al. 2018) Interestingly, alteration in *FLNC* genes have been linked to myofibrillar myopathy (MFM), a type of muscular dystrophy that affects muscle function and causes muscle weakness (Selcen and Engel 2011, Bührdel, Hirth et al. 2015). Some patients suffer from both MFM and cardiomyopathy and some develop either MFM or cardiomyopathy. To comprehend in detail the contribution of FLNC to cardiac phenotypes, we developed zebrafish loss-of-function models for two *flnc* paralogous genes, *flnca* and *flncb.* Zebrafish are a useful model to study cardiovascular disease, due to the unique features of embryos that allow researchers to study heart development, even when defects are severe. This project was implemented with the aim of determining FLNC`s functional role in development of cardiac defect in zebrafish.

A genetic model system for FLNC depletion is needed to address the question of why different mutations of FLNC lead to different types of cardiomyopathies, and to better understand the roles of FLNC in the embryonic heart. For initial studies, we reported that the knockdown of *flncb* is associated with heart defects in embryonic zebrafish. The phenotype is characterized by increased retrograde flow, and decreases in cardiac contractility, stroke volume, cardiac output and heart rate (Begay, Tharp et al. 2016).

In this chapter, I provide an introduction to the zebrafish model and its advantages for the study of embryonic heart function. Then, I summarize the history of cardiac muscle concepts and

classification. Lastly, I describe the filaminC structure and its function in skeletal and cardiac muscles development.

Zebrafish and Developmental Biology

Taxonomic classification

Table 1.1: Taxonomic classification of zebrafish (see www.itis.gov: Danio rerio).

Kingdom	**Animalia**	**multicellular organisms**
Phylum	Chordata	
Subphylum	Vertebrata	
Class	Actinopterygii	Class of ray-finned fish
Subclass	Neopterygii	
Infraclass	Teleostei	bony fishes
Superorder Order	Ostariophysi	
Order	Cypriniformes	Order of cyprinids, minnows, suckers
Superfamily	Cyprinoidea	
Family	Cyprinida	carps and minnows
Genus	Danio	
Species	Rerio	
common name	zebrafish or zebra danio	

Natural habitat of zebrafish

Zebrafish are small, bony fish, which fall under the Teleost infraclass of the cyprinid family (See Table 1.1). The Teleost clade includes other model organism such as pufferfish (*Takifugu rubripesnd, Tetraodon nigroviridis*) and medaka (*Oryzias Latipes*) (Nusslein-Volhard and Dahm 2002).

The geographic range of zebrafish is from Pakistan to Burma and from Nepal to Indian. They live in warm, fresh water and may be found in small streams, rivers and other channels (Fig. 1.1A) (Spence, Fatema et al. 2006, Engeszer, Patterson et al. 2007, Spence, Gerlach et al. 2008, Whiteley, Bhat et al. 2011, Arunachalam, Raja et al. 2013)). Adult zebrafish are typically striped with varied pigmentation and they are usually small with an anterior/posterior length of less than two inches (Fig. 1.1B) (Engeszer, Patterson et al. 2007). Adults display sexual dimorphism, with males displaying an enhanced fusiform, pinker coloration and more linear body shape whereas females are paler, with a protruding belly (Kimmel, Ballard et al. 1995). The average of lifetime of wildtype zebrafish in a laboratory is 42 months (Gerhard, Kauffman et al. 2002).

Embryonic development of zebrafish

Spawning of zebrafish occurs during the early morning hours. The male quickly pursues a female, while making an effort to nudge her sides. A receptive female will begin releasing eggs that will be fertilized by the males swimming adjacently. Following fertilization, the embryos sink to the silty substrate for protection from adults, which may prey on them. Development occurs rapidly (Kimmel, Ballard et al. 1995).

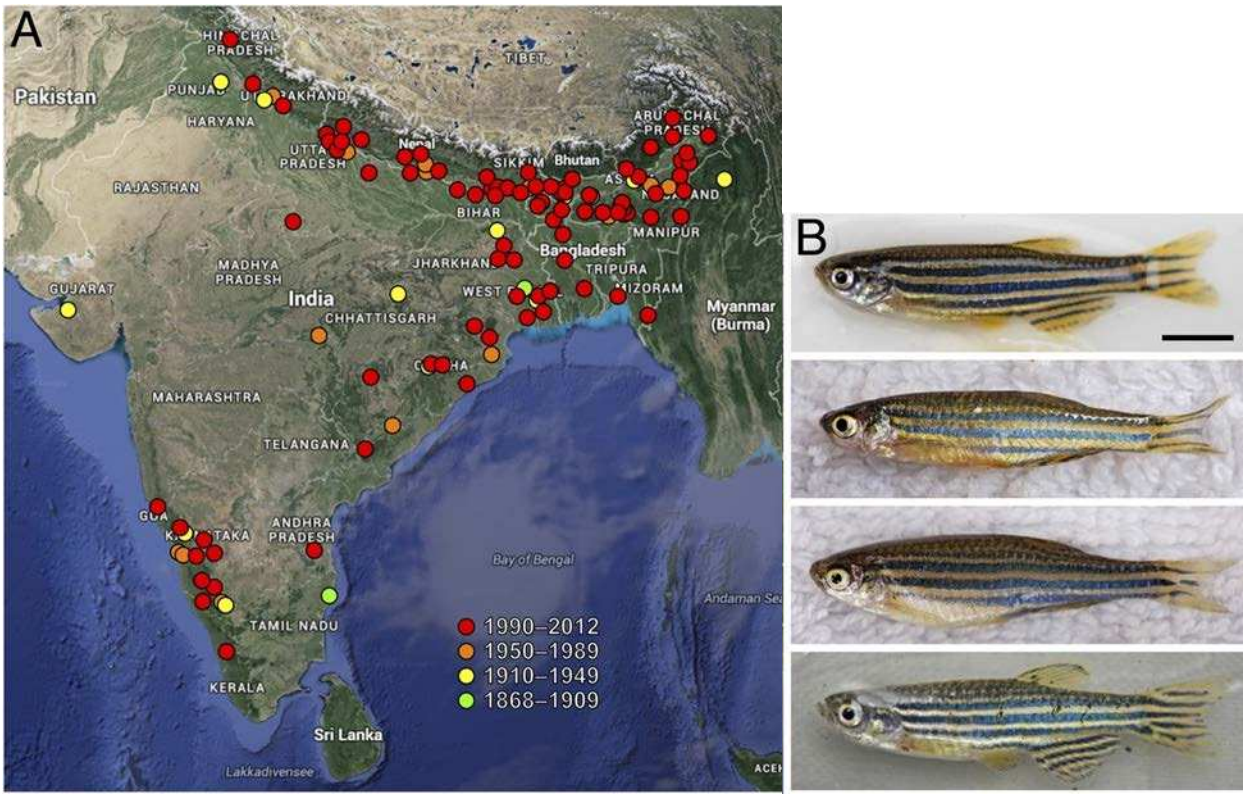

Figure 1.1 Zebrafish and their geographic range.
(**A**) Places in Nepal, Pakistan and Burma where zebrafish naturally distributed (Engeszer, Patterson et al. 2007)
(**B**) Zebrafish representative of different populations in northeastern India. Males are the upper two fish while females are the lower ones. Males have yellow or pink color and cylinder shape while females have silver color and big belly. Scale bar: 5 mm. Image credits: D Parichy.

In 1995 Charles Kimmel and his colleagues defined a major series stages of zebrafish embryonic development that occur during the first three days of post fertilization (dpf). The stages are named based on their morphological features and they are seven stages, which includ zygote, cleavage, blas- tula, gastrula, segmentation, pharyngula, and hatching periods (Fig 1.2) representing all developmental stages from the zygotic to segmentation period. The following table presents all stages and delineate the significant events that happen in each period.

Table1.2. Early zebrafish embryos stages (Kimmel, Ballard et al. 1995)

stages	Hour post fertilization (hpf)	Important events occur during development period
Zygote	0	-One cell and yolk form. -Yolk free cytoplasm begins segregating toward animal pole (Fig. 1.2a).
Cleavage	3/4	-Rapid and synchronous divisions occur for cell cycles 2 through 7. (Fig. 1.2b-g).
Blastula	2 1/4	-Cell cycles 8 and 9 occur rapidly and metasynchronously (Fig. 1.2 h-i). -The embryo undergoes the midblastula transition (MBT) transition. - The yolk syncytial layer (YSL) starts forming (Fig. 1.2j-k). -Epiboly starts (Fig. 1.2p).
Gastrula	5 1/4	-Epiboly continues (Fig1.2 q-u). -Morphogenetic cell movements of: involution, convergence, and extension occur to produce the embryonic axis and primary germ layers.
Segmentation	10	-Growth of somites, pharyngeal arch primordia, neuromeres -Primary organogenesis. -The tail appears and the embryo becomes elongated. -Differentiation of the first cell morphologically. -Embryo movement is evident. (Fig. 1.2v-z)

Pharyngula	24	-Pigmentation and fins developed - Body axis becomes straight, and touch reflex appears. - Circulation begins
Hatching	48	-Embryos continue growing rapidly.-Rapid completion of morphogenesis involving cartilage development in head and pectoral fins. -Asynchronous hatching occurs
Early larva	72	-Most of morphogenesis completed and embryos continue to grow rapidly. -Inflation of the swimming bladder -Food intake and avoidance behaviors started -Extension of the ventral yolk in both directions

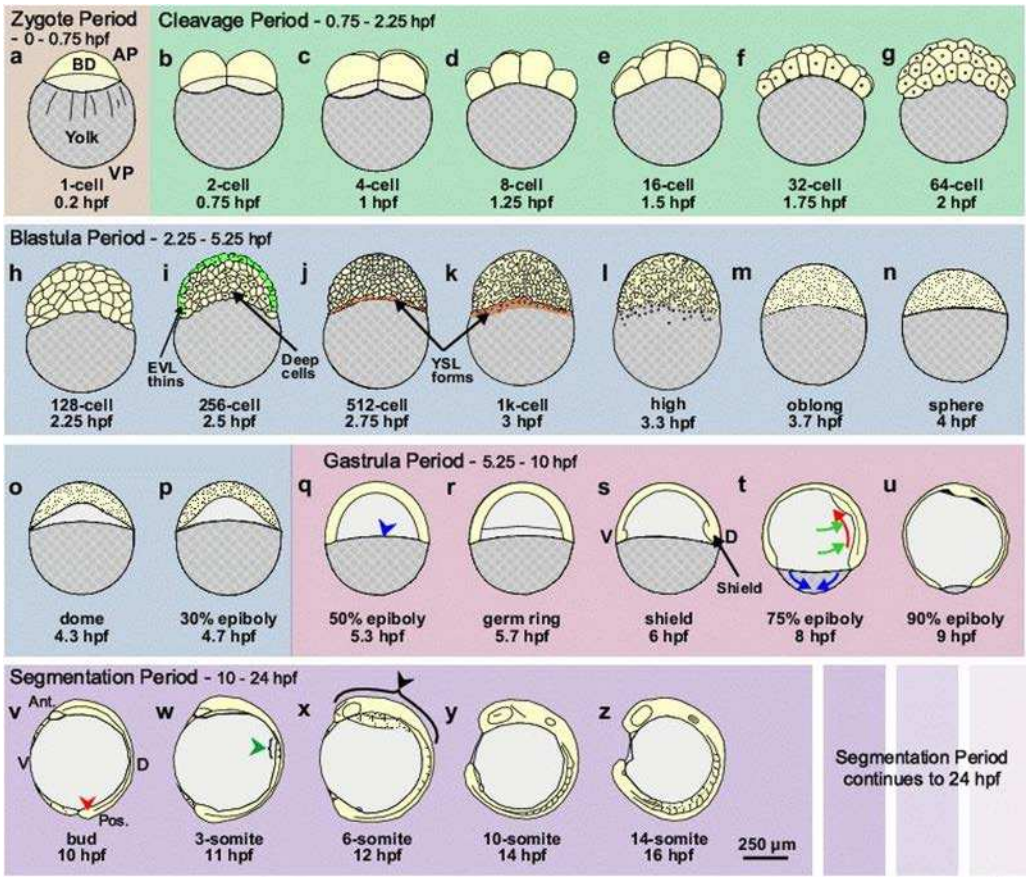

Figure 1.2 Schematic representation of early zebrafish development stages.
The cleavage period (panels b–g) running from the 2-cell to 64-cell stage, immediately comes after the brief Zygote Period (panel a). This brief Zygote Period takes place during the single-cell stage of the embryo. The period for the Blastula (panels h-p) covers from the 128-cell stage to the 50% epiboly stage (i.e., from 2.25 hour post fertilization (hpf) to 5.3 hpf). Panels i, and j and k respectively indicate the enveloping layer (EVL) and yolk syncytial layer (YSL) formations. The period of Gastrula (panels q-u) covers from the time Blastula period (BP) ends at 50% epiboly (i.e., 5.3 hpf) through the bud stage at 10 hpf, after which is the beginning of segmentation. This schematic demonstrates that the beginning stages of the period of segmentation (panels v-z) are from the bud stage at 10 hpf to the 14-somite stage at 16 hpf. Animal pole and vegetal pole, together with, anterior, posterior and are refereed in the figure respectively as AP and VP, as well as, Ant., Pos. (Kimmel, Ballard et al. 1995).

Zebrafish as a model organism

Overview

In 1992, George Streisinger was the founding researcher who established the use of zebrafish as a laboratory animal. After that, zebrafish (*Danio rerio*) research has been growing rapidly since 1992 based on a percentage of National Institutes of Health (NIH)-funded R01 grants and as a percentage of publications in MEDLINE (Lauer, 2016) (Fig. 1.3). This little fish provides many advantages as a model for the study of development and organogenesis in a vertebrate (Stainier 2001, Bournele and Beis 2016, Gut, Reischauer et al. 2017). Zebrafish are productive. That is, when a single pair goes through the mating process, hundreds of offspring can be produced in one morning. Second, the embryos of zebrafish develop externally. Additionally, they are transparent, an aspect that allows visualization of morphogenesis directly throughout the first week of development. Third, the reproductive cycle of the embryo is short; specifically, the formation of larva from the egg takes only a few days. Fourth, large numbers of fish can be maintained in the small space of a laboratory. Fifth, the genomic of zebrafish is fully sequenced (Postlethwait, Yan et al. 1998). Moreover, small size of zebrafish embryos and adult enable researchers to perform whole organism transcriptomic (Reischauer, Stone et al. 2016) and proteomic (Nolte, Hölper et al. 2015, Reischauer, Stone et al. 2016). Additionally, the zebrafish is suitable for genetic manipulations. Such genetic manipulations may include; forward genetic screens using established mutagenesis protocols, reverse genetic studies via targeted morpholino knock down, CRISPR and TALEN approaches, as well as the creation of transgenic animals in which expression of integrated genes occurs with spatial or temporal specificity. Lastly, many databases have been created to provide various data about zebrafish genome such as gene function, expression, and

mutant lines and markers. For example, zebrafish information network (zfin) is the most zebrafish informative database (Westerfield, Doerry et al. 1998, Sprague, Bayraktaroglu et al. 2006).

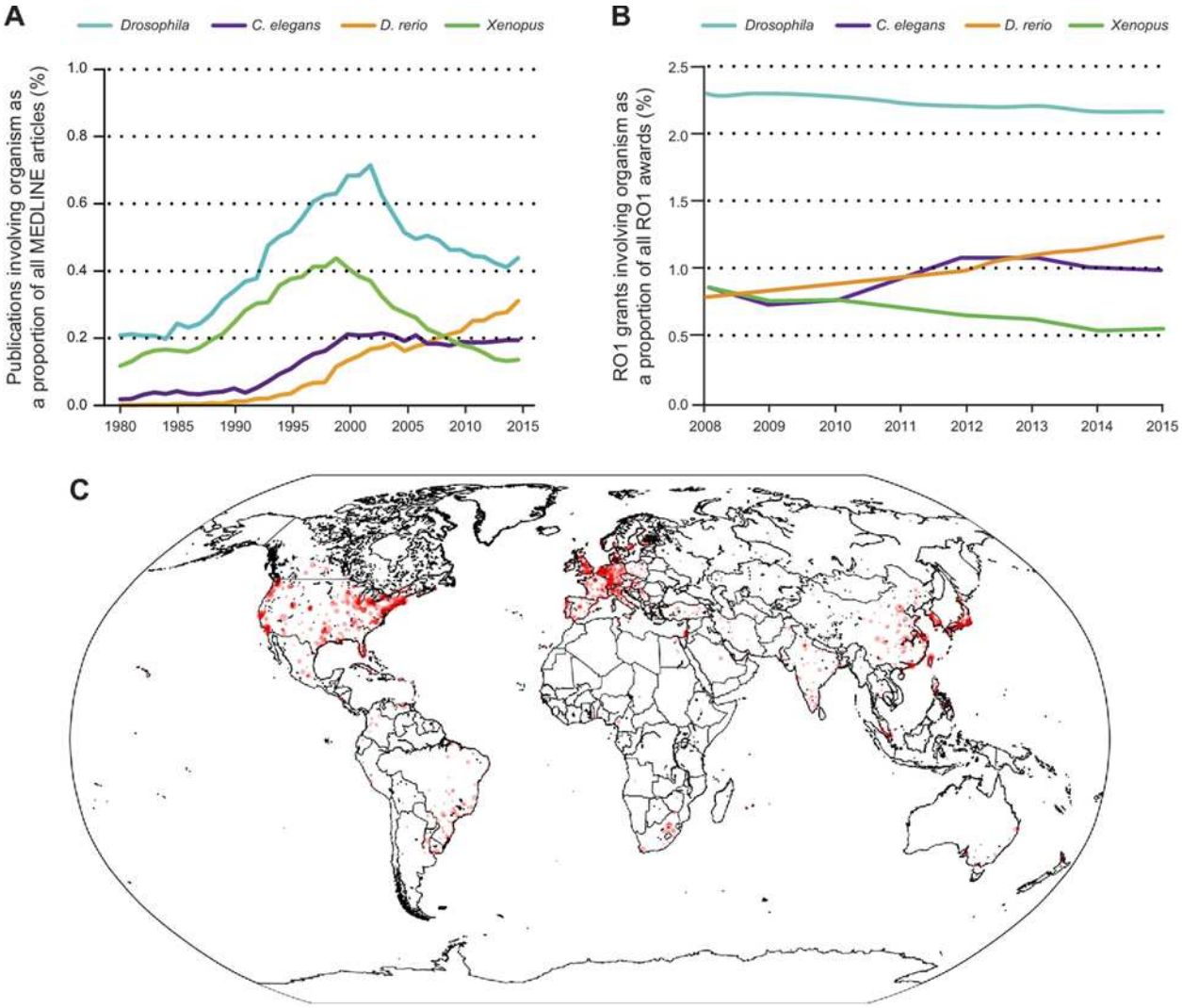

Figure 1.3 Zebrafish research across the world.

(A) *Drosophila*, *C. elegans*, *Danio rerio*, and *Xenopus* are the four most frequently utilized research organisms as ranked by percentage of publications listed in MEDLINE.
(B) The percentage of NIH R01s that involve zebrafish research for recent years.
(C) The location of zebrafish research labs around the world, based on the listed affiliations of authors of zebrafish papers in a MEDLINE search, based on Geo tagging(Gut, Reischauer et al. 2017).

Advantages of zebrafish as a cardiovascular model

Several unique features make zebrafish powerful model to study human disease especially cardiovascular disease and give us ability to elucidate the mechanisms that are incorporated in this disease (Bakkers 2011, Bournele and Beis 2016, Gut, Reischauer et al. 2017, Yalcin, Amindari et al. 2017). In the following list, I enumerate some of the most important characteristics of zebrafish for the study of cardiac development:

-Embryos are transparent for a week, which allow tracking cardiac development, contraction, blood flow in vivo.

- Embryos share many features of cardiac physiology with humans, such as: heart forming with chambers contract and pump blood to all body organs (Fig1.4) , and the heart rate 120-180 beats per minute much closer to human heart rate (Baker, Warren et al. 1997).

- Embryos obtain sufficient oxygen by passive diffusion during the first seven days. Therefore, the phenotype of severe heart defects in mutant embryos can be analyzed (Fig1.4).

- The ability to quantify shear stress set on endocardial cells of the embryos.

-The conduction system of zebrafish is similar to the human.

In their recent review article, Bournele and Beis nicely review genetic techniques, and describe several examples in which zebrafish have been used to identify gene pathways and function (Bournele and Beis 2016).

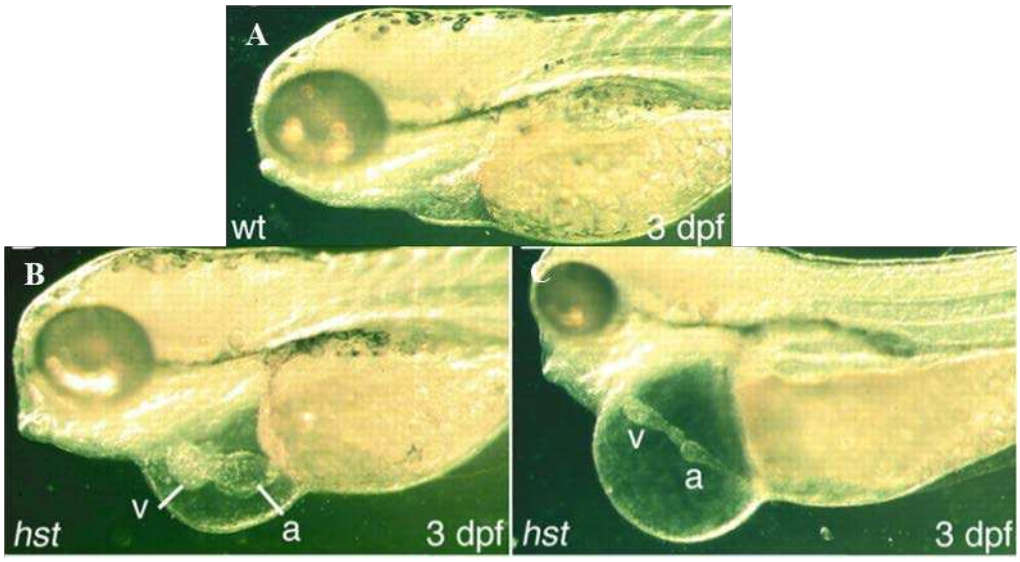

Figure 1.4 Cardiac phenotype in heart string (hst) mutant embryos.
(A) 3-day post fertilization (dpf) wild type embryos.
(B), (C) hst mutant siblings possess pericardial edema that is mild to severe and a stretched heart that is un-looped. (Garrity, Childs et al. 2002)

A brief description of embryonic zebrafish heart development

The heart is the first organ to function in the animal (Stainier 2001, Bakkers 2011). The zebrafish heart comprises only two chambers, the atrium and ventricle (Fig. 1.5H). The embryonic heart of the zebrafish is composed of three cellular layers: the endocardium, myocardium and pericardium (Fig. 1.5H). The endocardium is an endothelial lining that is connected with the rest of the vasculature. On the other hand, the myocardium is the muscle of the heart that undergoes rhythmic contractions to cause circulation of blood. The pericardium covers the outside of myocardial layer.

Heart formation passes through many major events that happen in chronological order. The origin of cardiac muscle is the anterior lateral plate mesoderm while the origin of skeletal muscle is both the paraxial mesoderm and lateral plate mesoderm. Table (1.3) presents a brief description of the main processes that happen during embryonic zebrafish heart development (Fig. 1.5).

Table1.3 Major events of embryonic zebrafish heart development (Yelon, Horne et al. 1999) (Christoffels, Habets et al. 2000, Forouhar, Liebling et al. 2006) (Yelon 2001, Beis, Bartman et al. 2005).

Main events	Description
Cardiac cells Specification	-Cardiogenic specification begins before gastrulation at 5hpf. -Myocardial atrial and ventricle progenitor cells are organized in the lateral marginal zone. - Endocardial atrial and ventricle progenitor cells are spread widely over the marginal zone.
Differentiation and bilateral heart fields migration and fusion	-At the 6-8 somite stage, the differentiating cardiomyocytes tend to move towards the midline to arrive at lateral plate mesoderm. -A cardiac cone forms at the midline when the two populations fuse.
Endocardium formation	-At the 25 somite stage, endocardial cells move first towards the mid-line then myocardial cells follow. - Cardiomyocytes migrate in an anterior to posterior direction.
Myocardial tube formation and rotation	-The venous pole of the heart tube is located at the left side. - The heart arterial pole is still at the mid-line.

	-At 22-24hpf, the heart cone elongates and the heart tube begins to beat.
Heart looping and chamber ballooning	-At 36hpf, the cardiac looping process starts in the heart tube. - The ventricle bends to right and the atrium is placed to the left of the midline. -The chamber ballooning process occurs, which defines two basic events: *The ventricle and atrium become distinct and attain their specific shapes with defined regions of inner and outer curvature. *Chambers attain the right size and placement.
Formation of atrioventricular valves	-At 48hpf within the endothelial layer of the heart, the endocardial cushions are formed, which are precursors to the valves. -Cardiac jelly (an extracellular matrix) is also formed between the endocardium and the myocardium. -By 105hpf the endocardial cushions expand and differentiate to form valve leaflets. -The atrioventricular valve is located between ventricle and atrium, and ensures the unidirectional circulation of blood.

Conduction system	-Approximately at 24hpf cardiomyocytes begin contract. -At 36-40hpf circulation observed

These morphological events are under both genetic and biomechanics control. Zebrafish mutants retrieved following mutagenesis screens have remained relevant in the identification and characterization of relevant pathways and genes (Kupperman, An et al. 2000).

Researchers continue to face the challenge of elucidating fully all the steps of heart generation. However, the transparency of the zebrafish embryo as well as the use transgenic zebrafish lines where specific tissues can be labeled using fluorescent reporters have made defined heart formation steps possible (Stainier 2001).

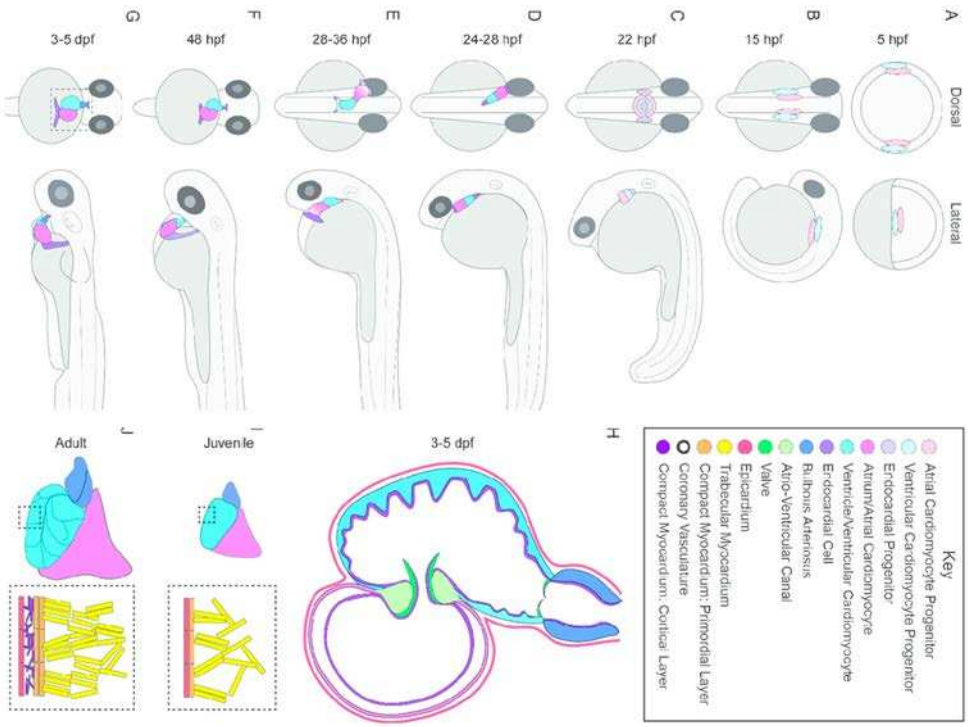

Figure 1.5 Zebrafish Heart Development stages. (From A to G) development of the heart viewing it from the lateral and dorsal sides from 5 hpf embryos to 5 days after fertilization (dpf) larvae. (A) The location of cardiac progenitors is at the adjacent margin and the ventricular progenitors are much nearer to the margin, compared to the atrial progenitors at 5 hpf; (B) There is bilateral migration of Cardiac progenitors to the frontal lateral plate mesoderm by 15 hpf; (C) There is fusion of cardiac progenitors and emerging endocardial cells in the formation of the cardiac disk which by 22 hpf starts frequent contractions between 22 and 24 hpf. (D) The elongation of disk into the linear heart tube takes place from 24 to 28 hpf and then starts the migration leftward; (E) The leftward migration of linear heart tube remains and then begins the looping. Simultaneously, adding of second heart field cells from 28 to 36 hpf is made to the major and intravenous poles which is depicted with shades; (F) The formation of the double chambered heart has completed by 48 hpf; (G) The formation of bulbous arteriosus takes place at the outflow tract; (H) The view of the heart's cross-section from 3 to 5 that features the primary location of trabeculae in the outer wall of the ventricle and cardiac valves, as well as the heart's covering by the epicardium; (I) The rotation of atrium and ventricle in-between the stages of the larva and the juvenile in a manner of the atrium being dorsal with regards to the ventricle. There is complexity of the internal topology featuring a trabecular myocardium that is spongy and outer dense myocardium known as the primordial layer; (J) the coronary arteries are the additional adult heart features feeding ventricle and the dense myocardium expansion through CMs cortical layer addition (Brown, Samsa et al. 2016).

The zebrafish genome

The zebrafish's genome is made up of 25 chromosomes and is approximately 1.7 gigabases in size (Nusslein-Volhard and Dahm 2002) while human genome consists of 23 pairs of chromosomes and is around 3.200 gigabases in size (Morton 1991). A process termed the teleost-specific genome duplication (TSD) occurred in evolution, leading to a doubling of the zebrafish genome. Thus, ancestral genes are often represented in the zebrafish genome by two daughter genes called paralogue (Glasauer and Neuhauss 2014). Even though the duplication event encompassed the whole genome of the teleost lineage, it was succeeded by rapid divergence and gene loss. As a consequence, paralogs remain for approximately 20% of the zebrafish genes. Therefore, in most cases, zebrafish gene paralogs are considerably diverged, rendering the study of functions of individual genes relatively simple (Jaillon, Aury et al. 2004, Woods, Wilson et al. 2005). In their study published in Nature, (Howe, Clark et al. 2013) found evidence for a high degree of similarity between protein-coding human and zebrafish genes. Overall, about 70% of zebrafish genes have a single human orthologue (Fig 1.6). Additionally, 84% of human genes associated with familial diseases demonstrate phenotypic similarities in zebrafish mutants for the orthologus gene.

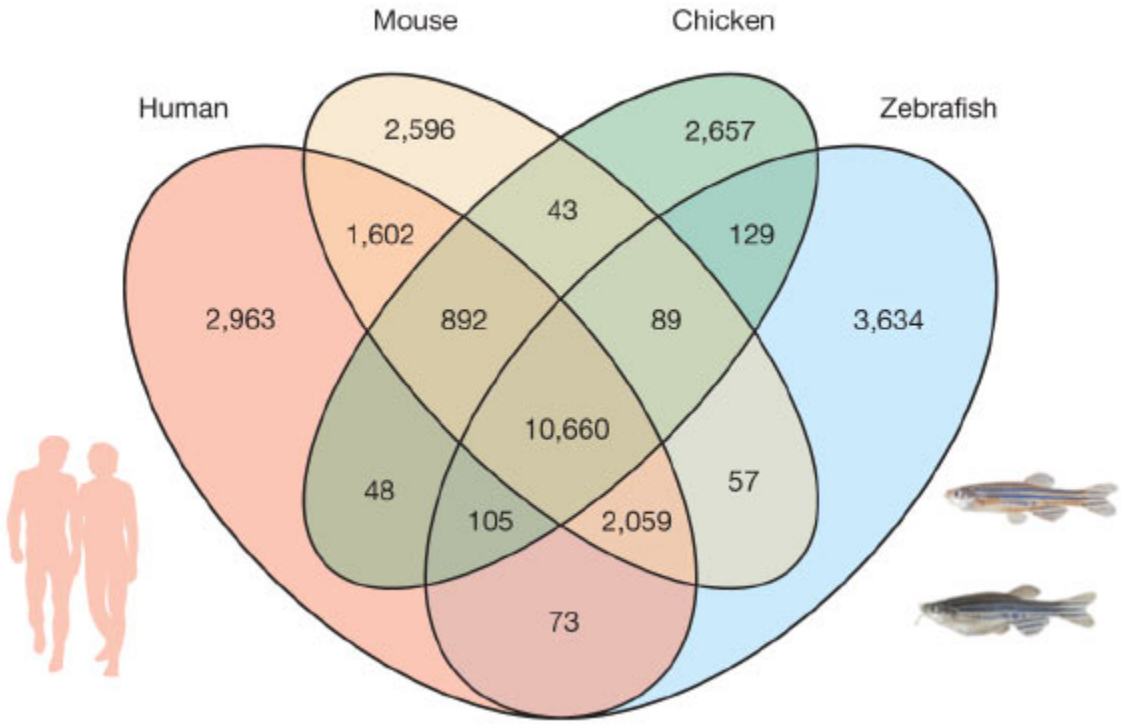

Figure 1.6 The zebrafish, human, mouse and chicken genomes share orthologous genes, with an estimated10, 660 genes common to all four species (Howe, Clark et al. 2013).

Aquarium and laboratory strains:

The following strains of zebrafish and transgenic lines were used in my research:

WIK: Tubingen wildtype fish catch in India (Spence et al., 2008).

***Tg (cmlc2: GFP)*:** The cardiomyocyte light chain2 (cmlc2; also known as myl7) promoter drives the expression of green fluorescent protein (GFP) throughout the cardiomyocytes of both chambers (Huang, 2003).

***Tg (cmlc2: cypher-eGFP)*:** Cypher is a z disc protein. The cmlc2 promoter drives the expression of a cypher-eGFP fusion protein throughout the z discs of myocardial cells (Yang, 2012).

Additionally, I used different mutant lines that were obtained from the Zebrafish International Resource Center (zirc), including: *flncasa24724*, *flncbsa15601*, *flncbsa11171*, and *flncbsa20217*

For more details on mutant lines. **See** https://zebrafish.org/home/guide.php

Cardiomyopathy

History of the concept of Cardiomyopathies

The concept of myocardial disease has an interesting and evolving history. Prior to the 20th century, most chronic myocarditis was credited to nonvalvular heart disease. In 1891, Krehl, a physician in Leipzig, applied the term idiopathic disease to heart muscle and linked it to heart failure, rather than valve disease. Then in 1901, Josserand and Gallavardin of Lyon coined the term primary myocardial disease, which opened the gate to additional etiology. During the period from 1933 to 1950, pathologists including Shields Warren and Henry Christian made an effort to diagnose and investigate the causes of myocardial disease that lead to heart failure (Abelmann 1984, Davies 1984, Braunwald 2017).

In 1957, the theory of cardiomyopathy was first introduced by Wallace Brigden, who provided descriptions of the different clinical manifestations of these conditions. Additionally, Bridgen identified possible causes of cardiomyopathies, which include both inherited forms and those arising from pathological causes like inflammation and necrosis (Brigden 1957, Abelmann 1984, Davies 1984). A great deal of attention was then paid to cardiomyopathies, and extensive studies were performed by (Goodwin and Oakley 1972). Afterward, the causes of cardiomyopathies were clarified with the increasing availability of sensitive imaging and genetic testing (Abelmann 1984, Davies 1984, Maron, Towbin et al. 2006, Arbustini, Narula et al. 2013, Arbustini, Narula et al. 2014, Braunwald 2017).

Cardiomyopathy definition

The definitions and classification schemes of cardiomyopathy are periodically made available by the World Health Organization (WHO) (Richardson 1996, Sisakian 2014) and national and continental cardiac societies. The American Heart Association's most recent definition was released in 2001 (Maron, Towbin et al. 2006, Arbustini, Narula et al. 2013): *"Cardiomyopathies are a heterogeneous group of diseases of the myocardium associated with mechanical and/or electric dysfunction that usually (but not invariably) exhibit inappropriate ventricular hypertrophy or dilatation and are due to a variety of causes that frequently are genetic. Cardiomyopathies either are confined to the heart or are part of generalized systemic disorders."*

Classification of Cardiomyopathies

Goodwin developed a classification paradigm for cardiomyopathies based on changes in the structure and function of heart muscle. This classification scheme includes dilated (previously

known as congestive) cardiomyopathy (DCM), hypertrophic cardiomyopathy (HCM), and restrictive (previously known as constrictive) cardiomyopathy (RCM) (Goodwin, Gordon et al. 1961, Goodwin and Oakley 1972, Goodwin 1974, Arbustini, Narula et al. 2013, Braunwald 2017). In more recent years, the fourth category, arrhythmogenic right ventricular cardiomyopathy (ARVC), was added (Boffa, Thiene et al. 1991, Richardson, McKenna et al. 1996, Corrado, Basso et al. 2017).

In 1995, the World Health Organization (WHO) and the International Society and Federation of Cardiology (ISFC) classified the cardiomyopathies into two main groups depend on the source of causes. The first group encompasses the "specific cardiomyopathies", which are the heart muscle diseases linked to myocarditis. Myocarditis is a viral infection that causes inflammation when active, and leads to chronic DCM in 5%-10% of all patients (Kawai 1999). The second group encompasses the "primary cardiomyopathies", which include diseases derived from the myocardium itself. This group consists of different types of cardiomyopathies, such as DCM, HCM, RCM, and ARVC (Hughes and McKenna 2005). Each of these categories is further subdivided based on pathogenesis; these pathologies include cardiomyopathy secondary to a universal disorder or an infection, as well as cardiomyopathy due to inflammation or an inherited disorder. In many cases, identification of pathogenesis cannot be clearly deduced for the patient, and those individuals are thus labeled as idiopathic cardiomyopathies (Arbustini, Narula et al. 2013).

The MOGES classification for cardiomyopathy, which received the endorsement of the World Heart Federation, was advanced by Arbustini et al., (Arbustini, Narula et al. 2013). This new MOGES system classification describes many aspects of the cardiomyopathies. The different letters in "MOGES" each represent part of the classification. M refers to the phenotype (ex. DCM

and HCM). O denotes organ involvement (for example, with/without the involvement of extracardiac cells). G describes genetic transmission (for example,. autosomal dominant or recessive). E refers to pathogenesis (for example, causal gene and mutation). Finally, S shows the stage of the disease (Arbustini, Narula et al. 2013, Elliott 2013, Arbustini, Narula et al. 2014, Mayosi 2014).

A major trigger of heart disease in every age group is inherited cardiomyopathy, which normally manifests near the onset of adolescence or early adult life. These illnesses often severely burden both patients and their family members (Watkins, Ashrafian et al. 2011). Genetic variation has different impacts in all the inherited cardiomyopathies, with many different rare mutations in numerous disease genes present within each category (Fig. 1.7). Nonetheless, advances in technology make it possible for families to regularly undergo genetic testing (Kamisago, Sharma et al. 2000). The following section describes the definitions and molecular genetic causes of several types of cardiomyopathies.

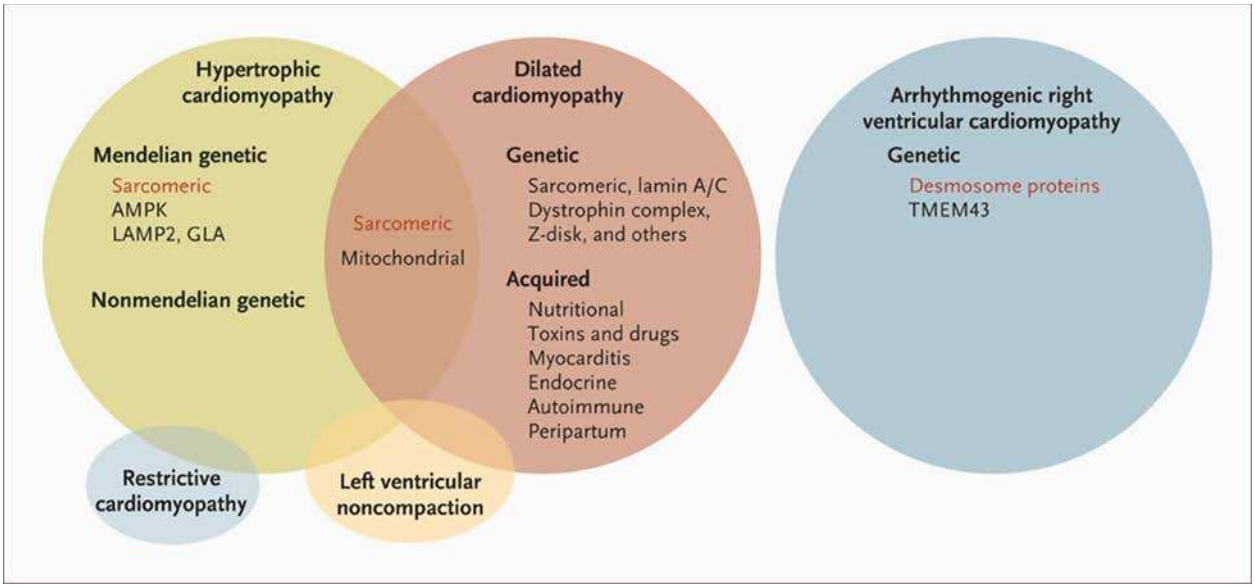

Figure 1.7 Inherited Cardiomyopathies Clinical Categories and their Genetic Basis: Some disease genes may cause either hypertrophic cardiomyopathy or dilated cardiomyopathy. Fewer genes are in common between restrictive cardiomyopathy and left ventricular noncompaction.

The appearance of Arrhythmogenic right ventricular cardiomyopathy is presented here as a genetically different grouping, in spite of the fact of the impossibility of easily distinguishing its clinical phenotype from that of dilated cardiomyopathy.

The genetic classes listed in red represent the overwhelming major causes of within the respective groupings (Watkins, Ashrafian et al. 2011).

Dilated Cardiomyopathy (DCM)

Definition

The major features of dilated cardiomyopathy involve the enlargement of the left ventricle and systolic dysfunction, together with myocyte death and myocardial fibrosis (Fig. 1.8) (Davies 2000) (Watkins, Ashrafian et al. 2011, Merlo, Cannatà et al. 2018). People can suffer from DCM at various ages, but most DCM cases occur in the third decade of life. The estimated occurrence of DCM ranges from 1/2500 up to 1/250, and the data exhibit a 3:1 male to female ratio (Merlo, Cannatà et al. 2018). In some cases, dilated cardiomyopathy is inherited with other cardiac traits (for example, conduction disorder) and/or noncardiac traits (for example, sensorineural hearing loss) (Watkins, Ashrafian et al. 2011).

Genes that have been linked to DCM

Familial DCM varies genetically; causal mutations have been identified in more than 50 genes. Most of these mutations are in genomic regions encoding protein critical for function of the costamere, the boundaries of the sarcomere (Z-disc), mitochondria, desmosomes, nuclear membrane, or RNA-binding proteins. Therefore, a broad variety of pathological mechanisms result in DCM (Davies 2000, Hughes and McKenna 2005, McNally, Golbus et al. 2013, McNally and Mestroni 2017). The following paragraphs describe the most common genes that have been associated with DCM.

Genes encoding cardiac costameric proteins have been implicated in DCM. Mutations in dystrophin, a rod-shaped cytoplasmic protein expressed in cardiac and skeletal muscles that localizes to the subsarcolemma, for example, are associated with X-linked DCM, as well as cardiomyopathy (Feng, Yan et al. 2002).

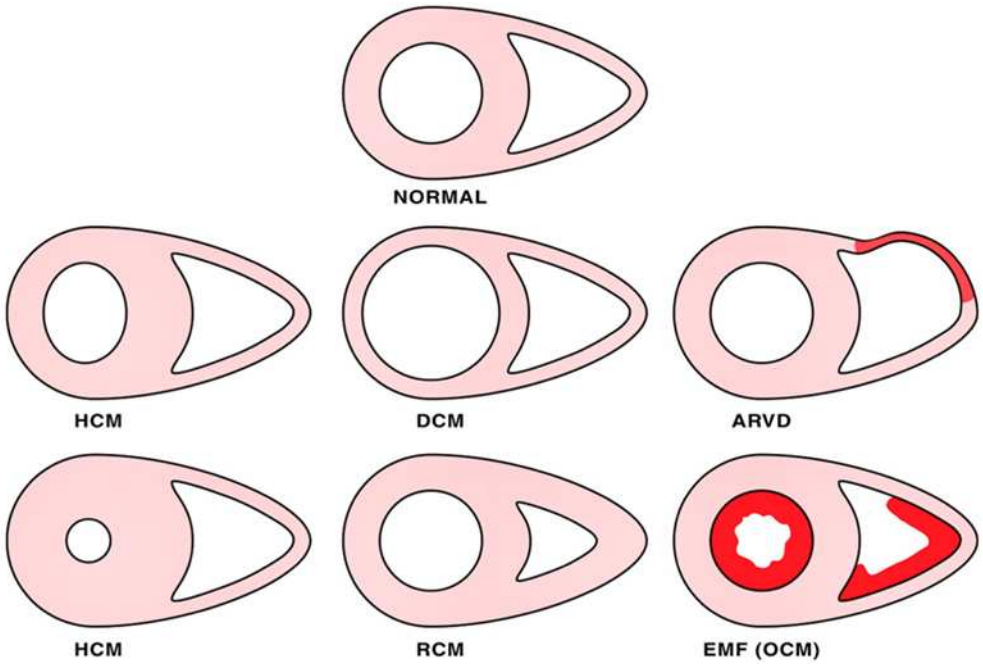

Figure 1.8 Classification of cardiomyopathy diseases according to the world health organization (WHO). This schematic represents cross cut for right and left ventricle at mid septal level of different types of cardiomyopathies in human as defined by the WHO. The ventricular shape changes due to abnormalities in cardiac function. Hypertrophic cardiomyopathy (HCM) can be either symmetric or asymmetric and the wall thickness of left ventricle is increased. Dilated cardiomyopathy (DCM) develops thin wall. The shape of the left ventricle looks closely normal in restrictive cardiomyopathy (RCM) however the myocardium fails to relax in diastole (Davies 2000). In the condition of arrhythmogenic right ventricular dysplasia (ARVD), the myocytes are replaced with transmural and some fibroses causing dilation in the left ventricle. Obliterative cardiomyopathy (OCM) is characterized by developing thrombus on the apex and inflow endocardium of either ventricle chambers.

Sarcoglycan genes encode transmembrane proteins that link the cortical actin fibers to the extracellular matrix. Mutations in the sarcoglycan genes, together with dystrophin mutations, produce cardiomyopathy that, on most occasions, is linked to muscular dystrophy (Tsubata, Bowles et al. 2000) (Watkins, Ashrafian et al. 2011, McNally and Mestroni 2017).

Furthermore, genes implicated in DCM commonly include the proteins that encode the sarcomere, which is the basic contraction unit of muscle. One gene linked to DCM is *titin* (*TTN*), which encodes a giant sarcomeric protein in the heart. The contributions made by TTN variants account for 20 to 25% of nonischemic DCM (Herman, Lam et al. 2012). *Myosin heavy chain 7 (MYH7), cardiac troponin 2 (TNNT2),* and tropomyosin 1 (*TPM1)* are the most commonly mutated sarcomere genes in DCM, based on the latest data from clinical genetic testing. Mutations in these genes explain ~2% to 4% of DCM cases (Kamisago, Sharma et al. 2000, Pugh, Kelly et al. 2014, McNally and Mestroni 2017).

Lamins are another group of genes involved in DCM. The *LMNA* gene encodes both lamins A and C via differential splicing at the 3′ end, leading to two proteins. LMNA is an intermediate filament usually expressed in differentiated somatic cells (Lu, Muchir et al. 2011). Approximately 5 to 8% of genetic DCM is due to *LMNA* missense or truncation mutations (Parks, Kushner et al. 2008). Additionally, numerous dominant mutations in *PLN*, whose protein product is phospholamban, are linked to DCM. PLN is an important protein which regulates Ca^2 cycling and enhances cardiac output by mediating β-adrenergic effects (Liu, Morales et al. 2015). Another gene linked to DCM is *RNA-binding motif 20* (*RBM20*), a ribonucleic acid (RNA) binding protein gene, which is highly expressed in atria and ventricles. Mutations in *RBM20* contribute to 1-5% of DCM cases (Li, Morales et al. 2010). The main sodium channel that the heart expresses is encoded by the ion channel gene *SCN5A*. Missense mutations in *SCN5A* have been shown to cause a greater risk of

arrhythmia and DCM (McNair, Sinagra et al. 2011) (Watkins, Ashrafian et al. 2011, McNally and Mestroni 2017).

In more recent times, *filamin C* (*FLNC*) mutations have been associated with DCM. Filamin C links cortical actin fibers to transmembrane proteins and interacts with many Z-disc proteins (Golbus, Puckelwartz et al. 2014, Begay, Tharp et al. 2016, Begay, Graw et al. 2018, Nozari, Aghaei-Moghadam et al. 2018)

Hypertrophic Cardiomyopathy (HCM)

Definition

Hypertrophic cardiomyopathy (HCM) is characterized by an increased wall thickness of the left ventricle, symmetrically or asymmetrically, and a reduced size of the ventricular cavity (Fig 1.8). In some cases, patients with HCM develop a secondary disease, such as hypertension or aortic valvular stenosis. The other histological features of HCM, which are considered the hallmarks of hypertrophic cardiomyopathy, include myocyte disarray and fibrosis. This heart phenotype varies among individuals who suffer from familial HCM, and has an estimated occurrence in the population of 1/500 (Davies 1984, Hughes and McKenna 2005, Watkins, Ashrafian et al. 2011, Hensley, Dietrich et al. 2015, Maron, Udelson et al. 2015).

Genes that have been linked to HCM

HCM is a common genetic disease with variable expression characters and is associated with more than 1500 mutations in 11 genes (Maron, Towbin et al. 2006, Maron, Udelson et al. 2015). Mutations in one or more of the nine sarcomere genes cause 60% of HCM cases. These genes encode for components of the heart's contractile apparatus. Of these nine genes, the majority of known mutations occur in four of them: the β-myosin heavy chain gene *MYH7* (20–30%), the

myosin-binding protein C gene *MYBPC3* (30–40%), the cardiac troponin T gene *TNNT2* (10%), and the cardiac troponin I *TNNI3* (7%). In other sarcomere genes, mutations are very uncommon (Richard, Charron et al. 2003, Hughes and McKenna 2005, Kimura 2008, Hensley, Dietrich et al. 2015).

On the other hand, mutations in two genes encoding non-sarcomeric proteins also produce the hypertrophy phenotype. Both proteins are involved in cardiac muscle metabolism and are responsible for cardiac glycogen storage disease. One of these gene is *PRKAG2*, which encodes the γ-2-regulatory subunit of the AMP-activated protein kinase (AMPK) and interacts with numerous signaling cascades (Maron, Towbin et al. 2006, Watkins, Ashrafian et al. 2011). The other gene is *LAMP2,* which encodes lysosome-associated membrane protein 2 and causes Danon-type storage disease. Certainly, more studies are needed to identify many other mutations in sarcomeric and metabolic genes that cause cardiac hypertrophy (Maron, Towbin et al. 2006).

Arrhythmogenic Right Ventricular Cardiomyopathy (ARVC)

Definition

ARVC is an uncommon form of a progressive, chronic, and inherited cardiac disorder with an estimated prevalence of 1/5000 in the general population. Myocardium fibrofatty replacement is the major feature of ARVC, predominantly in the right ventricle (and some in the left ventricle as well) (Fig 1.8) (Davies 2000, Maron, Towbin et al. 2006, Sen-Chowdhry, Morgan et al. 2010, Hall, Sutanto et al. 2018).

Genes that have been linked to ARVC

Mutations in genes responsible for encoding desmosomal proteins lead to ARVC. Desmosomes play a role in cell-to-cell adhesion and connect membrane proteins from the cytoplasmic domain to the intermediate desmin filaments of myocardium. These desmosomal proteins include smoplakin, plakoglobin, plakophilin 2, desmoglein 2, and desmocollin 2 (Watkins, Ashrafian et al. 2011, Corrado, Basso et al. 2017, Hall, Sutanto et al. 2018).

Alternatively, mutations in non-desmosomal genes develop atypical ARVD/C forms. These genes include the *growth factor beta 3* (*TGFB3*) and *transmembrane protein 43* (*TMEM43*) (Beffagna, Occhi et al. 2005, Merner, Hodgkinson et al. 2008, Lazzarini, Jongbloed et al. 2015). Although researchers have identified several gene mutations that cause ARVC, additional future studies are required to identify other disease genes.

In most cases, cardiomyopathy is a genetic disease. In the sections above, I listed numerous genes associated with different types of cardiomyopathy, and identified variant mutations helps to explain the mechanisms that lead to myocardium disorders. Although researchers have identified several gene mutations that cause myocardium disorders, many gene mutations are still unknown, or more data is required to significantly correlate them to cardiomyopathies. One such example is FLNC, which is a sarcomeric protein that links the cortical actin to transmembrane proteins such as integrin through it interaction with several proteins in the costamere. FLNC is expressed in skeletal and heart muscle; thus, FLNC may play a role in cytoskeleton organization (Dalkilic, Schienda et al. 2006, Fürst, Goldfarb et al. 2013). A few previous studies investigated the role of FLNC in heart development. Fujita and his colleagues used medaka as a model, and Begay and her colleagues (which includes myself and Dr. Garrity) used zebrafish as a model to test the role of FLNC in heart muscle development (Fujita, Mitsuhashi et al. 2012, Begay, Tharp et al. 2016).

Additionally, other studies have linked the FLNC varients to various human cardiomyopathies: three to DCM (Begay, Tharp et al. 2016, Reinstein, Gutierrez-Fernandez et al. 2016, Nozari, Aghaei-Moghadam et al. 2018), two to ARC (Begay, Graw et al. 2018), one to RCM (Brodehl, Ferrier et al. 2016), and one to HCM (Valdés-Mas, Gutiérrez-Fernández et al. 2014). Despite these prior studies, the mechanism by which FLNC mutation can lead to cardiomyopathies is poorly understood. In my dissertation project, I used zebrafish to study FLNC function and to model cardiac muscle disease, contrasting several FLNC alleles. Indeed, this project provided more data about the relationship between FLNC and cardiomyopathy, and explained some mechanisms that lead to this disease.

Filamin C and myopathies

Filamin (FLN)

The FLN genes encode large homodimer proteins of 240-260 kDa, which are essential for cellular differentiation (Gorlin, Yamin et al. 1990, Razinia, Mäkelä et al. 2012, Sethi, Seppälä et al. 2014). Vertebrates have three different genes in the filamin family; these genes are *filamin A* (*FLNA)*, *filamin B* (*FLNB)* and *filamin C* (*FLNC)*. The three human filamin proteins (FLNA, FLNB, and FLNC) show strong (around 70%) homology across the entire amino acid sequence (Patrosso, Repetto et al. 1994, Chakarova, Wehnert et al. 2000, van der Flier and Sonnenberg 2001).

Filamin genes (FLNs) are distributed throughout the animal kingdom and conserved across species. FLNs are found in vertebrates and many diverse organisms, such as amoebas, nematodes and insects (Razinia, Mäkelä et al. 2012). The number of FLN Ig domains and splice variants is different across species (Noegel, Rapp et al. 1989, Vargas, Sansonetti et al. 1996, Fucini, Köppel et al. 1999, Razinia, Mäkelä et al. 2012). FLNs have particular characteristics that contribute to their impact in the cell, which include actin cross-linking and providing a scaffold for other

proteins. Mutations in FLN family genes have been linked to a wide range of diseases and complex phenotypes, and are involved in different interactions and processes (Razinia, Mäkelä et al. 2012).

Structure

Each human FLN subunit is comprised of an N-terminal actin binding domain (ABD) followed by 24 β-pleated sheet immunoglobulin-like domains (IgFLN 1-24), which are collectively referred to as the rod region (Fig 1.9). The FLN actin binding domain has two calponin homology domains (CH1 and CH2). Two flexible hinge areas reside within the 24 Ig FLN domains, one between Ig domains 15 and 16 (H1) and one between Ig domains 23 and 24 (H2); both hinge regions precede the FLN dimerization domain (Fig. 1.9) (Pudas, Kiema et al. 2005, Nakamura, Osborn et al. 2007). When two filamin molecules self-associate via their carboxy-terminal dimerization domains, they give rise to an enlarged Y-shaped homodimer, thereby forming flexible links between two actin filaments (Fig. 1.9) (Himmel, van der Ven et al. 2003, Pudas, Kiema et al. 2005, Sjekloća, Pudas et al. 2007). FLNC differs from FLNA and FLNB in that it contains an insert of 81 amino acids in repeat 20 (Gorlin, Yamin et al. 1990, van der Flier and Sonnenberg 2001, Lad, Kiema et al. 2007, Sethi, Seppälä et al. 2014). Remarkably, over 90 proteins interact with FLNs through the Ig domains in the C terminus (Nakamura, Stossel et al. 2011).

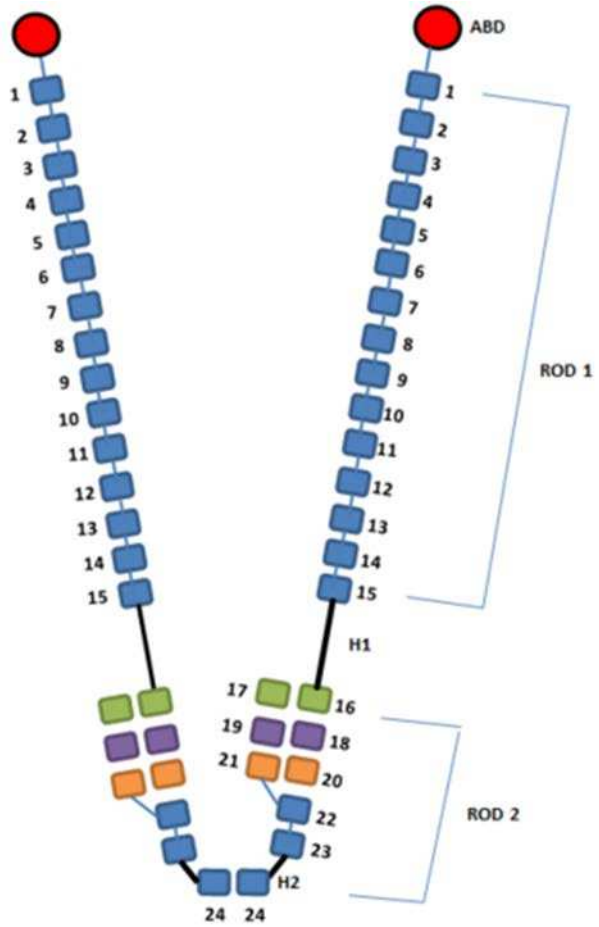

Figure 1.9 Schematic representation of the Filamin dimer structure based on the human protein. The actin binding domains (ABDs) are shown as red circles at the N terminus, with the 24 Ig domains following them (Sethi, Seppälä et al. 2014).

Cellular localization of filamin isoforms

Human FLNA, FLNB, and FLNC show overlapping tissue and cellular expression patterns. By far, FLNA and FLNB are most widely expressed, and in high abundance (Gorlin, Yamin et al. 1990, Takafuta, Wu et al. 1998, Xu, Xie et al. 1998). FLNA expression is required for normal cardiac and vascular development (Feng, Chen et al. 2006, Hart, Morgan et al. 2006). A heterozygous nonsense mutation in human FLNA results in a neuronal migration defect, leading to peri-ventricular heterotopia (Fox, Lamperti et al. 1998), while a missense mutation of FLNA causes cardiac valvular dystrophy (Kyndt, Gueffet et al. 2007).

FLNB is essential for skeletal and microvascular development (Zhou, Tian et al. 2007), and certain mutations in FLNB cause defective vertebral segmentation, skeletogenesis, and joint formation (Krakow, Robertson et al. 2004, Lad, Kiema et al. 2007).

FLNC restricts its expression to the cardiac and skeletal muscles (KOTELIANSKY, GLUKHOVA et al. 1986) and is required for normal myogenesis (Dalkilic, Schienda et al. 2006, Lad, Kiema et al. 2007). Several studies of skeletal muscle FLNC have demonstrated that the protein is localized at the Z-disc and myotendinous junctions, while in the cardiac muscle the intercalated disks and Z-disc are also enriched with FLNC. Additionally, FLNC also localizes to the muscle's sarcolemma, though in low amounts, and cross-links thin filaments at their ends in the myofibrillar Z-discs (Fig1.10) (Price, Caprette et al. 1994, Thompson, Chan et al. 2000, van der Ven, Obermann et al. 2000, Razinia, Mäkelä et al. 2012).

Beyond the sarcomere per se, FLNC links the costameric complexes with Z-disc proteins. In this context, FLNC has a role in force transmission from the sarcomere to the sarcolemma (Peter, Cheng et al. 2011). In cultured human skeletal muscle cells, FLNs may localize along actin stress

fibers and the cortical actin network, and are frequently found in migrating cells at the base of their membrane ruffles (Chiang, Greaser et al. 2000, van der Ven, Obermann et al. 2000).

Biological function of filamin family proteins

FLNs play important roles in the cell development including:

Organization of actin cytoskeleton

FLNs interact with F actin and cross-link actin filaments. Many factors play a role in the arrangement of actin filaments into orthogonal networks and parallel fibers. The high ratio of the frequent interaction of actin binding protein (ABP) filamins to actin proteins leads to tighter networks of actin (Cunningham, Gorlin et al. 1992). For example in the study was done in vitro using rabbit skeletal muscle F-actin, a molar ratio of 1:50 ABP filamin :actin leads to the formation of parallel bundles of actin filaments, while an orthogonal network of actin is promoted when the stoichiometry is 1:(150-740) (Brotschi, Hartwig et al. 1978, van der Flier and Sonnenberg 2001). Moreover, the type of actin cross-linking proteins present influences the type of actin network built. For example, an *in vitro* mixture of FLN and α-actinin results in the formation of dense actin fibers, while the presence of single FLN only in the mixture leads to orthogonal networks (Schollmeyer, Rao et al. 1978). Additionally, the structure of the filamen variant has an effect on actin fiber organization. For instance, a lack of the first H1 region of FLN variants prevents the flexibility of the filamin rod domain and leads to packed filamin dimers, which form rigid actin fibers instead of orthogonal networks (van der Flier and Sonnenberg 2001). Although the above studies were done for ABP filamin in general (before the three types of FLNs discovered) the roughly 70% amino acid homology of FLNA and FLNB with FLNC suggest the probability that FLNC interactions with actin are of functional importance. Overall, these data point to the functional impact that filamin interaction with actin has on organization of the cytoskeleton.

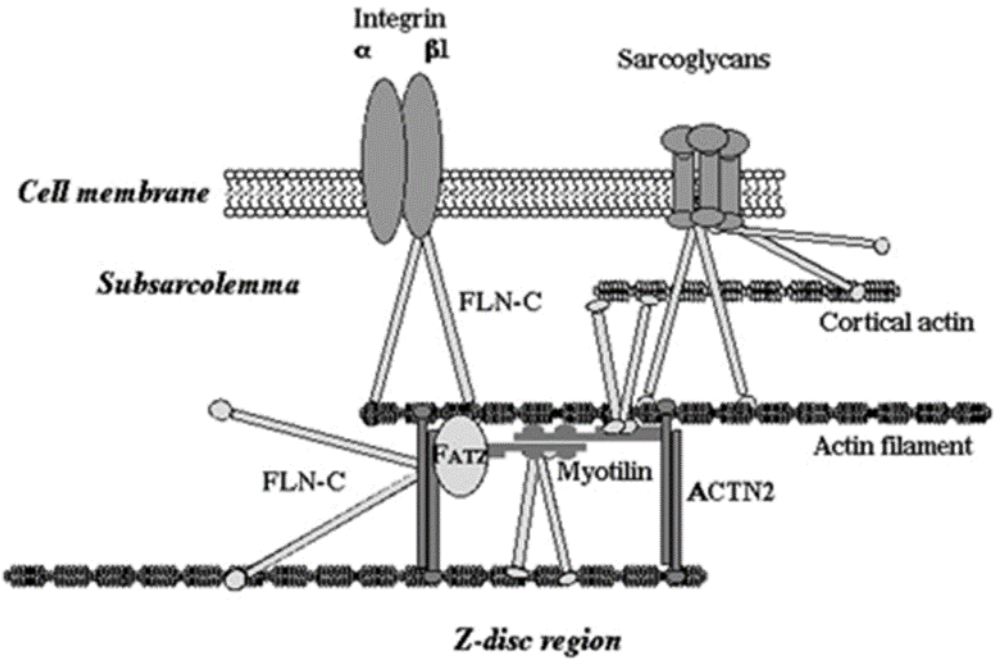

Figure 1.10 Schematic of intracellular Filamin C localization within the costamere. The filamin-C (represented here in the form of a tail-to-tail connected dimer) links the cytoplasmic domain of β1 integrin, as well as γ and δ sarcoglycans at the sarcolemma. FLNC also links actin filament to sarcolemma via N-terminal (Gontier, Taivainen et al. 2005).

Anchoring of transmembrane proteins

Numerous transmembrane receptors interact with the filamin Ig repeat domains, including Integrin, Glycoprotein-Ib K, and N-sarcoglycans. Some of these transmembrane proteins bind to one or many Ig repeat domains found in the carboxy-terminal region of filamin (Loo, Kanner et al. 1998, Takafuta, Wu et al. 1998, Xu, Xie et al. 1998, Thompson, Chan et al. 2000). Thus, filamins promote the anchoring of cortical actin and stress fibers to the transmembrane receptors (van der Flier and Sonnenberg 2001). FLNC interacts with γ- and δ-sarcoglycans, which are localized to the sarcolemma of the muscle cell membrane and are responsible for anchoring the actin cytoskeleton to the extracellular matrix (ECM) (Thompson, Chan et al. 2000, Löwe, Kley et al. 2007). Many sarcolemma proteins, such as sarcoglycan, localize improperly and form intracellular aggregations in patients who have mutations in FLNC (Kley, Hellenbroich et al. 2007, Löwe, Kley et al. 2007). In general, FLNC has a role in linking actin fibers to cell membrane through interaction with numerous transmembrane proteins.

Scaffolding of signaling molecules

GTPases of the Rho family regulate cytoskeleton dynamics and cell protrusions. FLNs are associated with several signaling molecules through its carboxy-terminal repeats, such as FLNA's interaction with the small GTPases, Rho and Rac (UEDA, OHO et al. 1992, van der Flier and Sonnenberg 2001, Razinia, Mäkelä et al. 2012). The interactions between FLNs and signaling molecules facilitate many different cell processes including the formation of filopodia (Ohta, Suzuki et al. 1999) and cell migration (Ueda, Ohta et al. 2003, Razinia, Mäkelä et al. 2012). Hence, FLNs are considered to be scaffolding proteins for several signaling molecules.

Besides the organization of actin filaments, FLNC interacts with other proteins, the myozenins and myotilin which are the Z-disc proteins (Fig. 1.11) (Fürst, Goldfarb et al. 2013) .

Myofibrillar myopathy (MFM) related to FLNC

Myofibrillar myopathies (MFMs), which were first identified in 1969, are a group of progressive inherited muscle disorders that usually result in severe disability and early death. MFM symptoms usually begin at an age of 35-50 years. Most patients with MFMs suffer from progressive muscle weakness over years, and as a result they develop respiratory failure and cardiac disease. Children and infants with MFMs can experience severe, progressive respiratory failure, cardiomyopathy, and arrhythmias. The cardiac defect is characterized by conduction blocks, diastolic dysfunction, and left ventricular hypertrophy (Claeys and Fardeau 2013, Fürst, Goldfarb et al. 2013, Latham and Lopez 2015).

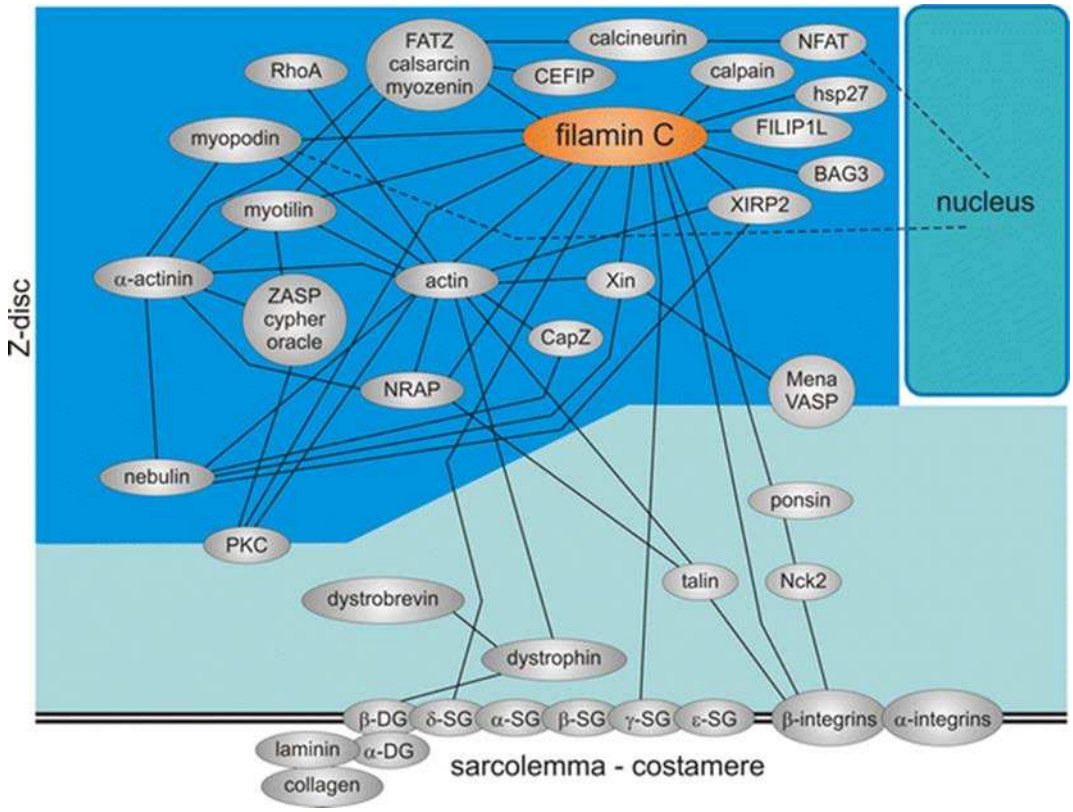

Figure 1.11 Schematic diagram illustrates the FLNc's complex interactome within the Z-disc and at the sarcolemma (Fürst, Goldfarb et al. 2013).

The observation of MFMs through histopathology reveals the disintegration of myofibrils at the Z-disc, dysfunction of the mitochondria, and accumulation of intramyoplasmic protein aggregates. MFMs are caused by mutations in genes located at or associated with Z-disc proteins, including desmin, filamin C, plectin, VCP, FHL1, ZASP, myotilin, αB-crystallin, BAG3, and DNAJB6. Fifty percent of gene mutations causing MFMs have been identified, while the remaining half are still unknown. Amelioration and causative therapy techniques to remedy this disorder are not yet available (Maerkens, Olivé et al. 2014, Latham and Lopez 2015, Winter and Goldmann 2015, Vincent, Grady et al. 2016).

Researchers have reported many cases that link MFMs to the *FLNC* gene in populations across the world. The number of identified *FLNC* mutations causing MFMs has been increasing, and the mutations are often in different functional domains, resulting in various clinical phenotypes characterized at the cellular level by improper localization or aggregation of the filamin protein (Löwe, Kley et al. 2007, Valdés-Mas, and Gutiérrez-Fernández et al. 2014). Mutations in FLNC-Ig-like domains 7, 22, and 24 were shown to cause cardiomyopathy, weakness in limb-girdle muscles, and atypical protein aggregation (Vorgerd, van der Ven et al. 2005, Shatunov, Olivé et al. 2009, Luan, Hong et al. 2010, Tasca, Odgerel et al. 2012). The protein aggregation leads to muscle degeneration. The disruption of interaction sites and dimerization domains of FLNC results in the accumulation of many muscle proteins in insoluble cytoplasmic aggregates and produces disease. These mutations could explain how FLNC aggregation is toxic (Dalkilic, Schienda et al. 2006, Ruparelia, Zhao et al. 2012). Alternatively, patients with mutations in the actin-binding domains (ABD) or Ig-like domain 15 mostly demonstrate weakness in the distal muscles and no cardiomyopathy or common pathology (Duff, Tay et al. 2011, Guergueltcheva, Peeters et al. 2011, Miao, Su et al. 2018) (Fürst, Goldfarb et al. 2013).

FLNC mutations that are presently recognized are demonstrated on the provided mutation chart (Fig 1.13) (Fürst, Goldfarb et al. 2013).

Animal Models for FLNC function:

Mouse

The *FLNC* Δ41-48−/− mouse model is the only model for Flnc mutation that has been designed thus far. Dlkilic and his colleagues expected a severe phenotype in the Flnc mice KO model. Thus, they created a mouse model where the last eight exons (41-48) of the *FLNC* gene were deleted, similar to the FLNA truncation mutation that leads to a partial loss of function phenotype

in human patients. The Flnc knockout allele causes severe skeletal muscle deformities on the infiltration of connective tissue into the intercostal muscles and the diaphragm, which in turn resulted in a weakened ability to breath. Due to this, mice homozygous for the knockout allele died at birth. The skeletal muscles of these mice have less mass, and the number of muscle fibers is reduced. The heterozygous mice were fertile and viable with no deformities. This process illustrated that the heterozygous mice of truncated Flnc do not result in an obvious phenotype. (Dalkilic, Schienda et al. 2006).

Medaka

A mutation in the *flnca* gene of medaka, a teleost fish, was found in *zacro* (*zac*) mutants. *zac* mutants contain a nonsense mutation predicted to encode a truncated protein in the 15th immunoglobulin-like repeat of *flnca*. In this mutation, the skeletal muscle fibers are degenerated and disorganized at 4 days and 5 hours post fertlization. The myocardial layer of the heart also ruptures once the heart starts beating, leading to an abnormally-developed heart. In addition, filamin C protein is aggregated at myotendinous junctions, and the myofibrils are disconnected from the sarcolemma and intercalated disks. The embryos possessing the *zac* phenotype were homozygous for the mutant allele. A series of morpholino-based antisense RNA experiments yielded a similar phenotype to the *zac* mutant. This study suggested that filamin C is important for maintaining the structural integrity of cardiac and skeletal muscles (Fujita, Mitsuhashi et al. 2012).

Zebrafish

The *stretched out* (*sot*) mutation is an *flncb* nonsense mutation that causes a premature stop codon at exon 30 out of 48, which is predicted to encode a protein that eliminates of the C-terminal half of the protein, including the interaction sites and dimerization domains. In this mutant, muscle

fibers break and the skeletal muscle becomes defective, causing protein aggregation. This mutation is a novel zebrafish model of a myofibrillar myopathy associated with filamin. When the two *FLNC* paralogs (*flnca* and *flncb*) are knocked down by morpholinos, the result is the same as the *sot* mutant phenotype of skeletal muscles features but stronger than *sot* single mutant (Rubarelia, 2012).

In addition, at 48 and 72 hpf, zebrafish embryos injected with *flncb* morpholino were observed to show systolic dysfunction. It was characterized by dysmorphic cardiac chambers, pericardial edema, and looping defects. The ultrastructural study of these embryos revealed that the myofibrils had low numbers of successive sarcomeres, or that the myofibrils were in irregular alignment with the Z-discs (Begay, Tharp et al. 2016).

Dissertation Aims

Although mice, medaka, and zebrafish filamin C models exhibit abnormal skeletal muscle development, they each have limitations for the study of the relationship between filamin C and heart development or cardiomyopathy. Mice are dead at birth or display no cardiac phenotype in filamine C mutants (Dalkilic, Schienda et al. 2006). While medaka *zac* mutant shows cardiac phenotype, we need more research to see if the heart phenotypes was similar to phenotypes appears in medaka.

In this work, I used zebrafish as a model system to determine the impact of a lack of Flnc on heart development. I addressed several open questions in the field. First, the possibility for genetic (functional?) redundancy between the two paralogous *flnc* genes. Second, the phenotypic effects of a nonsense *flnc* mutation on the heart. Third, the differences in phenotype between null mutants

and putative truncation mutants. Fourth, whether the truncation mutants show more severe or different phenotypes than the full loss-of-function alleles, which would suggest that the truncation protein is toxic.

This work examines the role of FLNC in z-disc formation and organization and how it affects sarcomere and myofibril development and assembly. Additionally, I investigated the the mechanisms of FLNC mutations that lead to cardiac muscle diseases. For example, how the absence of FLNC impacts the actin fibers network organization and which FLNC alleles lead to heart defects and/or skeletal muscle defects.

Aim 1: To test the hypothesis that *flnca* and *flncb* are required for normal heart development (Chapter 2).

Rational: FLNC is a large actin binding protein that localizes to Z-discs. FLNC is expressed in both heart and skeletal muscles. In this aim I used a morpholino approach to knockdown *flnca* and *flncb,* two paralogous genes in zebrafish, to determine the functions of each gene in early heart development. I analyzed the heart function of morphant embryos by measuring different morphological events such as heart rate, looping angle and chamber size.

Aim 2: To test the hypothesis that different FLNC mutant alleles differentially affect zebrafish heart development (Chapter 3).

Rational: In humans, mutations in FLNC cause MFM and/or cardiomyopathies, and these mutations occur across the large FLNC gene. In this aim, I used different *flnc* genetic lines from the following alleles: *flnca* sa24724, *flncb* sa15601, *flncb* sa11171 and *flncb* sa20217, which are nonsense mutations in *flnca* exon1, or *flncb* exons 1, 14, and 35, respectively (both genes span 48

exons in total). Both exon 1 alleles have a high probability of being null, whereas exon 14 or 35 alleles may produce a truncated protein. Using embryos of verified genotype, I analyzed the heart morphology and function of singly or doubly homozygous or heterozygous mutant embryos. Lastly, I compared the nature of defects among different *flnca* and *flncb* mutants, some of which make no protein and some of which make truncated proteins.

Aim 3: To test the hypothesis that FLNC mutants impact the cytoskeleton and Z disc arrangement and determine which alleles cause protein aggregation (Chapter 4).

Rational: Within the cell, FLNC protein localizes at the Z-disc and costamere of the heart and skeletal muscles. The main biochemical functions proposed for FLNC to date are linking cortical actin to several transmembrane proteins, thus strengthening costamere architecture, and interaction with many Z-disc proteins, thus facilitating sarcomere formation or stability. Moreover, researchers found that several mutations in Flnc lead to toxic protein aggregation, and patients with these mutations developed cardiac and/or skeletal muscle phenotypes.

In this chapter 1) I utilized immunohistochemistry, transgenic fish, and transmission electronic microscopy approaches to examine the organization of actin fibers and Z discs of *flnc*a and *flncb* mutant and morphant embryos. 2) I tested whether Flnc mutation leads to protein aggregation, which is a hallmark of myopathy disease. I performed trichrome staining on early mutant hearts from the different genetic lines.

Chapter 2: *flnca* and *flncb* are required for normal heart development

Introduction

Structure

Filamin (FLN) is a high molecular weight protein that associates with actin fibers (Wang, Ash et al. 1975). FLNs must homodimerize at their C-terminal ends. Vertebrate FLNs are comprised structurally of an N-terminal actin binding domain (the head) followed by 24 immunoglobulin-like domains (Ig) (the backbone), and dimerization domain at C-terminal (the tail) (Fig. 2.1A). The actin binding domain (ABD) of each FLN protein consists of two calponin homology (CH) domains: CH1 with an amino terminal and CH2 with a carboxyl terminal (Tyler, Anderson et al. 1980, Gorlin, Yamin et al. 1990, Hock, Davis et al. 1990). The FLN Ig domains 1-15 are defined as "rod1" and the Ig domains 16-24 are defined as "rod2", which specifically acts as an interaction module (Fig. 2.1B) (Ruskamo and Ylänne 2009). Filamin genes have been identified in at least 2 kingdoms: Animalia (including *Caenorhabditis elegans, Drosophila melanogaster, Gallus gallus domesticus, and Mus musculus*), and Protista (including *Dictyostelium discoideum, Entamoeba histolytica*). The only known variability in FLN structure between the organisms is the number of Ig repeats (Hock, Davis et al. 1990, Wilson, Ainscough et al. 1994).

The human genome encompasses three FLN genes, FLNA, FLNB, and FLNC, which are 70% identical at the amino acid level. Furthermore, FLNC contains an 81 amino acid domain that encodes Ig repeat 20, not present in FLNA or FLNB (Patrosso, Repetto et al. 1994, Chakarova, Wehnert et al. 2000). Human FLNA, B, and C have overlapping cellular and tissue expression patterns. FLNA and B isoforms are largely ubiquitously expressed and FLNB expression varies among tissues. (Gorlin, Yamin et al. 1990, Takafuta, Wu et al. 1998, Xu, Xie et al. 1998). In

contrast, FLNC is mostly expressed in the cardiac and skeletal muscle (Thompson, Chan et al. 2000).

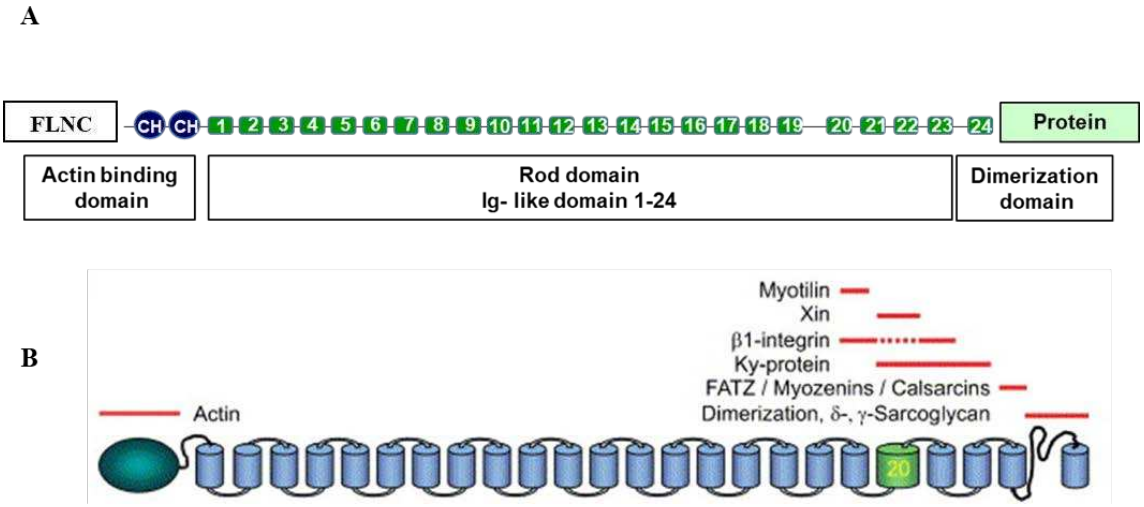

Fig. 2.1: **Schematic representing the filamin C protein.** (**A**): The actin binding domain is located at the N-terminus, followed by 24 Ig repeats of filamin domains. The FLNC Ig domains 1-15 are described as rod1 and 16-24 as rod2 (Ruskamo 2009).
(**B**): filamin C protein interaction domains (van der Ven, 2006)

Functions

In general, FLNs play an important role in actin organization and membrane stabilization. FLNs mediate anchoring of cortical actin and actin stress fibers to transmembrane receptors and serve as a scaffold for signaling. Additionally, FLNs link actin filaments in an orthogonal network and parallel bundles (Brotschi, Hartwig et al. 1978, Dabrowska, Goch et al. 1985). Moreover, FLNs interact with several transmembrane proteins. For example, FLNC binds to proteins at the plasma membrane, including integrins and γ and δ sarcoglycans (Sharma, Ezzell et al. 1995, Loo, Kanner et al. 1998, Pfaff, Liu et al. 1998, Thompson, Chan et al. 2000, Zent, Fenczik et al. 2000).

FLNC

In the skeletal muscle, FLNC protein is found in high abundance in Z-lines and myotendinous junctions. Additionally FLNC connects the cortical actin cytoskeleton to plasma membrane

proteins in low abundance (Gomer and Lazarides 1981, Gomer and Lazarides 1983, Pavalko, Otey et al. 1989, Thompson, Chan et al. 2000, van der Ven, Obermann et al. 2000). In cardiac muscle, FLNC protein is also detected at Z-disc and at intercalated discs (Koteliansky, Glukhova et al. 1981, Price, Caprette et al. 1994).

The unique amino acid insertion at the 20th Ig-like repeat of FLNC facilitates interaction with Xin repeat proteins. Xin is the protein encoded by the human gene 'cardiomyopathy associated 1' (CMYA1). A study on neonatal mice and human cardiomyocytes indicated that Xin localizes with FLNC, Mena, and VASP in intercalated discs. This interaction is essential for actin organization and Z-disc assembly (Fig. 1.2B) (van der Ven, Ehler et al. 2006). FLNC interacts with two groups of ligands: (1) Z-disc proteins including myotilin (van der Ven, Obermann et al. 2000, Gontier, Taivainen et al. 2005) myopodin (Linnemann, van der Ven et al. 2010), calsarcin (Faulkner, Pallavicini et al. 2000, Takada, Vander Woude et al. 2001, Frey and Olson 2002), and nebulette proteins (Holmes and Moncman 2008) and (2) proteins associated with the sarcolemma such as the Nebulin Related Anchoring Protein (NRAP)-talin complex (Lu, Carroll et al. 2003) and the ponsin-Nck2 complex (Zhang, Liu et al. 2007, Gehmlich, Hayess et al. 2010). In chicken embryos, FLNC was discovered to be expressed early in Z-bodies, which are the precursors to Z-discs and observed during sarcomerogenesis. FLNC interacts with many Z-disc components which suggests an essential role in mediating Z-disc and myofibril formation during the early stages of the Z-disc development (Price, Caprette et al. 1994, Fürst, Goldfarb et al. 2013). In a study using cultured mammalian CHO cells (the ATCC line), researchers found that FLNC interacts with costameric β1A integrin to anchor premyofibrils to sarcolemma. Alternatively, in mature muscle cells FLNC indirectly links myofibrils to sarcolemma- associated integrin through the above mentioned protein complexes (van der Ven, Obermann et al. 2000, Gontier, Taivainen et al. 2005).

Myopathy diseases

A relationship has been established between FLNC and muscle disease. Myofibrillar myopathies (MFM) are a group of heredity human skeletal muscle diseases that lead to severe muscle weakness and physical disability (Fürst, Goldfarb et al. 2013). MFM is characterized by protein aggregation, myofibrillar degeneration, and mitochondrial dysfunction. Most MFM diseases are caused by mutations in about ten genes encoding sarcomeric proteins including FLNC, desmin, myotilin, and Z-band alternatively spliced PDZ-motif (ZASP) (Schröder, Vrabie et al. 2007, Schröder and Schoser 2009). Several studies of patients who suffered from muscle weakness were shown to exhibit FLNC mutations which underlie the MFM disease (Kley, Hellenbroich et al. 2007, Shatunov, Olivé et al. 2009, Avila-Smirnow, Béhin et al. 2010, Luan, Hong et al. 2010, Kley, Serdaroglu-Oflazer et al. 2012, Tasca, Odgerel et al. 2012).

In the last few years, mutations in FLNC alleles were linked to cardiomyopathy diseases including hypertrophic cardiomyopathy, dilated cardiomyopathy, and restricted cardiomyopathy. However, few studies have investigated the functional relationship between cardiomyopathy and FLNC (Valdés-Mas, Gutiérrez-Fernández et al. 2014, Begay, Tharp et al. 2016, Brodehl, Ferrier et al. 2016, Tucker, McLellan et al. 2017, Nozari, Aghaei-Moghadam et al. 2018). One study used mice as a model to investigate the role of FLCN in myofibril development; however, mutant mice died soon after birth due to respiratory failure (Dalkilic, Schienda et al. 2006). Medaka, (*Oryzias latipes*) a teleost fish, is another animal model which has been investigated to determine the role of FLNC in heart and skeletal muscle development (Fujita, Mitsuhashi et al. 2012).

In the next section I will discuss these animal models in detail.

Animal models used to study FLNC

FLNC is a candidate gene that has been linked to cardiac muscle disorder. The *Flnc* Δ41-48 mouse lacks the final 8 exons of the protein, and is the only mouse model for the FLNC gene described to date (Dalkilic, Schienda et al. 2006). In this mouse model, the last eight exons (41-48) of the gene were deleted. Homozygous FLNC Δ41-48 ^{mice} exhibited severe abnormalities of skeletal muscle. These mice were dead at birth due to inability to breathe (Dalkilic, Schienda et al. 2006). In medaka a nonsense mutation in one of two paralogous FLNC genes (*flnca*) has been identified; these fish are called *zacro* (*zac)* mutants. Homozygous *zacro* embryos demonstrate disorganization of the skeletal muscle and heart muscle defects associated with the rupture of the myocardial layer. The injection of a *flnc* morpholino (MO) into medaka embryos resulted in a phenotype highly similar to homozygous *zacro* mutants (Fujita, Mitsuhashi et al. 2012).

The *zac* mutant of medaka focused on *flnca* whereas by sequence comparison *flncb* is most similar to human FLNC. Therefore, we need to develop an animal model to understand what the overall FLNC function is in heart development and what mechanisms lead to cardiac muscle diseases.

Zebrafish as a model organism

The zebrafish *Danio rerio* are considered a suitable model to study human heart disease because they have unique features that allow researchers to study the development of embryos with severe cardiac disease that is not possible in mammalian systems. The zebrafish has two *flnca* and *flncb* paralog genes, which are 80% identical in amino acid sequence. A mutation in the zebrafish *flncb* was identified in the *sot* mutant, which encodes a nonsense mutation in exon 30 out of 48 (Ruparelia, Zhao et al. 2012). The homozygous phenotype resulting from this mutation is characterized by skeletal muscle degeneration and protein aggregation, both of which are hallmarks of human MFM disease. Furthermore, this result was supported by MO antisense RNA

knockdown experiments that produced morphant phenotypes similar to homozygous *sot* mutant phenotypes (Ruparelia, Zhao et al. 2012).

Although the mouse, medaka, and zebrafish filamin C (*sot*) mutant models all exhibit abnormal skeletal muscle development, they have limitations regarding the relationship of filamin C and heart development or cardiomyopathy. In the mouse model, embryos are dead at birth and no cardiac phenotype appeared (Dalkilic, Schienda et al. 2006). While the medaka *zac* mutant did show a cardiac phenotype, it is not clear how well the phenotype correlates with human phenotypes. Thus, we need more research to see if the heart phenotypes was similar to medaka phenotypes. Additionally, medaka *zac* mutant is a mutation in *flnca*, which is a different gene than *flncb.* It is not clear whether the phenotypes of mouse, medaka, and zebrafish models lacking filamin C represent full loss of function or partial loss of function phenotypes. To better understand how mutations in FLNC contribute to cardiac phenotypes, we created zebrafish loss-of-function models for two *flnca* and *flncb* paralogous genes using a MO knockdown approach. Analysis of knockdown animals will enable us to address several outstanding questions about the functional importance of *flnca* and *flncb* in heart development. First, MO knockdown experiments are likely to mimic the full loss of function phenotype, assuming the MO efficiently knocks down the gene product. Second, a MO approach would allow comparison of zebrafish Flnca and Flncb morphant phenotypes to *zac* and *sot* mutants. Third, the relationship between the known human mutations in FLNC and cardiomyopathy disease is still unclear and some evidence suggests haploinsufficiency as a mechanism whereas other data suggest possible dominant negative effects from truncated proteins (Valdés-Mas, Gutiérrez-Fernández et al. 2014, Begay, Tharp et al. 2016). Zebrafish MO studies could test the hypothesis that haploinsufficiency, created by FLNC depletion, is sufficient

to produce cardiac dysfunction. In addition, we will test the hypothesis that the two *flnca* and *flncb* paralog genes are redundant. Lastly, although data from MO knockdown can be rapidly generated, using MO has limitations such as the toxicity issues and off target effect, the MO stability is reduced when stored in aqueous solution (Bedell, Westcot et al. 2011). To improve the strength and specificity of knockdown by using MO, best practices for design, storage, preparation, and use of the oligos should be followed. Additionally, it is critical to perform carful control experiments to determine the efficacy of knockdown. Phenotypic rescue by mRNA injection into morphant embryos is considered one of the strongest tests for specificity of phenotypes (Moulton 2017) .

Results

Genetic conservation:

To determine which paralog (*flnca* or *flncb*) is most closely related to humans, the amino acid sequences of *flnca* and *flncb* (GenBank Accession number*: flnca* CU302436 and *flncb* AL954190) were aligned with other vertebrate FLNC proteins (*Homo sapiens*, and Mus musculus). *Danio rerio flnca* and *flncb* are 2719 and 2743 amino acids in length respectively. *flncb* was the most similar to the human FLNC protein (83% amino acid identity with *H.sapiens*) although *flnca* was also highly conserved (79% identity) (Fig. 2.2).

FLNC morpholino knockdown and phenotypic analysis:

Phenotype analysis

To functionally examine whether *flnca* or *flncb* is essential for heart development, a MO targeting *flnca* translation (*flnca* MO) and a MO that interferes with *flncb* pre-mRNA splicing (*flncb* SD-MO) were used (Ruparelia, Zhao et al. 2012). Zebrafish embryos were coinjected with P53MO to

reduce off-target defects, which could include ectopic upregulation of the P53 pathway (Campbell, Sinagra et al. 2013). By 48hpf, 90% (135/150) of embryos injected with 90µM of ATG-blocking *flnca* MO + P53 MO and 83% (166/200) embryos injected with 250µM splice-blocking morpholino *flncb* MO + P53 MO displayed cardiac phenotypes, including a cardiac looping defect, abnormal chamber morphology, and reduced contractility. By 72hpf, *flnca* morphant embryos exhibited variable cardiac phenotypes, which we further classified as "severe" or "mild" (Fig. 2.3E). 33.3% (50/150) of *flnca* morphant embryos showed severe cardiac phenotypes characterized by weak contractility, collapse of both cardiac chambers, lack of circulation, and pericardial edema. In addition, 56.6% (85/150) displayed mild cardiac phenotypes such as dilation of chambers and moderate pericardial edema (Fig. 2.3). In addition, all *flnca* morphant embryos swam showed a slower swim escape response when touched lightly with a probe compared to the wild type. 86% (129/150) had a curved tail and abnormal body axis. Likewise, at 72hpf, *flncb* morphant embryos exhibited variable cardiac phenotypes. 10% (20/200) of *flncb* morphant embryos showed a severe phenotype including a collapsed heart and pericardial edema (Fig. 2.3) and 73% (146/200) had mild cardiac phenotypes as described in (Begay, Tharp et al. 2016) as well as moderate pericardial edema and an elongated atrium. On the other hand, single *flncb* morphant embryos didn't show any morphological skeletal muscle defect. In addition, the singly-depleted *flnca* or *flncb* morphant embryos died by 7-8 days post fertilization.


A
Zebrafish flnca
Zebrafish flncb
Human FLNC
Mouse FLNC

A

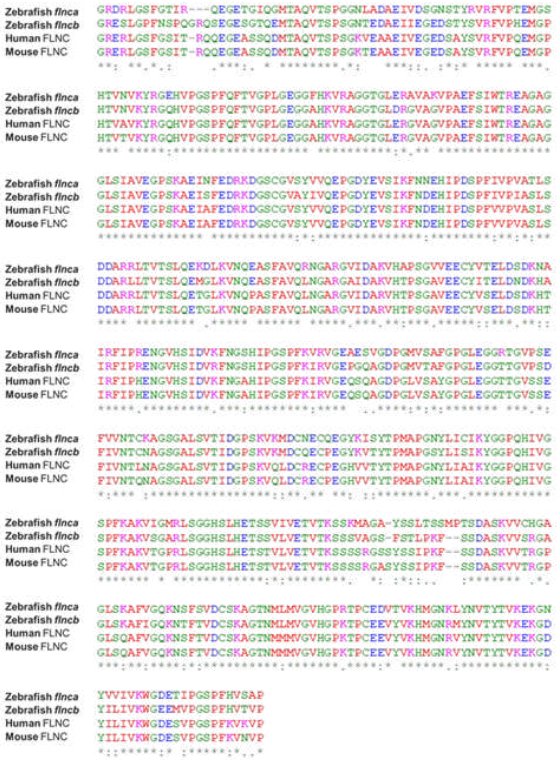

B

Percent amino acid Identity Matrix - created by Clustal2.1

	Zebrafish *flnca*	Zebrafish *flncb*	Human FLNC
Zebrafish *flncb*	81.56		
Human FLNC	79.72	83.91	
Mouse FLNC	79.84	83.66	98.31

Fig 2.2: The zebrafish *flnca* and *flncb* protein sequences are highly conserved. **(A)** ClustalW alignment of predicted FLNC sequences from *H. sapiens*, and *M.-musculus* with the predicted FLNCA and FLNCB protein sequences from the teleost species *D.rerio.* Colors indicate similar types of amino acids: green = polar, Orange = nonpolar, pink = basic, blue = acidic. **(B)** Table represents the percent identity of zebrafish FlncA and FlncB amino acids with human and mouse filamin C.

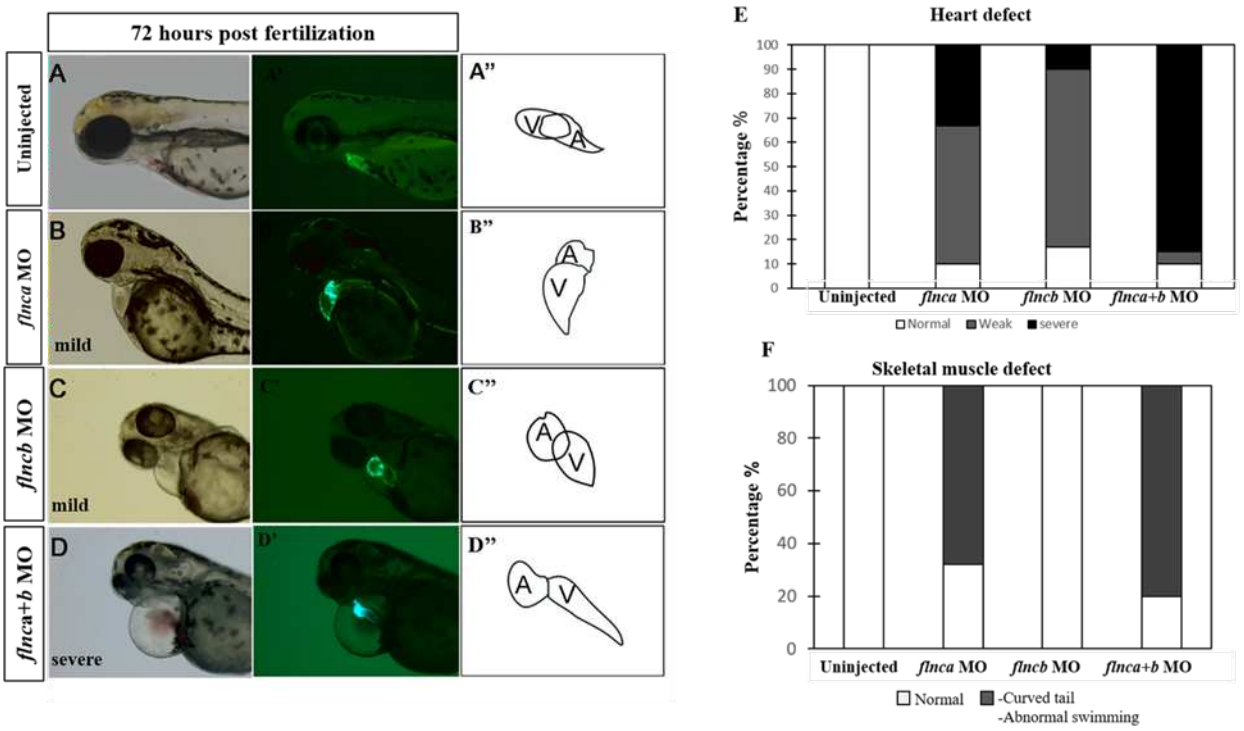

Fig. 2.3: Embryos depleted by *flnca* or *flncb* MO display cardiac abnormalities.
(A, B, C, D) Bright field imaging (lateral view) for uninjected, *flnca* MO,*flncb* MO, and *flnca+flncb* MO embryos. (A', B', C', D') Images from the transgenic line *Tg(Cmlc2: EGFP)* showing the green fluorescent protein (GFP) expressed in hearts of uninjected, *flnca* MO, *flncb* MO, and *flnca+flncb* MO embryos. (A'', B'', C'', D'') Tracings of hearts in uninjected, *flnca* MO and *flncb* MO embryos indicate morphant embryos showed dilated or collapsed atrium, and cardiac edema when compared to uninjected embryos. (E-F) The percentage of *flnca* MO, *flncb* MO, *flnca+b* MO embryos that displayed cardiac and skeletal muscle defects; n= 150, 200, 120 respectively.

Double knockdown

Since the *flnca* and *flncb* gene sequences exhibit a high degree of conservation, it was possible that the paralogs retained a degree of redundancy in function. To determine whether double MO knockdown of *flnca* and *flncb* would exhibit more severe cardiac defects (such as extreme chamber dilation, or a silent heart) than single *flnca* or *flncb* morphants, we coinjected *flnca* MO and *flncb* MO into embryos. At 72hpf, 90% (108/120) of doubly morphant embryos exhibited dilated heart chambers, weak contractility, slow circulation, and pericardial edema. Of these phenotypes, 85% (102/120) of embryos scored with severe cardiac defects whereas only 5% (6/ 120) displayed mild cardiac defects. In addition, 80% (96/120) had curved tails and were touch-sensitive (Fig.2.3). The doubly-depleted *flnca*+*flncb* morphant embryos died by 7-8 days post fertilization. The data support the conclusion that the double *flnca* and *flncb* knockdown caused a more severe cardiac phenotype. Notably, single MO knockdown produced a higher percentage of embryos showed a visible heart phenotype and a greater proportion of affected hearts exhibited the strong phenotype. Overall, these data support the hypothesis of genetic redundancy between *flnca* and *flncb*.

Looping angle

After initial phenotype scoring at 72 hpf, additional knockdown hearts were examined at an earlier stage (48 hpf). This early stage represents approximately the earliest time that phenotypes are reliably detectable, and scored for particular features affecting cardiac morphology and chamber development, as well as heart function. Cardiac looping is a progressive morphological event that converts the linear heart tube to a C-shape, and later, into a more complex shape. The "cardiac looping angle" refers to the angle formed between the atrioventricular junction [AVJ] of the heart and the anteroposterior [A/P] axis of the embryo as shown in diagram (Fig.2.4B) (Chernyavskaya, Ebert et al. 2012). We used a transgenic line that expressed GFP driven by the *cardiomyocyte light*

chain 2 (*cmlc2*) promoter, *Tg (cmlc2: EGFP*), to visualize the heart chambers. At 48hpf, the wildtype larvae zebrafish displayed normal progress in heart morphogenesis, with an average looping angle of 21.35° (Fig. 2.4C). However, the ANOVA test demonstrated that hearts of *flnca* MO, *flncb* MO, and *flnca+b* MO-injected embryos displayed significantly larger looping angles than uninjected controls, averaging 73.9°, 56.8°, and 70.1°, respectively, indicating that hearts were delayed or restricted in their transition from a linear heart tube (~26 hpf) to a normally looped heart tube.

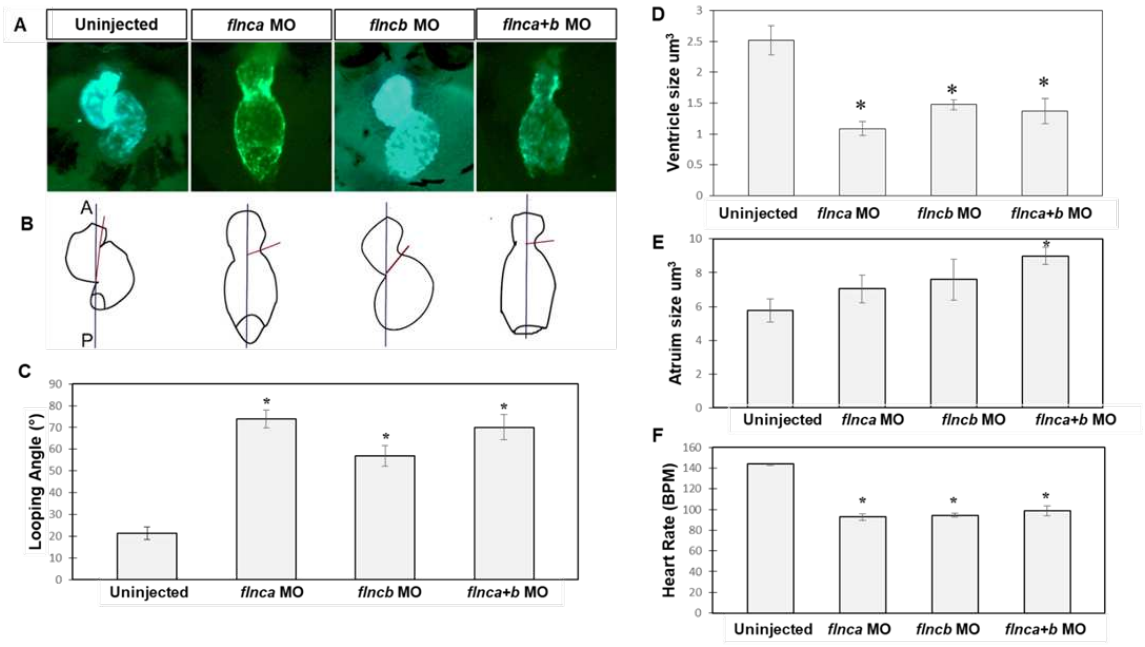

Fig. 2.4: *flnca* and *flncb* morphant embryos exhibit cardiac defects at 48hpf.
The looping angles, which is the angle formed between the atrioventricular junction [AVJ] of the heart and the anteroposterior [A/P] axis of the embryos, were determined at 48hpf for *flnca* MO and *flncb* MO embryos. **(A):** Ventral views for transgenic *Tg(Cmlc2: GFP)* embryos representing GFP-expressing hearts of uninjected and morphant embryos. **(B):** Trace of the hearts in (A), used to calculate looping angle. (**C):** looping angle average, calculated from 15 embryos per genotype. **(D):** The average size of the ventricle at 48hpf, calculated from 15 embryos per genotype. **(E)**: The average size of the atrium at 48hpf, calculated from 15 embryos per genotype. **(F):** The average heart rate in beats per minute (BPM) determined at 48hpf from 20 embryos per genotype. Significant differences between group means as determined by one-way ANOVA are reported (*P=<0.001for heart rate *P=<0.001 for looping angle *P=<0.001 for ventricle size *P= 0.133 for atrium size). (a= anterior, p= posterior of the embryos)

Chamber size

The size of the atrial and ventricular chamber was measured at 48hpf based on images of *Tg (cmlc2: EGFP*) hearts. The depletion of *flnca*, *flncb*, and *flnca+b* by MO reduced the average ventricle chamber size to 1.08um^3, 1.47um^3, and 1.36um3 respectively, compared to the average wildtype ventricular volume of 2.5um3 (Fig 2.4D). The atrium size of *flnca* and *flncb* injected embryos were measured similarly to ventricle size but no significant differences were noted. However, in double *flnca+b* knockdown zebrafish embryos, the atrium size was enlarged with an average volume of 8.99um^3 compared to the average wildtype volume of 5.77um^3 (Fig. 2.4E). Overall, the ANOVA test demonstrated that *flnca*, *flncb* and double *flnca +b* morphant embryos showed a statistically significant decrease in ventricle size, but only *flnca+ b* showed a statistically significant decrease in atrial. Taken together, the results on looping angle and chamber size provide evidence that FLNC is required for normal heart morphology and indicate that *flnca* and *flncb* function is required in both cardiac chambers.

Heart rate

Heart rate was measured here as a simple rubric to evaluate cardiac function. The heart rate was counted in beats per minute (bpm) at 53hpf embryos. Compared to wildtype embryos (144.2 bpm), the heart rates of *flnca* MO, *flncb* MO and *flnca+b* MO-injected embryos were significantly reduced, averaging 92.75 bpm, 94,6bpm, and 98.8bpm respectively (Fig. 2.4F). Generally, the ANOVA test demonstrated that *flnca*, *flncb*, and *flnca+b* morphant embryos exhibited low heart rate. Based on these results, the depletion of either *flnca* or *flncb* is sufficient to produce weak cardiac muscle contractility.

Zebrafish *flncb* is required for sarcomeric arrangement and Z-disc assembly

The sarcomere is the repeating segment between two Z-discs and delimits the basic unit of contractility (Krans 2010). Thus, the Z-disc represents the boundaries of the sarcomeres, which appear as a series of dense lines in cross sections of striated muscles. The sarcomeres are anchored to actin filaments via proteins in the Z disc (Franzini-Armstrong and Porter 1963, Luther 2009). Based on data above, heart rate and heart contractility was reduced in *flnca* and/or *flncb* MO-injected embryos. We therefore hypothesized that the contractile mechanism was compromised in these hearts, and either the formation or maintenance of sarcomeres might be abnormal. To determine how filamin C proteins affects sarcomere organization and Z-disc stability we performed a TEM study on hearts of 72hpf uninjected and *flncb* MO-injected embryos (Fig 2.5). By 72hpf, heart of uninjected embryos had clearly developed myofibrils uniformly arrange in repeated sarcomere units, linked by distinct Z-discs of uniform thickness and width (Fig 2.5A). Alternatively, hearts of *flncb* MO-injected embryos showed myofibrils not consistently aligned in successive and parallel sarcomeres (Fig 2.5B-D). Z-disc were irregular in thickness, width, and electron density and sometimes absent, In most cases, however, thick and thin filaments arranged into normal hexagonal lattices, as shown in cross-section. We conclude that the early sarcomerogenesis was initiated but did not proceed normally and the myofibril growth was diminished. Additionally, small and large vacuoles appeared in the cardiomyocytes of *flncb* MO-injected embryos in close association with the cell membrane (Fig. 2.5E), suggesting the possibility that intercellular attachments were disrupted, and that cells had begun to separate. Taken together, these data support an important role for *flncb* in development or maintenance of sarcomere structure and cardiomyocyte intercellular attachment.

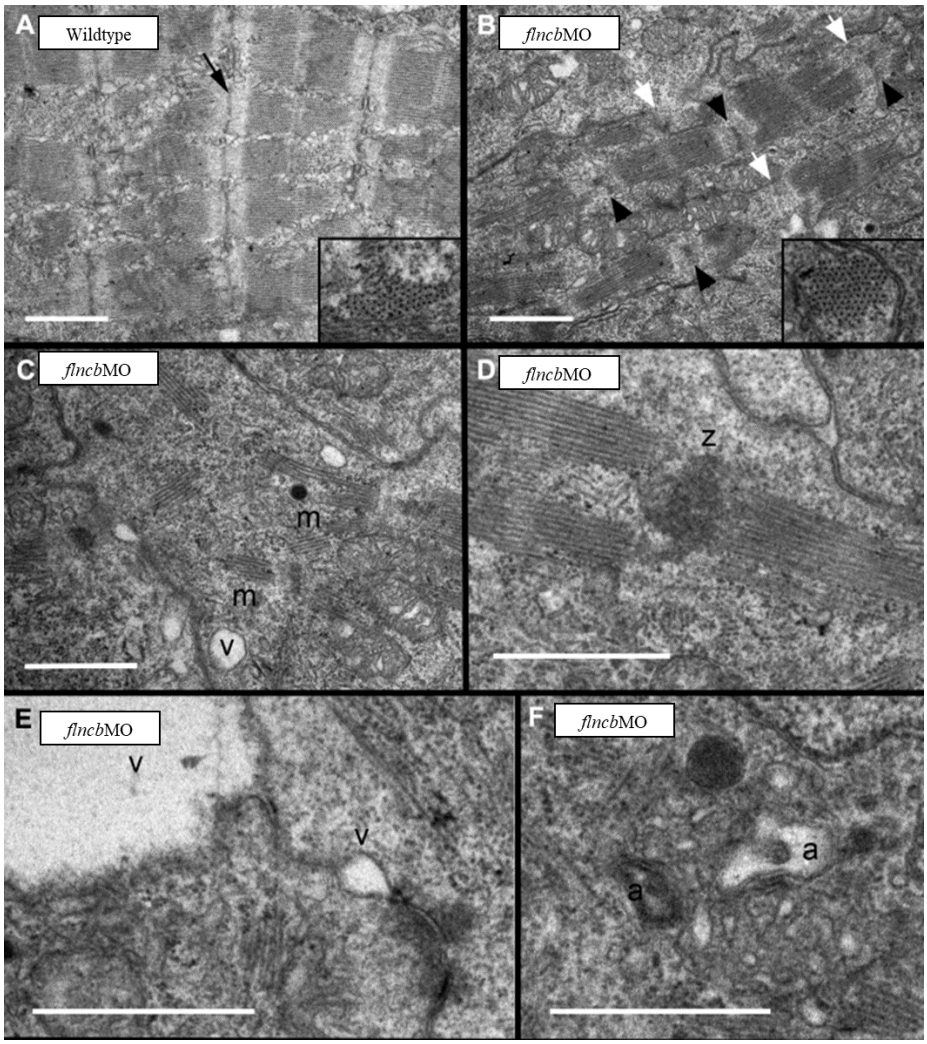

Fig. 2.5 Ultrastructural Analysis Indicates Deficiencies in Sarcomere Organization and Z-Disc Formation.

Transmission electron micrographs of zebrafish ventricle at 72 hpf indicate that **(A)** wild-type embryos had assembled several consecutive sarcomeres with clearly distinct Z-discs (black arrow), whereas *flncb*+p53 MO hearts **(B to F)** show evidence of disorganized ultrastructure. **(B)** Most Z-discs were diffusely stained, irregular in shape (black arrowheads), or seemingly absent (white arrowheads). Insets: Cross section through myofilament bundles indicated a normal primary organization of thick and thin filaments in hexagonal lattices in flncb-depleted hearts. **(C)** Sarcomere arrangement in myofibrils (m) was often nonconsecutive, with **(D)** multiple sarcomeres sometimes adjoined to a mass of Z-disc-like material (z). **(E)** Small vacuoles (v) were often present between or near the plasma membranes of adjacent cardiomyocytes. These vacuoles could be large, creating a gap between adjacent cells. **(F)** Autophagic vesicles (a) were observed.

Discussion

Our study shows that indeed, *flnca* and *flncb* genes have essential roles in cardiac morphogenesis. Zebrafish have two *flnc* paralogous genes (*flnca* and *flncb*), which are around 82% identical at the amino acid level. However, the zebrafish *flncb* paralog is most closely related to the human FLNC, as it is ~ 84% identical at the amino acid level compared to *flnca* with ~80% identity. The major findings in this study are: First, knockdown of *flnca* or *flncb* by MO causes abnormal heart development, indicating that both genes are required for normal heart formation. Second, double knockdown of *flnca+flncb* exhibits more severe phenotype than single knockdown indicating that they are partially redundant. Third, *flncb* depletion (but not flnca?) alters the ultrastructure of sarcomeres, indicating that *flncb* is required for normal sarcomere assembly or maintenance.

Human *FLNC* is expressed in both skeletal and cardiac muscle. In medaka, *flnca* is likewise expressed in skeletal and cardiac muscle (Fig 2.6), while no data has been published about medaka *flncb* expression (Fig 2.6) (Fujita, Mitsuhashi et al. 2012). In zebrafish, previously reported *in situ* hybridization experiments showed that the expression of *flncb* is restricted to skeletal muscle and cardiac muscle (Fig 2.7) (Ruparelia, Zhao et al. 2012). Prior RT-PCR data from the Garrity lab provided evidence for *flnca* expression in zebrafish cardiac muscle at 72hpf. Thus, in many species, FLNC genes are expressed at a time and place consistent with critical roles in cardiac development.

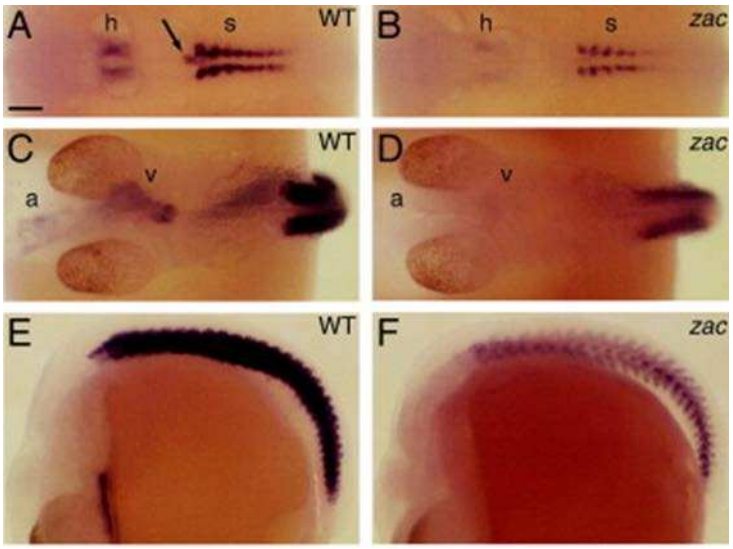

Fig 2.6 *flnc*a expression in the medaka notochord and cardiac and skeletal muscles.
(A, C, E): Wild-type and **(B, D, F):** zacro mutant embryos. **(A, B)** at stage 22 and **(C–F)** stage 27, whole-mount RNA in situ hybridization analysis of *flnc* expression. (Fujita, Mitsuhashi et al. 2012).

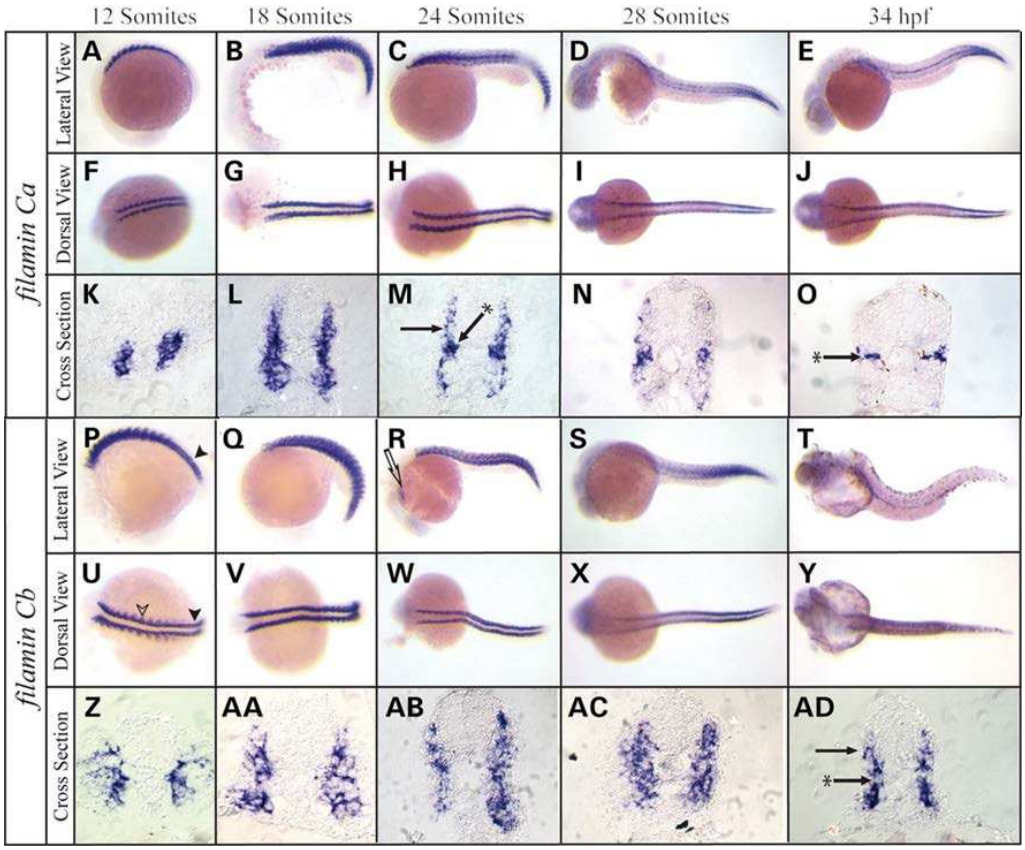

Fig 2.7. The *flnca* and *flncb* expression during zebrafish development (Ruparelia, Zhao et al. 2012).

In humans, several studies have linked variation in FLNC sequence to cardiomyopathies (Valdés-Mas, Gutiérrez-Fernández et al. 2014, Begay, Tharp et al. 2016, Begay, Graw et al. 2018, Nozari, Aghaei-Moghadam et al. 2018). This data was only correlative to cardiomyopathy and was not sufficient to show whether FLNC mutation caused cardiomyopathy. We used zebrafish as a model to better understand the mechanism by which *FLNC* mutations might cause cardiomyopathies. Knock-down of *flnca* or *flncb* via MO injection resulted in abnormal heart and skeletal muscle development. The *flnca* MO targeted the region of *flnca* encoding the translation start site, with the expectation that mRNA could be transcribed but not translated. The *flncb* MO targeted the splice site region of *flncb* (Ruparelia, Zhao et al. 2012). A deficiency of either Flnca or Flncb disrupted cardiac morphogenesis, affecting looping morphogenesis, contractility, and blood flow.

These phenotypes were somewhat stronger in *flnca* knockdown embryos than in *flncb* knockdown embryos, especially with regard to the looping angle and decrease in ventricle size. Loss of filamin C in medaka causes heart defects in the ventricular myocardium and was lethal (Fujita, Mitsuhashi et al. 2012), similar to the *flnca* MO and *flncb* MO phenotypes. In a prior report, colleagues and I found that hearts of *flncb* knockdown embryos at 48hpf exhibited an increase in retrograde flow, as well as lower cardiac output, stroke volume, and heart rate; these data were measured using a high speed camera (Fig 2.8) (Begay, Tharp et al. 2016). Cardiac defects in zebrafish *flnca* and *flncb* knockdowns share some phenotypic features with some patients who suffer from dilated cardiomyopathy, such as poor systolic function which alters the pattern of blood flow, and low cardiac output (Begay, Tharp et al. 2016). Between 7-10 dpf, all single and double *flnca* and *flncb* knockdown embryos died due to heart failure, which suggests the importance of FLNC for heart development. Mutations in essential zebrafish cardiac genes generally cause embryos to die at 7dpf, since at this age embryos are no longer able to acquire oxygen by diffusion, but require a beating heart (Pelster and Burggren 1996, Schwerte 2009).

The particular timing of *flnca* and *flncb* phenotypes, which occurred well after heart tube development, suggests that the defects affect the growth and differentiation of heart tissue, but not specification of early cardiac progenitor cells in the heart field. Our data point to a critical function of FLNC around 48 hpf and beyond, when the looping process starts in the heart tube and the atrioventricular formation proceeds.

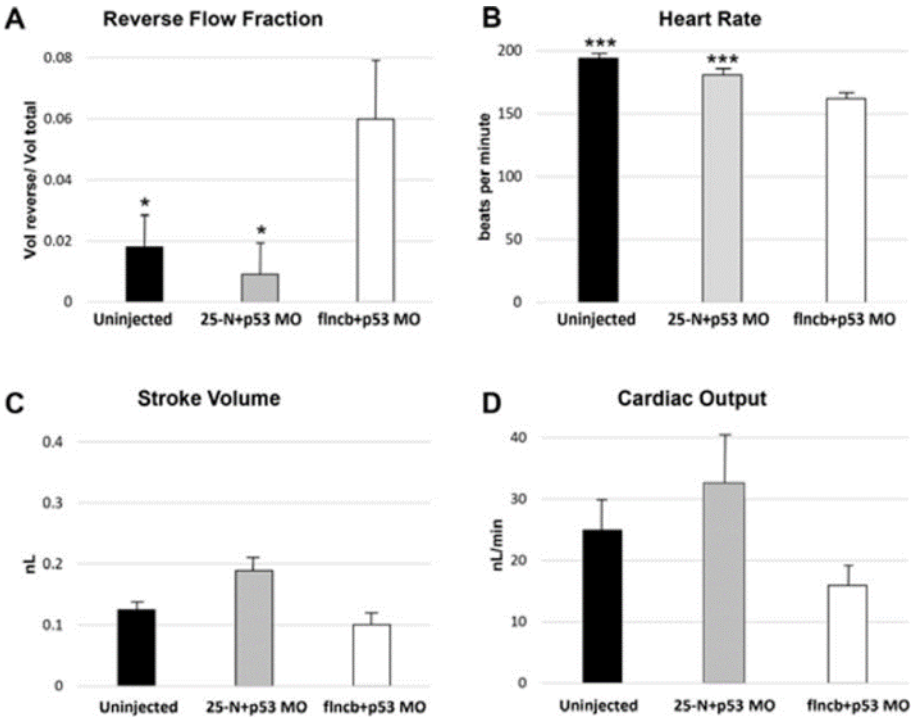

Fig. 2.8: Morphological analysis demonstrating impaired cardiac function of *flncb*+p53 MO injected zebrafish embryos. High-speed videos of hearts in 48 hours post fertilization (hpf) embryos were analyzed using custom MATLAB software (Westerfield 1993, Kimmel 1995). Embryos injected with *flnc*+p53 MO (n=21) were compared to uninjected controls (n=17) and controls injected with a scrambled morpholino (25-N+p53 MO; n=11). **(A)** Mean reverse flow fraction (+SE) for each treatment [uninjected: 0.017, 25-N+p53 MO: 0.008, *flncb*+p53 MO: 0.061. Significant differences were observed for *flncb*+p53 MO injected relative to controls by ANOVA ($P=6.1\times10^{-5}$). Follow-up Tukey tests indicated differences between *flncb*+p53 MO and uninjected embryos (P=0.023); and *flncb*+p53 MO compared to 25-N+p53 MO (P=0.007), but no difference between the controls (P=0.420). **(B)** Mean heart rate (+SE) for each treatment [uninjected: 193.5 beats per minute (bpm), 25-N+p53 MO: 181.0 bpm, *flncb*+p53 MO: 162.0 bpm (ANOVA $P=2.1\times10^{-7}$). *flncb*+p53 MO decreased the heart rate at 48 hpf compared to both uninjected embryos and 25-N+p53 MO injected embryos. (***P=0.001, ***P=0.005, respectively, by Tukey Test); heart rates of uninjected vs. 25-N+p53 MO were not different (P=0.118). (C) Mean stroke volume (+SE) for each treatment [uninjected: 0.125 nL, 25-N+p53 MO: 0.185 nL, *flncb*+p53 MO: 0.100 nL]. No significant difference was detected between treatments (Kruskal-Wallis one-way ANOVA on ranks; P=0.482). **(D)** Mean cardiac output (+SE) for each treatment [uninjected: 24.4 nL/min, 25-N+p53 MO: 32.6 nL/min, flncb+p53 MO: 16.0 nL/min]. No significant difference was detected between treatments (Kruskal-Wallis one-way ANOVA on ranks; P=0.293) (Begay, Tharp et al. 2016).

Additionally, FLNC has a known role in skeletal muscle and mutations may lead to MFM. Human FLNC mutations lead to myopathies with myofibril disorganization, and these patients suffer from myofibril myopathy and/or cardiomyopathy (Vorgerd, van der Ven et al. 2005, Kley, Hellenbroich et al. 2007, Shatunov, Olivé et al. 2009, Luan, Hong et al. 2010). *flnca* knockdown embryos exhibited a skeletal muscle phenotype at 48 hpf, with slower swimming behavior compared to *flncb* knockdown and uninjected embryos. *flncb* morphant embryos still have the functional part of the protein, *flnca* MO targets translation start site while *flncb* targets splice site, which could explain the difference between *flnca* and *flncb* knockdown phenotypes. This study was limited since these observations were qualitative, and the skeletal muscle defect will be measured by performing touch evoked assays and label the actin fibers of skeletal muscle with phalloidin to examine the actin fibers organization and formation.

Given the high degree of sequence identity between the two paralogs, we hypothesized that the protein products would show a measure of functional redundancy. If true, we would predict that double knockdown phenotypes will be more severe than single knockdown phenotypes. Double knockdown of *flnca* and *flncb* indeed caused more severe cardiac and skeletal muscle phenotypes than single knockdowns. Thus, our data provide clear support for partial functional redundancy in cardiac phenotypes. With regard to skeletal muscle, *flnca* knockdown caused stronger defects than *flncb* knockdown. In fact, no detectable defects were discerned for *flncb* knockdown embryos using a simple qualitative assay. However double knockdown produced a slightly stronger phenotype than *flnca* knockdown alone. In a prior study of skeletal muscle at the 26somite stage, Ruparelia and colleagues found that double *flnca*+*flncb* knockdown caused more severe broken skeletal muscle fibers and protein aggregation compared to single *flnca* or *flncb* morphant embryos (Ruparelia, Zhao et al. 2012).

FLNC is expressed in Z-disc which provides the boundary of the sarcomere and connects the myofibrils to the action filaments (Franzini-Armstrong and Porter 1963). We hypothesized that FLNC had a role in sarcomere assembly. The ultrastructural study of *flncb*-injected embryos revealed that the myofibrils exhibited low numbers of successive sarcomeres, or that the myofibrils were in irregular alignment with the Z-discs. This phenotype shares some features with skeletal muscle phenotypes of mice with Flnc Δ41-48 deficiency, such as dissolution of Z-discs and development of autophagic vesicles (Chevessier, Schuld et al. 2015). The autophagic vesicle is a cell component that promotes clearing of the cytosolic components such as aggregated (presumably misfolded) proteins, and damaged organelles (Glick, Barth et al. 2010). Protein aggregation is considered a hallmark of MFM (Ruparelia, Zhao et al. 2012) and also has been observed in human heart tissue (Valdés-Mas, Gutiérrez-Fernández et al. 2014). Protein aggregation was not assayed in this MO study because it is presumed to represent a condition of little to no FLNC protein production. More studies are needed to determine whether *flncb* mutant phenotypes associated with truncated alleles would show protein aggregation and/or myofibril degeneration in cardiac muscle.

The current MO data demonstrate that FLNC is required for normal heart development and indicate that the loss of *flnca* and/or *flncb* leads to cardiac dysgenesis through defects in cardiac morphology, ultrastructure, and biomechanical dynamics. However, a limitation of this study is that MO reagents may cause off target effects, and may not achieve 100% efficacy in gene knockdown, although we attempted to mitigate this potential problem by coinjecting the embryos with p53 MO to reduce off-target effects. To better interpret the efficacy of MO knockdown, a Western blot procedure using antibodies specific to FLNCa and FLNCb could be used to determine whether any translated protein is present in knockdown animals. When the MOs were originally

designed, Ruparelia and colleagues (Ruparelia, Zhao et al. 2012) performed RT-PCR to confirm that knockdown occured when using *flncb* MO, as well as using antibody against *flnca* to confirm that knockdown occured for that gene too. Flnca and Flncb antibodies are available now from several companies. Using human tissue, found that FLNC protein is decreasing in patients who is suffering from DCM (Begay, Tharp et al. 2016). More experiments need to be done to confirm the linkage between FLNC and myocardial diseases. The generation of mutant Flnca and Flncb zebrafish lines is recommended to resolve the limitations of the MO data. Moreover, zebrafish is a suitable model to determine how different alleles may affect cardiac muscle development. The next chapter presents a comparison of different *flnca* and *flncb* alleles in zebrafish heart development.

Materials and Methods:

Zebrafish husbandry

Zebrafish strains and larvae were maintained, raised, and staged using standard protocols, as previously described (Westerfield 1993, Nusslein-Volhard and Dahm 2002). All animal work was approved by the Colorado State University Animal Care and Use committee (IACUC). Fish were developed at 28℃, which is the appropriate temperature for normal development as described by (Kimmel, Ballard et al. 1995). Tricaine methane sulfonate (3-amino benzoic acidethylester, Sigma) was used to anesthetize fish at a final concentration of 0.16% in E3 embryo medium (5 mM NaCl, 0.17 mM KCl, 0.33 mM CaCl, and 0.33 mM MgSO4 in H_20).

Morpholino Injections

All antisense MO oligonucleotides were synthesized by Gene Tools (California). The translation blocking *flnca* MO (*flnca* MO: CATGGTGGGACTGCTGCTTTTATAC) was designed against the region of *flnca* encoding the translation start site. For *flncb* knockdown, the single splice *flncb* MO (*flncb* MO: GAGTTTTCTAATGGCCCTTACCTGC) was used. This MO was designed by (Ruparelia, Zhao et al. 2012). 1-4 cell embryos were injected with 90 µM *flnca* MO, 250 µM *flncb* MO, or coinjected with 80 µM *flnca* MO and 230 µM *flncb* MO together. All zebrafish embryos were coinjected with 150 µM P53MO to reduce off target defects related to ectopic upregulation of the P53 pathway, and consequent non-specific cell death. To identify well injected embryos 1:10 10x rhodamine was used with the MO mix and 0.3x Danieau's buffer was used. The only embryos that scored positive for rhodamine after gastrulation were retained for subsequent analysis.

Before injection, the embryos were transferred using a fire-polished Pasteur pipette from a petri dish to an injection plate. 1-2 cell embryos were injected with MO using a Femtojet (Eppendorf). We used injection needle from 0.75mm inner diameter borosilicate capillary tubes (World Precision Instruments, Sarasota, FL) and pulled on a Sutter P97 Flaming/Brown Micropipette puller using the following program: Heat: 715, Pull: 60, Velocity: 80, Time: 200.

Zebrafish Imaging

48 and 72 hpf live larvae were anesthetized using 5ml of 1mg per 1ml tricaine (i.e. MESAB) and placed on 2% low melt agarose for imaging. All samples were visualized and imaged using an Olympus SZX12 Fluorescent stereo-dissecting microscope and microscope-mounted Olympus U-

CMAD3 digital camera, then captured using SPOT software imaging (Diagnostic Instruments, Inc.). Adobe Photoshop software was used to resize images and adjust the white balance.

Cardiac Morphology

Transgenic line embryos *Tg(cmlc2: EGFP)* were injected with MOs to image cardiac specific fluorescence. 48hpf larvae were anesthetized using MESAB and mounted into a petri dish containing 2% low melt agarose. All samples were visualized and captured using Olympus SZX12 fluorescent stereo-microscope and Spot Insight IN1120 digital camera. We determined the looping angles by measuring the angle formed between the atrioventricular junction [AVJ] of the heart and the anteroposterior [A/P] axis of the embryos using ImageJ software. The chamber sizes, which is (volume/ (10^5)), were determined by measuring chamber volume through the following formula ((4/3) *3.14*a*b^2) (a is the middle of the anterior and posterior axes, b is the widest part of the chamber). One way ANOVA and Turkeys analysis were used to determine if there is significant different between the means of groups. Lastly, Post processing was done by using Adobe Photoshop software.

Transmission electron microscopy (TEM)

Uninjected and *flncb* morphant embryos were fixed and proceeded for TEM according to the manufacturer's instructions (Ebert, Hume et al. 2005). Samples were sectioned to Silver to pale-gold sections (60nm-90nm) by using a diamond knife on a Reichert Ultracut E ultramicrotome (Leica Microsystems AG, Wetzlar, Germany). Then, sections were mounted on formvar-coated slot grids and stained with uranyl acetate and lead citrate. Lastly, The JEOL JEM-1400 TEM (Peabody, Massachusetts) operated at 100 kV was used to observed all samples.

Chapter3: Using zebrafish as a model of filaminC cardiomyopathy

Introduction

Overview of Cardiomyopathy

Cardiomyopathies are a group of cardiac muscle diseases characterized by abnormal function and/or structure of the myocardium which cause arrhythmia, heart failure and sudden death (Hughes and McKenna 2005, Sisakian 2014). According to the European Society of Cardiology, cardiomyopathies are categorized traditionally into four types: dilated cardiomyopathy (DCM), hypertrophic cardiomyopathy (HCM), arrhythmogenic right ventricular cardiomyopathy (ARVC) and restrictive cardiomyopathy (RCM). DCM and HCM are the most common forms which have a prevalence of (1:2500, 1:500) respectively (Maron, Towbin et al. 2006, Elliott 2013). DCM is characterized by dilation of one or both ventricles combined with systolic dysfunction while HCM exhibits a thickened left ventricle with impaired relaxation (Maron, Towbin et al. 2006, Shi, Chen et al. 2018).

Inherited cardiomyopathies are the most prominent cause of morbidity and mortality in both children and adults (Hughes and McKenna 2005, Watkins, Ashrafian et al. 2011). Each category of familial cardiomyopathies, which are genetically heterogeneous, relates to several genes and encompasses many different alleles. Additionally, various mutations in the same gene can cause different disorders (Watkins, Ashrafian et al. 2011).

Sarcomere cardiomyopathies

The sarcomere is the basic contractile unit of the myofibril (Harvey and Leinwand 2011). Sarcomere cardiomyopathies are inherited disorders that cause HCM and/or DCM by disturbing the contractile function and changing the myocardial structure (Garfinkel, Seidman et al. 2018).

Familial HCM contributes to 30%-60% of HCM cases. Mutations in seven sarcomere genes link to HCM pathogenicity, including *MYH7* and *MYBPC3*, which are identified in 75% of familial HCM cases, and *MYL2, MYL3, TPM1, TNNT2, TNNI3, ACTC1* which account for less than 10% of cases (Burke, Cook et al. 2016, Garfinkel, Seidman et al. 2018). On the other hand, DCM is a common heart muscle disease caused by several factors such as acquired toxicity, metabolic insults, or sarcomere gene mutations. Inherited mutations account for 25%-60% of all DCM cases. Of note, more than 25% of DCM cases have been linked to truncation mutations in the *TTN* sarcomere gene (Vikhorev, Smoktunowicz et al. 2017). Mutation in other sarcomere genes that may lead to DCM include *MYH7, MYBPC3, TNNT2,* and *TPM1* and each gene can exhibit various alleles causing DCM (Marian, van Rooij et al. 2016, Garfinkel, Seidman et al. 2018).

Although researchers have identified more than a thousand different mutations in multiple human genes that cause hypertrophic, dilated, restrictive, and arrhythmogenic cardiomyopathies, for many other genes, insufficient data exists to determine whether mutations significantly correlate to cardiomyopathy (Dellefave and McNally 2010, Jefferies and Towbin 2010, Valdés-Mas, Gutiérrez-Fernández et al. 2014, McNally and Mestroni 2017).

Filamin C and heart myopathies

Filamin-related cardiomyopathy derives from mutations in *filamin C* (*FLNC*). Mutations in *FLNC* were first identified as a cause for familial myofibril myopathy (MFM) (Vorgerd, van der Ven et al. 2005) and distal myopathy (Williams, Reardon et al. 2005). Both myopathies are characterized by abnormal function and structure of skeletal muscle. Recently, a causative linkage between FLNC variants and cardiomyopathies has been proposed. FLNC mutations linked to HCM were first reported in 2014 with the identification of eight different mutations in FLNC in humans that developed HCM (Valdés-Mas, Gutiérrez-Fernández et al. 2014). Shortly thereafter, studies

reported the impact of FLNC variation in contributing to additional types of cardiomyopathy including DCM (Begay, Tharp et al. 2016, Reinstein, Gutierrez-Fernandez et al. 2016, Nozari, Aghaei-Moghadam et al. 2018), HCM with atrial fibrillation (Gómez, Lorca et al. 2017), and RCM (Brodehl, Ferrier et al. 2016). FLNC variant alleles that were recognized as a cause of MFM and/or cardiomyopathies appeared to be haploinsufficient, suggesting that the level of FLNC protein in the cell could be critical to normal function (Guergueltcheva, Peeters et al. 2011, Begay, Graw et al. 2018). The variability of phenotypes associated with different FLNC alleles is noteworthy and characterized at cellular level by mislocalization or aggregation of the filamin protein (Löwe, Kley et al. 2007, Valdés-Mas, Gutiérrez-Fernández et al. 2014). Protein aggregation characterized by accumulation of misfolded protein in the cytoplasm of the cell (Aguzzi and O'connor 2010). A list of all known human FLNC variant alleles that cause skeletal and cardiac myopathies is presented in (Fig 3.1) (Brodehl, Gaertner-Rommel et al. 2017, Tucker, McLellan et al. 2017). To date, the correlation between various mutations in the FLNC locus and the type of myopathies and/or cardiomyopathies represents a knowledge gap in the field which needs to be clarified. Moreover, some human FLNC alleles cause MFM and/or HCM show protein aggregations while others do not. It is still unknown if these aggregates are toxic to the cell or effect on the cell in different way.

FLNC structure and functions

In humans, the *FLNC* gene is composed of 48 exons which encode a protein of high molecular weight (291 kDa) which forms homodimers (van der Flier and Sonnenberg 2001). FLNC is one of the three filamin family members which are highly conserved at the N-terminus. The structure of FLNC consists of two calponin homology (CH) domains at N terminal (CH1, CH2) followed by a series of 24 immunoglobulin (Ig) repeats and C terminal domains (van der Flier and

Sonnenberg 2001, Nakamura, Stossel et al. 2011). In addition, FLNC interacts with numerous sarcomere proteins through its domain 20 which has been demonstrated as the interaction site for several proteins, including Xin (van der Ven, Ehler et al. 2006), KY (Beatham, Romero et al. 2004), myotilin (van der Ven, Wiesner et al. 2000) and cadherin (Guyon, Kudryashova et al. 2003, Tucker, McLellan et al. 2017). The expression of FLNC is most prevalent in the skeletal and cardiac muscle. Within the cell, FLNC localizes at the z-discs (a structure which joins sarcomeres) and intercalated discs (a structure which joins adjacent myocytes of heart muscle). In addition, FLNC protein localizes within the costamere in small amounts (Ruparelia, Zhao et al. 2012). Consistent with this subcellular distribution, FLNC plays an important role in organizing the sarcomeric components, and in linking the z-disc components and cortical actin fibers to the sarcolemma. Therefore, FLNC connects the mechanic system (sarcomere, and cytoskeleton) through the costamere to the cell surface via its interaction with membrane proteins such as integrin. In this role, FLNC functions as a scaffolding protein (Zhou, Hartwig et al. 2010, Tucker, McLellan et al. 2017).

Animal model

Recent studies have used animal models to investigate the role of FLNC in embryos that ultimate develop MFM or cardiomyopathy phenotypes. The only FLNC mouse model generated to date deletes the last eight exons (of 48 total) which would include the sarcoglycan and FATZ interacting sites and the FLNC dimerization domain (Dalkilic, Schienda et al. 2006). These mice exhibit severe skeletal muscle defects and die soon after birth. An electron microscopy study of skeletal muscle in homozygous mutant mice showed that the majority of sarcomere structure was abnormal. A small but significant number of fibers exhibited a rounded cell shape with central nuclei and disrupted z-discs accompanied by overlapping thick and thin filaments. However, in

these mice no cardiac defect was observed which suggests the possibility that of the truncated protein is still functional. Based on the absence of cardiac phenotypes, the generation of mice model is not useful to investigate the biology of cardiomyopathy (Dalkilic, Schienda et al. 2006). The medaka (*Oryzias latipes*) mutant zacro represents another model system that enables study of FLNC embryonic function. This mutant line has a mutation in *flnca,* one of two medaka paralogs of FLNC. Homozygous zacro mutants show defects in skeletal and cardiac muscle including enlargement of the cardiac chambers, along with disruption and degeneration of skeletal muscle (Fujita, Mitsuhashi et al. 2012).

The zebrafish genome encodes two FLNC paralogs, *flnca* and *flncb,* which are 70% identical to human FLNC at the amino acid level. A zebrafish mutant named *sot* (*stretched out*) in *flncb* was characterized and the mutation generates a stop codon at exon 30 (c.5056A>T; ENSDART00000026492) out of 48 exons. Homozygous *sot* mutants displayed skeletal muscle degeneration and intracellular protein aggregation which are two hallmarks of human MFM (Ruparelia, Zhao et al. 2012). Although the allele predicts the production of a truncated protein, it is not clear whether the protein is partially functional or represents the null phenotype.

In an initial approach to investigate the *flncb* null phenotype, I used morpholino injection procedures to knockdown FLNCb in zebrafish embryos. My data support a role for FLNC in modulating heart function and morphology (described in detail in chapter 2). In the previous chapter, the morpholino experiments data confirmed the functional importance of *flnca* and *flncb*, yet many outstanding questions and gaps in knowledge about FLNC still need to be addressed. First, are the *flnca* and *flncb* genes genetically redundant? If so, what does the full (double) loss of function phenotype tell us about collective FLNC function in the heart? Second, since morpholino data are consistent with a mechanism of haploinsufficiency, meaning that the absence of the

protein causes the phenotype, are there differences in phenotypes between null mutants and putative truncation mutants? Third, the truncation mutants might show more severe or different phenotypes than the full loss-of-function alleles, which would suggest that the truncation protein is toxic. Lastly, in an allelic series, does the severity of the skeletal muscle phenotypes coordinate with the severity of cardiac phenotypes? To answer these questions, we need to develop an animal model to investigate the linkage between FLNC and cardiomyopathy.

In this study, I compared four zebrafish *flnca* and *flncb* mutant lines which have nonsense mutations in different regions of the gene, either near the beginning or progressively later in the amino acid sequence. These alleles encode either complete loss of function alleles, or putative truncated proteins. I compared the morphological and functional phenotypes in homozygous mutant fish by measuring specific features including the heart rate, cardiac looping angle and chamber size. Additionally, I created doubly homozygous *flnca* and *flncb* mutant embryos to investigate whether the two genes are genetically redundant. Lastly, I characterized the skeletal muscle phenotype by performing a touch assay to determine the correlation between the mutation site and phenotype of skeletal and heart muscle.

Results

Genetic Analysis

To determine how closely *flnca* and *flncb* alleles of various species are related to humans, the amino acid sequences of *flnca* and *flncb* (GenBank Accession number: *flnca* CU302436 and *flncb* AL954190) were aligned with other vertebrate FLNC proteins (Homo sapiens, and Mus musculus). *Danio rerio flnca* and *flncb* are 2719 and 2743 amino acids in length respectively. *Danio rerio flnca* and *flncb* were highly similar to the human FLNC protein (79.7% and 83% amino acid identity). Interestingly, alignment of vertebrate filamin C amino acid sequences with zebrafish *flnca* and *flncb* identified highly conserved amino acid motif within several locations of *flnca* and *flncb* alleles. The *flnca sa24724* exon1 allele encodes a PWKKIQQNTFTRWCNEHLK conserved motif in which a nonsense mutation created a stop codon (Fig 3.1A). The *flncb* exon35 allele encodes a conserved motif, KDGTCTVSYLPTTPGDYNII, in which a nonsense mutation created a stop codon (Fig 3.1A). BLASTP analysis shows the zebrafish *flnca* motif is 100% conserved with other vertebrate FLNC proteins (Homo sapiens, and Mus musculus) (Fig. 3.1A). The *flnca sa24724* exon1 motif is predicted to encode part of the actin binding domain. The *flncb sa20217* exon35 motif is predicted to encode part of the Ig 17 domain; its' function is still unknown but this region resides near some known interaction domains (Sethi, Seppälä et al. 2014).

Comparative Analysis of Phenotypes for Various FLNC Alleles

Single mutant phenotype

To determine the role of two paralogous genes, *flnca* and *flncb,* and how different *flnca* and *flncb* alleles affect in zebrafish heart development and function, we examined the phenotypes associated with *flnca* and *flncb* mutant lines. The alleles examined include: *flnca* sa24724 (C>A mutation in

A

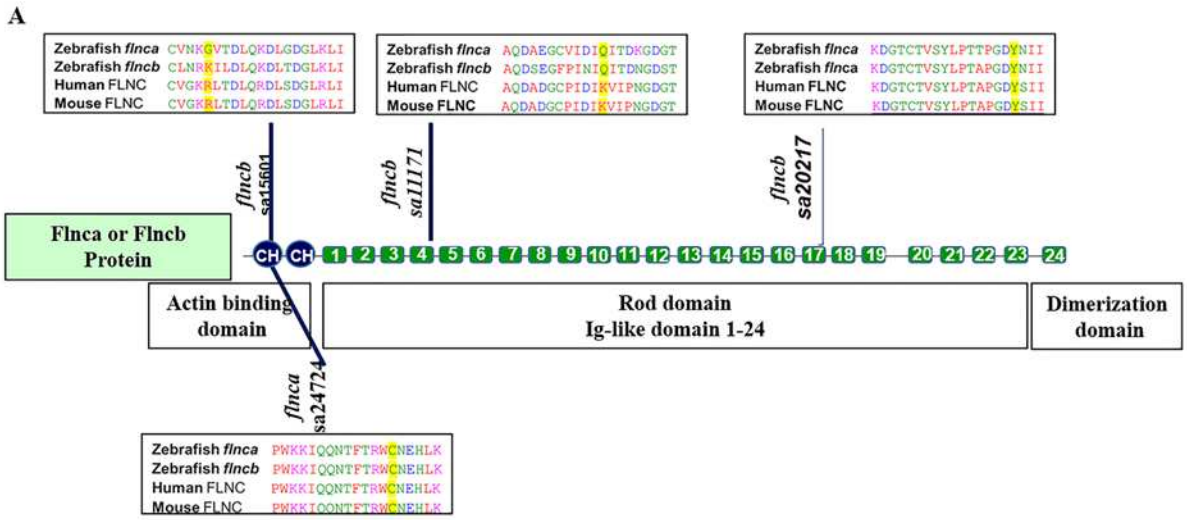

B

Gene name	Allele name	Exon affected	Amino acid affected	Type of mutation
flnca	sa24724	1 out 48 total	53 out of 2719	Nonsense
flncb	sa15601	1 out of 48 total	65 out of 2743	Nonsense
flncb	sa11171	14 out of 48 total	728 out of 2743	Nonsense
flncb	sa20217	35 out of 48 total	1936 out of 2743	Nonsense

Figure 3.1 various allelic series in *flnc* of zebrafish.
(A) Schematic representation of the domain structures of the Flnca and Flncb proteins, annotated with the positions of four mutations that affect heart and skeletal muscle development. The sequence alignment was generated using ClustalW. Amino acids in the human and mouse FLNC sequences that are homologous to the zebrafish mutation sites are highlighted in yellow. **(B)** Description of *flnca* and *flncb* alleles used in this study.

exon1), *flncb* 15601 (A>T mutation in exon1), *flncb* sa11171 (C > T mutation in exon14), and *flncb* sa20217 (C > A mutation in exon35). All alleles were obtained from the zebrafish international resource center (ZIRC) https://www.sanger.ac.uk/resources/zebrafish/zmp/. Sequencing determined that each allele has a single base-pair change which created a nonsense mutation (premature stop codon) (Fig. 3.2). For convenience, the four alleles are referred to here by the shorthand of *flnca* exon1, *flncb* exon1, *flncb* exon17, and *flncb* exon35.

After genotyping and identifying heterozygous adult fish, the heterozygous pairs of each allele were crossed. The expected genotype frequencies are 25% wildtype, 50% heterozygous and 25% homozygous. All embryos were scored for phenotypic features including: cardiac chamber deformation, cardiac looping angle, cardiac edema, cardiac arrhythmia, abnormal body axis, and touch insensitivity (an assay for swim escape behavior, which relies on skeletal muscle function). At least 500 embryos from at least 10 different heterozygous matings were scored for all lines. With reference to the scoring criteria, all progeny (wildtype, heterozygous, or homozygous) produced by crosses of heterozygous parents for *flnca* exon 1 or *flncb* exon1 exhibited normal heart and skeletal muscle morphology at 26hpf, 48hpf, and 72hpf. *flncb* exon14 embryos exhibited overtly normal heart formation and morphology, but a portion later demonstrated abnormal heart function, or swimming behavior at 48hpf (described in detail below). Moreover, 25%? of the heterozygous and homozygous embryos from these three lines survive and adults are viable and fertile (Fig 3.3A-D). More studies are needed to investigate whether all 25% homozygous embryos survive until adult stage, although substantial numbers do. This result suggests that if either *flnca* or *flncb* function is impaired by mutation, the paralogous gene provides functional redundancy. Alternatively, knockdown *flnca* or *flncb* via MO exhibited heart phenotype.

In contrast to the other alleles, at 48hpf homozygous mutant *flncb* exon 35 embryos do show morphological heart and skeletal muscle phenotypes. From a cross of two heterozygous parents, 25% of embryos are expected to display recessive phenotypes. We observed that 4.5% (10/221) of embryos exhibit heart defects including the following: 3.1% show mild edema, abnormal chambers, and faster heart rate, and 1.3% develop cardiac edema and collapsed chambers (Fig 3.3E, F). The percentage of embryos that displayed skeletal muscle defects are as follows: 7.6% (17/221) of embryos exhibited a curved tail and 20 %(45/221) showed slow swimming (Fig 3.4A). However, note that these percentages are below the expected 25%, suggesting that not all homozygous mutant *flncb* exon35 embryos displayed heart or skeletal muscle phenotypes. When heterozygous fish for this allele were crossed and the progeny were raised to adulthood and genotyped all survived fish (20 adults), no homozygous mutant adult fish were identified, which suggests that although some homozygous fish did not display overt defects, the majority did not survive to adulthood. Based on this result, the putative truncated products for *flncb* exon 14 and *flncb* exon35 show mild gain-of-function phenotypes, since in a direct comparison to a presumed null mutant (*flncb* exon1), the phenotype are more severe. Additionally, both *flncb* 14 and *flncb* exon 35(-/-) exhibit variable penetrance and expressivity because less than 25% of homozygous embryos exhibit detectable phenotypes and severity of heart phenotypes was variable among embryos. In contrast, we predicted that homozygous embryos of *flnca* exon1 or *flncb* exon1 represent examples of full loss- of-function alleles based on the site of stop codon near the 5' end of the gene. The *flnca* exon1 allele is encoding 53 amino acids while *flncb* exon1 allele is encoding 65 amino acids. We conclude that the putative null mutant for these alleles showed no overt phenotype.

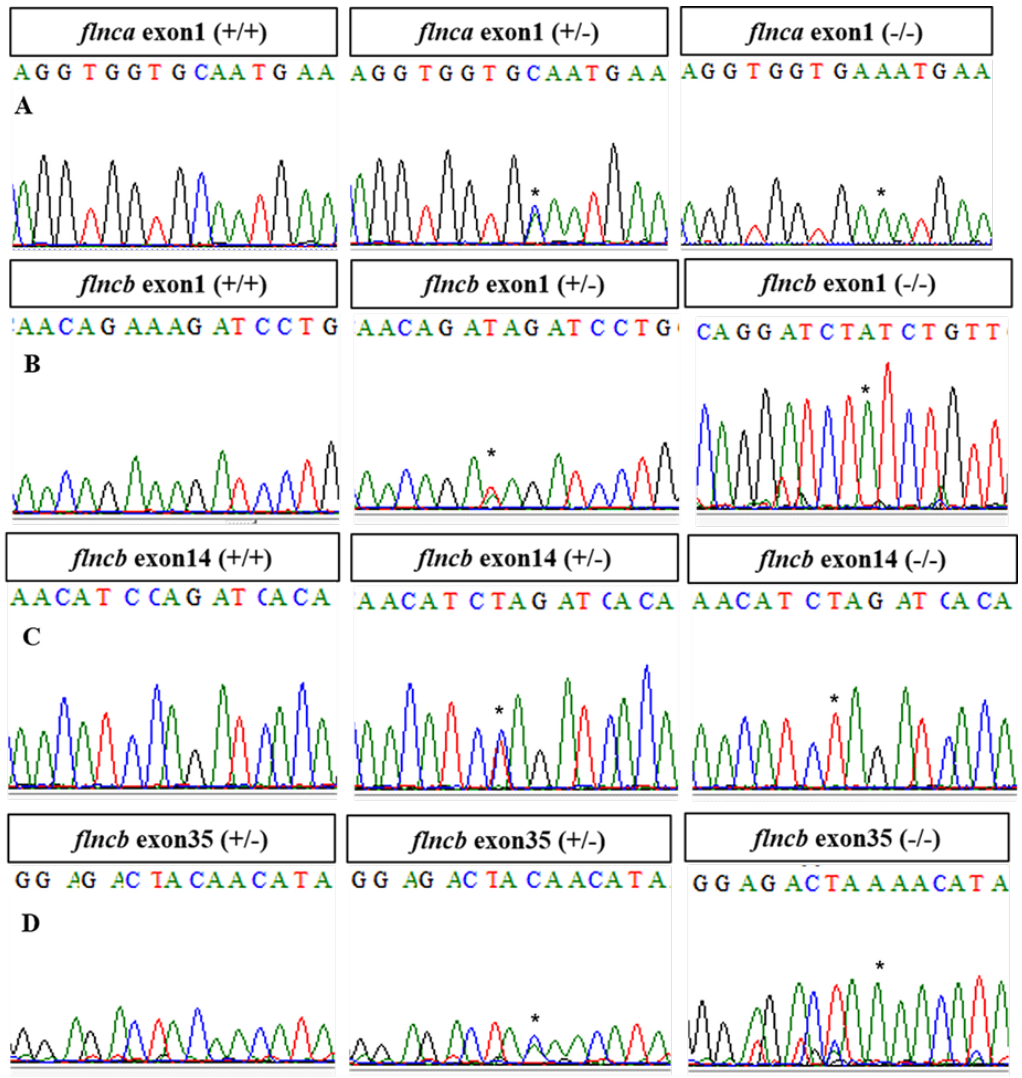

Figure 3.2 Mutations in zebrafish *flnca* and *flncb*

(A) Chromatogram showing the *flnca* sa24724 C>A mutation referred to in the text. This *flnca* exon1 heterozygous and homozygous nonsense mutation was identified in zebrafish.

(B) Chromatogram showing the *flncb* sa15601 A>T mutation referred to in the text. This *flncb* exon1 heterozygous and homozygous nonsense mutation was identified in zebrafish. A reverse complement primer was used for sequencing homozygous embryos.

(C) Chromatogram showing the *flncb* sa11171 C>T mutation referred to in the text. This *flncb* exon14 heterozygous and homozygous nonsense mutation was identified in zebrafish.

(D) Chromatogram showing the *flncb* sa20217 C>A mutation referred in the text. This *flncb* exon35 heterozygous and homozygous nonsense mutation was identified in zebrafish.

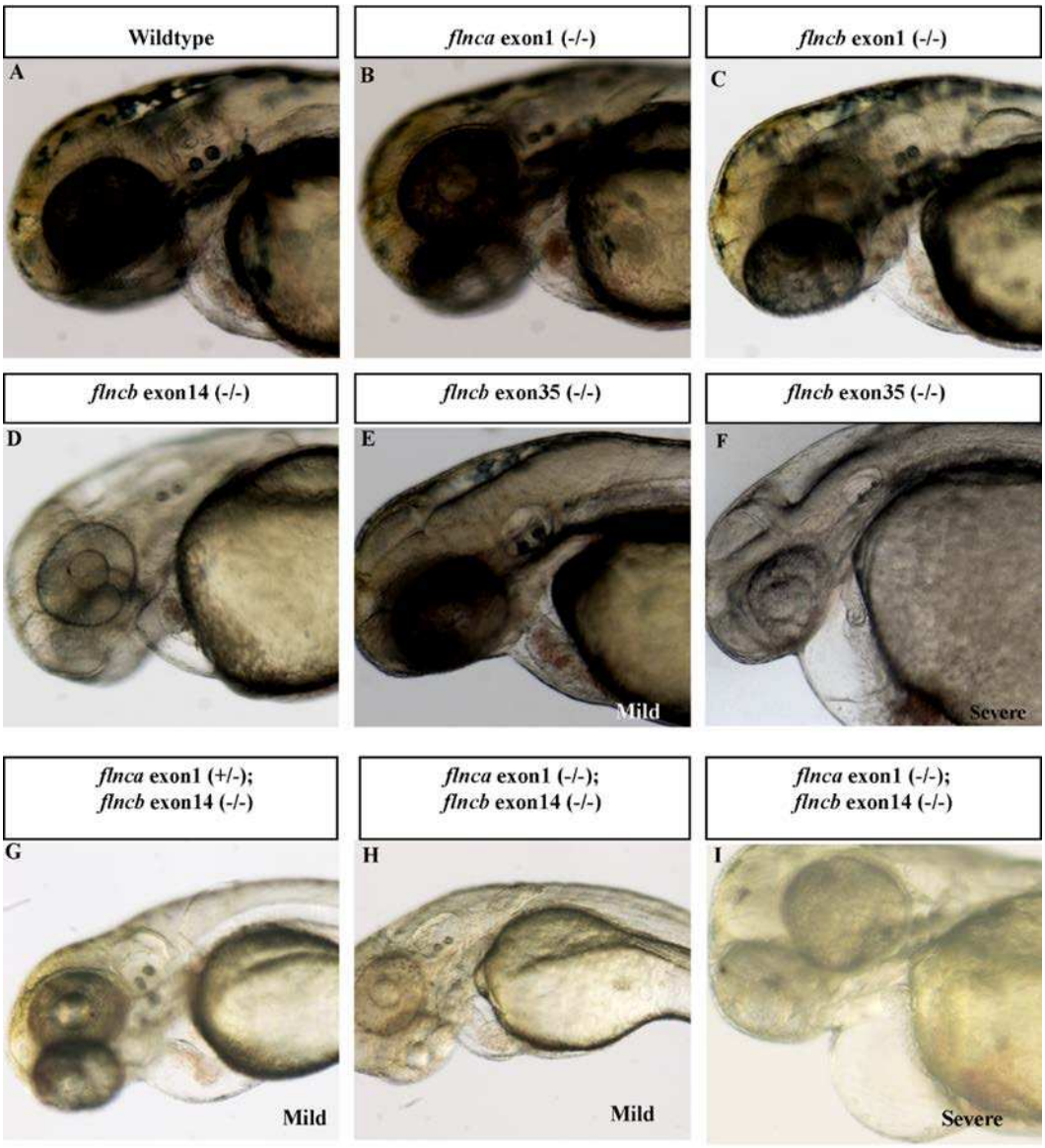

Figure 3.3 Cardiac phenotype in *flnca* and/or *flncb* mutant embryos. **(A-I)** lateral view of zebrafish embryos at 48 hpf. **(A, B, C, D)** wildtype and homozygous *flnca* exon1, *flncb* exon1, and *flncb* exon14 mutants, respectively, have normal heart morphology. **(E-F)** homozygous *flncb* exon35 mutant. **(E)** Mildly dilated chambers. **(F)** Severe pericardial edema and stretched chambers. **(G-H-I)** double *flnca* exon1+*flncb* exon14 mutant embryos **(G-H)** exhibited mild pericardial edema and dilated chambers. **(I)** Severe pericardial edema and stretched chambers.

Filamin C Redundancy

Both the *flnca* and *flncb* gene sequences exhibit a high degree of conservation, we hypothesized that the *flnca* and *flncb* paralogs retained a degree of redundancy in function. To determine the summative functions of *flnca* and *flncb* in zebrafish development, we created double mutant lines. Trans-heterozygous adults (heterozygous for *flnca* exon1 and *flncb* exon14) were intercrossed.

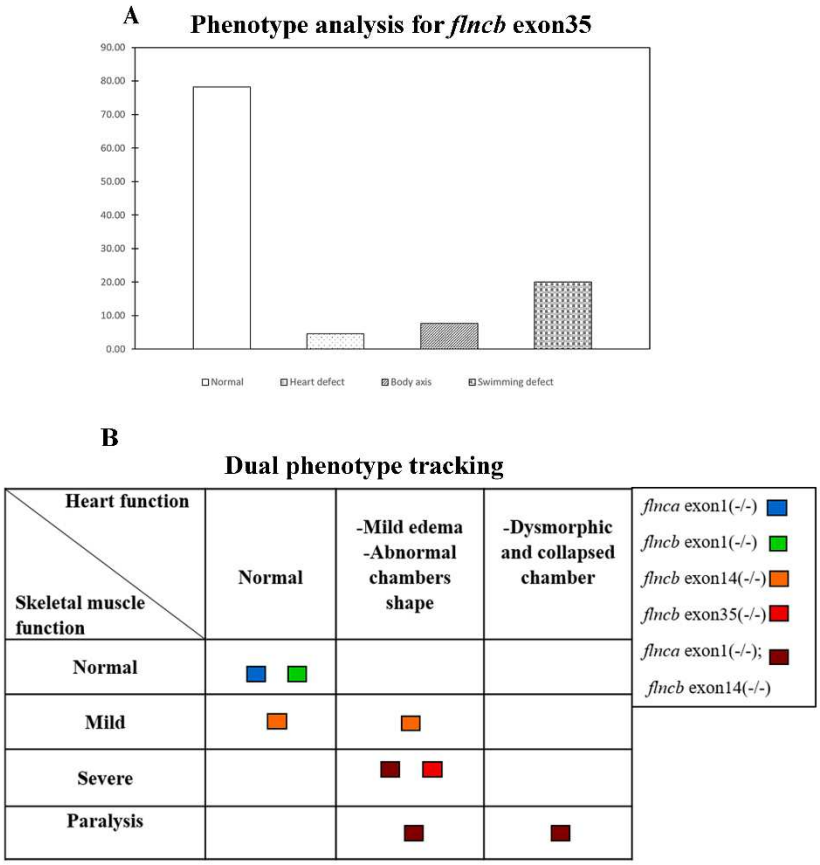

Figure 3.4 Synergistic effects of mutation of Flnc paralogs. (A) The percentage of embryos from *flncb* exon35 (+/-) parents with specific heart, body axis, and swimming phenotypes (n= 221). **(B)** The distribution of heart and skeletal muscle phenotypes amongst various *flnca* and *flncb* alleles, including *flnca* exon1 (-/-), *flncb* exon14 (-/-), *flncb* exon14 (-/-), and *flncb* exon35 (-/-) embryos.

Observed Phenotypes of Double Mutant Alleles.

The progeny of *flnca* exon1 (+/-), *flncb* exon14 (+/-) trans-heterozygote crosses were scored at 26hpf, 48 hpf, 72 hpf, and 6dpf for the following traits: cardiac chamber deformation, cardiac looping angle, cardiac edema, cardiac arrhythmia, abnormal body axis, and touch insensitivity. Upon crossing two trans-heterozygote *flnca* exon1 (+/-); *flncb* exon14 (+/-) adults, the progeny developed the following heart and skeletal muscle phenotypes by 48hpf, as summarized in (Fig 3.4A). Embryos were examined to determine whether the most severe cardiac and most severe skeletal muscle defects were coincident. As shown in (Fig 3.5b) 76.8% of progeny were overtly normal. 5.6% showed normal heart morphology but mild skeletal muscle phenotype (slow swimming) compared to wildtype. A total of 15.4% showed mild heart phenotype including mild cardiac edema, abnormal chamber shape, and abnormal heart beating. Among this group the skeletal muscle defects were variable, with 7.4% (28/371), 7.8% (29/371), and 0.2% (1/371) embryos showing mild swimming defects, severe swimming defects, or paralysis (Fig 3.3G,H) and (Fig 3.5B). A total of 1.8% displayed a severe heart phenotype characterized by dysmorphic and collapsed chambers and no circulation, and among these the skeletal muscle phenotypes were scored as 0.2% (1/371) with severe swimming defects, and 1.6% (6/371) with paralysis (Fig 3.3I) and (Fig 3.4B). Based on these results, double mutant embryos showed more severe phenotypes with regard to both heart and skeletal muscle. From a cross of trans-heterozygous parents, the predicted genetic frequency of doubly mutant embryos is 6.2% of the population. That number is close to the observed percentage of offspring with cardiac defects. However, the percentage of offspring with skeletal muscle defects is higher (~18%), suggesting that some portion of other genotypes such as *flnca* +/-; *flncb* -/- embryos also display phenotypes.

A

Expected Genotype frequencies

flncb \ *flnca*	(+/+)	(+/-)	(-/-)
(+/+)	6.2%	12.5	6.2%
(+/-)	12.5%	25%	12.5
(-/-)	6.2%	12.5	6.2%

B

Observed phenotype

Skeletal muscle function \ Heart function	Normal	- Mild edema - Abnormal shape	-Edema -Stringy
Normal	371/285 (76.8%)		
Mild (slow swimming)	371/21 (5.6%)	372/28 (7.4%)	
Severe (Very slow movement)		371/29 (7.8%)	371/1 (0.2%)
Paralysis		371/1 (0.2%)	371/6 (1.6%)

C

Dual phenotype tracking for double mutant embryos

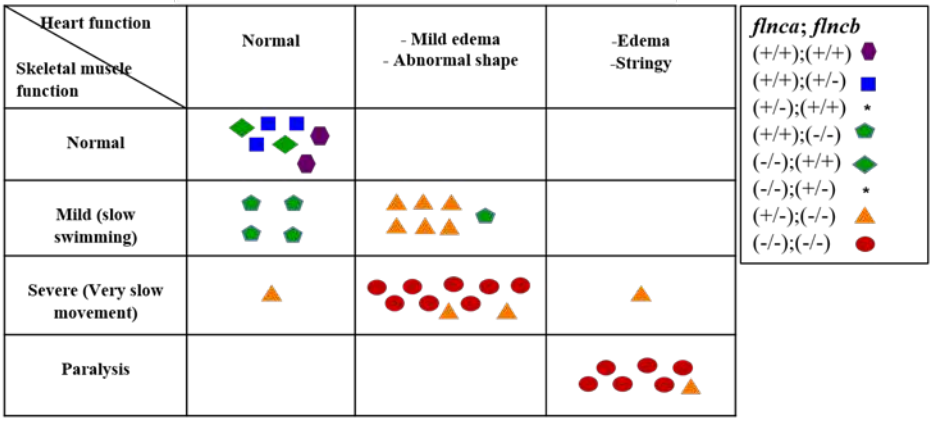

*Not found; expected phenotype is normal

Figure 3.5 Double Flnca+b mutation exhibits distinct heart and skeletal muscle morphological changes. (A) The expected genotype percentages of embryos obtained from a cross of two transheterozygous parents. **(B)** The percentage of observed phenotypes of embryos from a cross of two transheterozygous parents (*flnca* exon1 (+/-), *flncb* exon14 (+/-). The phenotypes are classified into normal, mild, or severe (skeletal muscle and/or heart) morphology (n=371). **(C)** Dual phenotype tracking of double *flnca+b* mutant embryos. Colored shapes represent numbers of sequenced embryos with particular genotypes. The top right box lists each genotype and its respective colored shape.

Genotyping Double Mutant by DNA Sequencing

To be able to match specific heart and skeletal muscle phenotypes to specific *flnc* genotypes, DNA from normal and phenotypically affected embryos was sequenced. A pool of 37 affected or non-affected embryos were picked at random from different mated trans-heterozygous pairs and digested to extract DNA for sequencing. The expected genotypes and the percentage of phenotypes that will be produced from mated trans-heterozygous *flnca* exon1 (+/-); *flncb* exon 14 (+/-) adults are listed in table (3.5A). As in the initial phenotyping experiments, heart and skeletal muscle phenotype were sub-classified by severity. The heart phenotypes consisted with three classes including: 1) normal heart morphology 2) mild heart phenotype (mild edema, and abnormal chamber shape), and 3) severe heart phenotype (dysmorphic and collapsed chambers, and no circulation) (Fig 3.5C). The skeletal muscle phenotypes were segregated to 4 classes based on the response to a light touch: 1) normal swimming and morphology, 2) mild (slow swimming), 3) severe (very slow movement), and 4) paralysis (no movement) (Fig 3.5C).

The phenotypic data was correlated with specific genotypes as follows (Fig 3.5C):

First, embryos with normal heart and skeletal muscle responses were sequenced and found to include the following genotypes: [*flnca* exon1 (+/+); *flncb* exon14 (+/+)], [*flnca* exon1 (+/+); *flncb* exon14 (+/-)], and [*flnca* exon1(-/-); *flncb* exon14 (+/+)]. However [*flnca* exon1 (+/-); *flncb* exon14 (+/+)], [*flnca* exon1 (-/-); *flncb* exon 14(+/-)], and [*flnca* exon1 (+/-); *flncb* exon 14(+/-)] were not identified among the limited pool of embryo DNAs sequenced but we expect these would be present in this group and could be identified in larger pools of sequenced embryos. Out of four possible *flnca* or *b* alleles in a cell, these genotypes all include either zero, one or two mutant alleles.

Second, among embryos with normal heart morphology, but mild skeletal muscle defects, a single genotype was observed: *flnca* exon1 (+/+); *flncb* exon14 (-/-). Thus, *flncb* loss of function is slightly more severe than *flnca* loss of function.

Third, a variety of phenotypes (heart: normal, mild or severe, and muscle: mild, severe or paralyzed) included embryos of the genotype *flnca* exon1 (+/-); *flncb* exon 14(-/-). We did not identify *flnca* exon1 (-/-); *flncb* exon 14 (+/-) in the pool. Embryos of the *flnca* exon1 (+/-); *flncb* exon 14 (-/-) genotype thus displayed both variable penetrance and variable expressivity. Overall, this data indicates that three mutant *flnc* alleles is generally more detrimental than two mutant alleles, at least in the case of full loss of *flncb*.

Fourth, the most severe phenotypic classes (heart: mild or severe, muscle: severe or paralyzed) included a majority of *flnca* exon1 (-/-); *flncb* exon 14(-/-) embryos as well as some *flnca* exon1 (+/-); *flncb* exon 14(-/-) embryos. This finding confirms the hypothesis of a degree of functional redundancy between the two paralogs.

flncb MO Knockdown and Single flnca Mutant Allele Phenotype

As an alternative approach to achieve complete *flnc* depletion, homozygous singly mutant *flnca* embryos were injected with *flncb* MO. Since only a limited number of embryos can be sequenced, we tested the consistency of the above observations by morpholino injections into single mutant lines. A previously validated morpholino targeting *flncb* pre-mRNA splicing (*flncb* SD-MO) was used (Ruparelia, Zhao et al. 2012). *flncb* MO was injected at a low dose that does not exhibit heart or skeletal muscle phenotype when injected. This approach allows comparison of frequency of *flnca* phenotypes with or without *flnb* MO knockdown, to determine whether *flncb* MO knockdown exerts synergistic effects. Zebrafish embryos produced by crossing adult *flnca* (+/-)

exon1 pairs were injected with *flncb* MO. Additionally, the embryos were co-injected with P53MO to reduce off-target defects, which occur due to ectopic upregulation of the P53 pathway (Campbell, Sinagra et al. 2013). By 48hpf, 12.9% of wildtype embryos injected with *flncb* MO exhibited mild cardiac edema (Fig 3.6A). However, among offspring of the *flnca* exon1 heterozygous parents (all injected with *flncb* MO) 46.5% displayed collapsed cambers, pericardial edema, and low circulation, and 18.6% showed dilated chambers and pericardial edema (Fig 3.6B, C). Thus, double knockdown embryos displayed a more substantial percentage of phenotypes than did *flncb* MO-only or *flnca* (-/-) embyros. The previous double mutant data suggested that genotypes lacking three or four copies would show stronger phenotypes. Of the expected 25% *flnca*(-/-), *flncb*-MO, and 50% *flnca*(+/-), *flncb*-MO embryos, the observed 46 percent with phenotypes support the conclusion that stronger phenotypes are produced when 3 or 4 of the paralogous gene copies do not encode protein product.

Stress Experiment

Another approach to test the collective function of *flnc* in the heart is to examine a sensitized condition. The homozygous single *flnca,* and *flncb* embryos showed at most minor phenotypes. If the embryos were subjected to temperature stress, they may exhibit a more obvious phenotype, or a greater percentage may show a detectable phenotype. At 48hpf wildtype, or *flnca* exon1 (-/-) or *flncb*(-/-) exon14 embryos with normal phenotype were subjected heat stress by incubating them at 37℃ for 24hrs. Indeed, by 72hpf, 15% of *flnca* exon1 (-/-) embryos subjected to heat stress showed an abnormal heart, compared to only 5% of wildtype embryos (Fig 3.7A, B, D). Remarkably, a much more robust effect occurred for heat-stressed *flncb* exon14 (-/-) embryos:

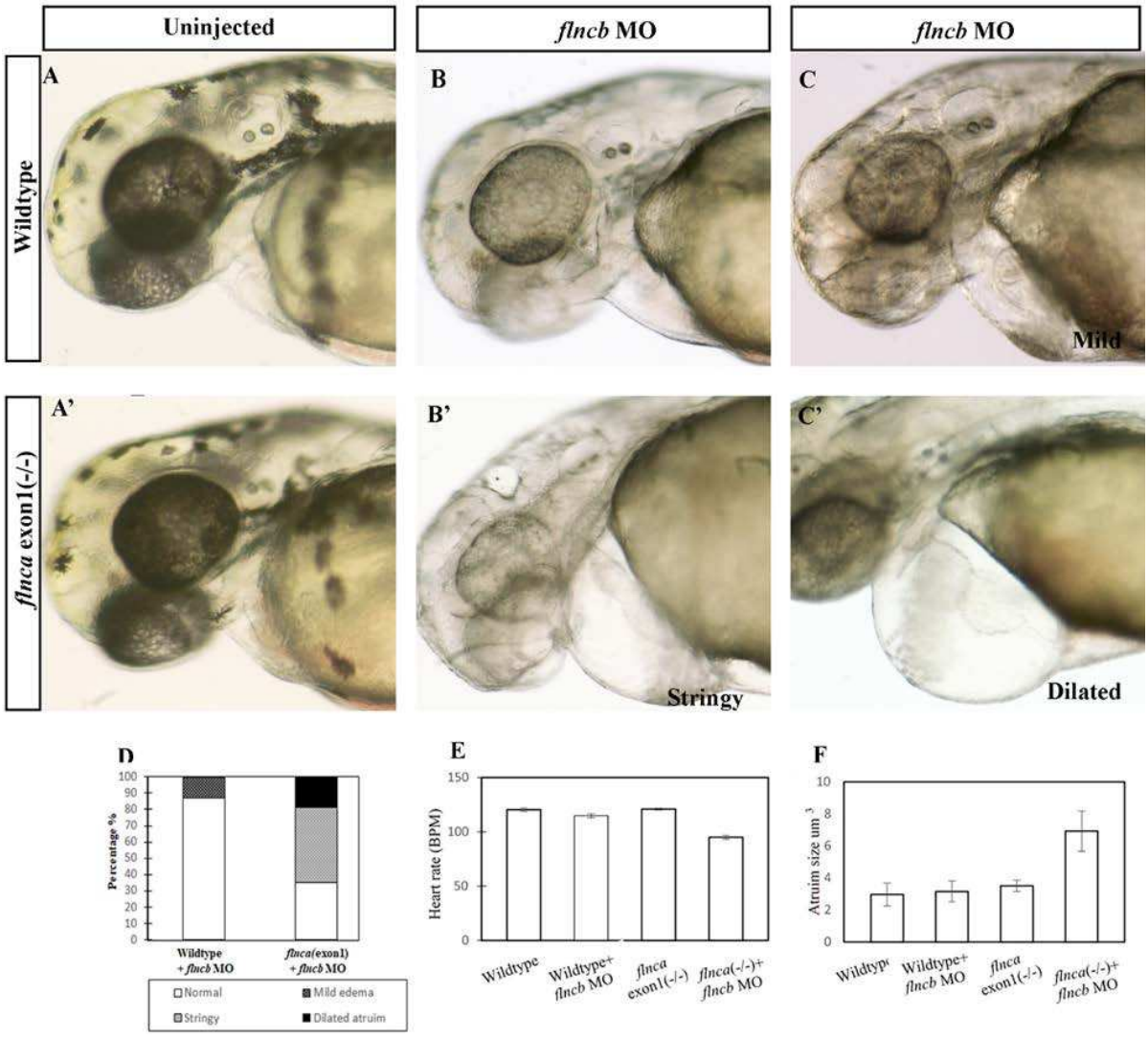

Figure 3.6 Double *flncb* MO, *flnca* exon1 (-/-) embryo have cardiac morphology defects. (A) Lateral bright field images of the heart area of wildtype and flnca exon1 (-/-) **embryos** injected with a low dose of *flncb* MO. **(A, A', B)** Normal heart chambers. **(C)** Mild pericardial edema. **(B')** Pericardial edema and stretched chambers. **(C')** Pericardial edema and dilated heart chambers. **(D)** The percentage of embryos who have either normal, dilated, stringy chambers, or mild edema (n=31, n= 86, respectively). **(E)** The average heart rate (BPM) for 53hpf embryos. Relative to controls, the *flnca* mutants injected with *flncb* MO had statistically different BPM as compared to wildtype embryos (ANOVA*P =1.059E-15, n=12). **(F)** Atrium size was determined by measuring chamber volume with the formula ((4/3) *3.14*a*b^2), where a is the middle of the anterior and posterior axes and b is the widest part of the chamber. Relative to controls, the *flnca* mutants injected with *flncb* MO displayed a significant increase in atrium size (ANOVA *P = 0.0057, n=7 for wildtype, 10 for wildtype +*flncb*MO, 11 for *flnca* exon1 (-/-) = 11, and 12 for *flnca* exon1+ *flncb* MO).

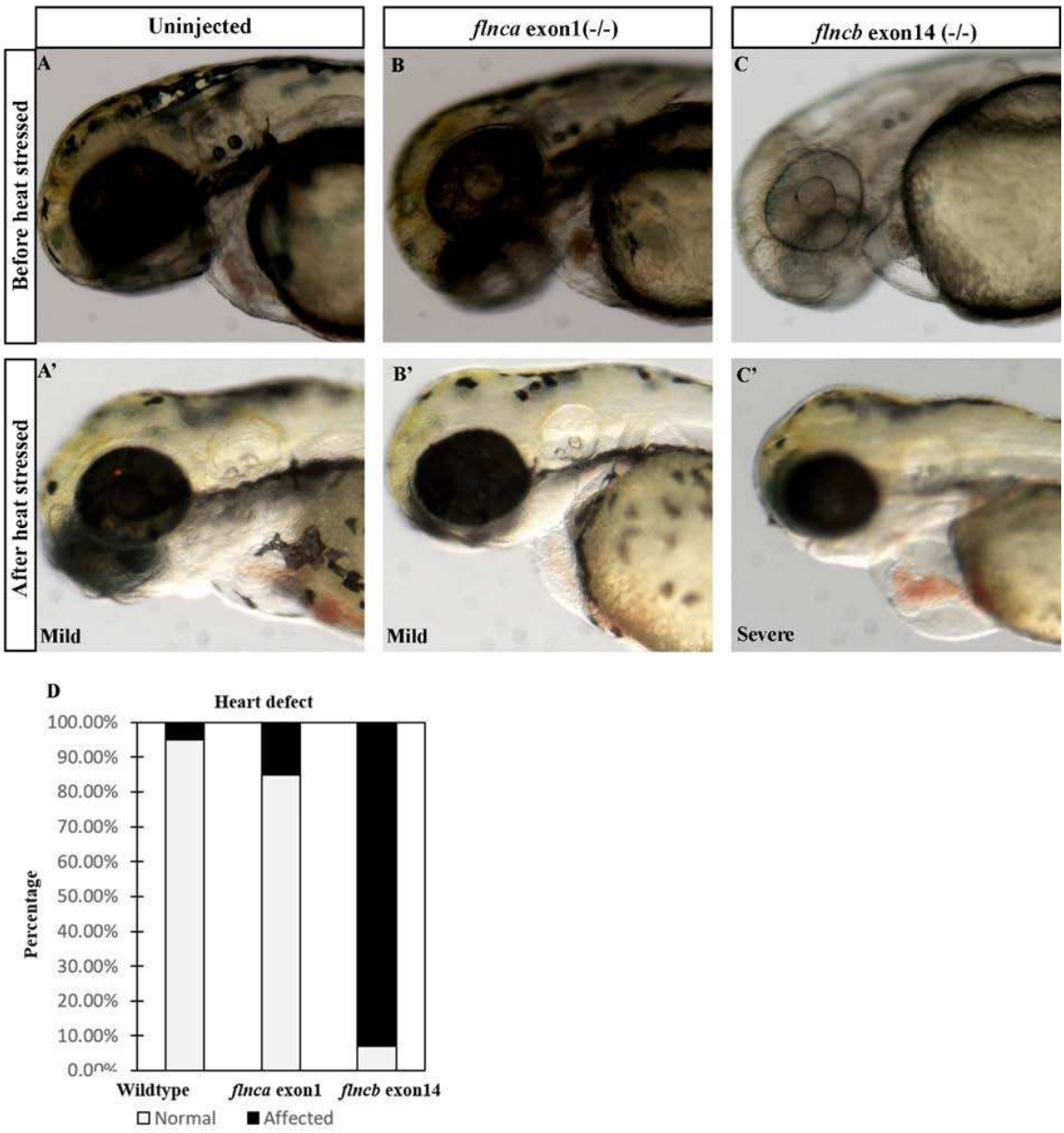

Figure 3.7 Exposed homozygous *flncb* exon14 to heat stress leads to cardiac morphology change. (A) Lateral brightfield images of the heart area of wildtype, *flnca* exon1 (-/-), and *flncb* exon14 (-/-) embryos, which were exposed to high temperature (37C) for 24 hours at 48hpf. **(A, B, C)** Cardiac morphology before incubation at high temperature was normal. **(A', B')** wildtype and *flnca* exon1 (-/-) embryos exhibited mild pericardial edema after exposed to high temperature. **(C')** *flncb* exon14 (-/-) embryos exposed to high temperature had severe pericardial edema and dilated chambers. **(D)** The percentage of embryos that have normal or mutant phenotypes (n=60 for wildtype, 66 for *flnca* exon1 (-/-), and 70 for *flncb* exon14).

92.8% showed mild heart phenotype including pericardial edema, mild dysmorphic chamber, and weak contractility (Fig 3.7C, D).

In the next series of experiments, the phenotypes of affected embryos were examined in more detail in order to understand the functional and morphological impact of loss of one or both *flnc* genes. The 48 hpf time point represents approximately the earliest time that phenotypes are reliably detectable; therefore, all quantitative morplogical analyses were carried out around this stage. Heart rate was measured slightly later (53 hpf) to assess function when cardiac looping was more mature.

Looping Angle

Cardiac looping is a progressive morphological event that converts the linear heart tube to a S-shape, and later, a more complex shape (Bakkers 2011). The cardiac looping angle refers to the angle formed between the atrioventricular junction [AVJ] of the heart and the anteroposterior [A/P] axis of the embryo as shown in diagram (Fig 3.8F) (Chernyavskaya, Ebert et al. 2012, Parrie, Renfrew et al. 2013).

Genetic lines

At 48hpf, the wildtype larvae zebrafish displayed normal progress in heart morphogenesis, with an average looping angle of 9.9°C (Fig 3.8A, G). However, hearts of double *flnca+b* (mild, stringy) displayed significantly larger looping angles, with average of 23.2°, and 52.7° respectively of *P*= 0.001, and 0.04 (Fig 3.8D-G). In addition, the more affected double *flnca*+b (stringy) looping angle significantly different compare to *flnca* exon1 (-/-), *flncb* exon 14, and double *flnc a+b* (mild) with *P*=0.006, 0.008, 0.03 respectively (Fig 3.8B-G). Since the variable data were not normally distributed, the Kruskal-Wallis One Way Analysis of Variance on Ranks was used to test whether

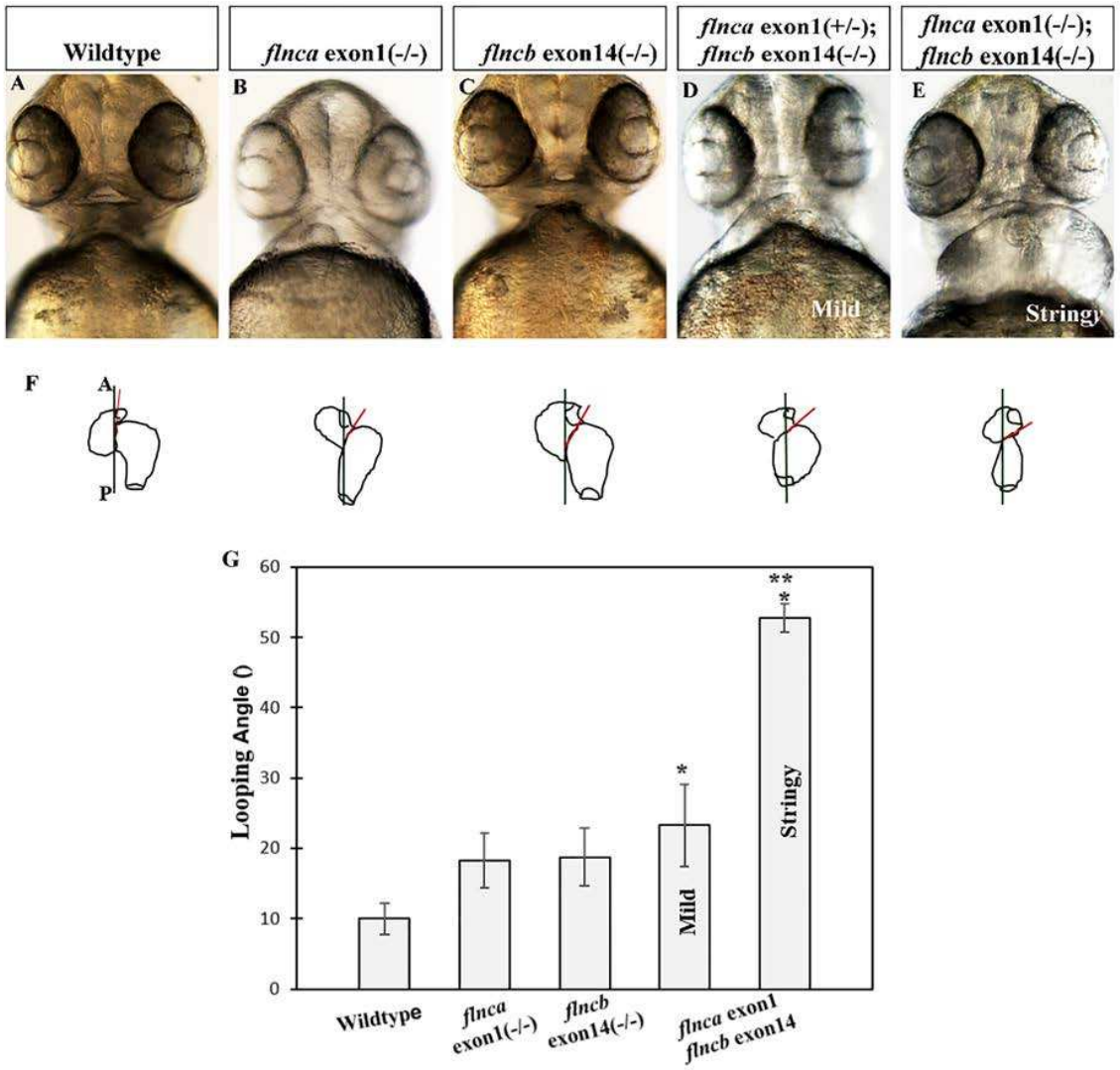

Figure 3.8 *flnca* and *flncb* mutants displayed cardiac defects at an early stage of development. The cardiac looping angle refers to the angle formed between the atrioventricular junction [AVJ] of the heart and the anteroposterior [A/P] axis of the embryo; this looping angle was calculated for *flnca* and/or *flncb* mutants. **(A-E)** Ventral view for wildtype, *flnca,* and *flncb* mutant embryos at 53hpf. **(D)** Mild cardiac phenotype of the double *flnca+b* mutant embryo**. (E)** Stringy cardiac chambers of the double *flnca+b* mutant embryo. **(F)** Diagram represents how the looping angle was measured for the hearts in **(A-E)**. **(G)** Relative to the wildtype, double *flnca+b* embryos (mild, stringy) exhibited significantly larger looping angles. (Tukey **P*=0.04 and <0.001, respectively.) The stringy double *flnca+b* hearts also showed significant differences as compared to the single *flnca*, *flncb*, and *double flnca+b* (mild) hearts. (Tukey ***P*=0.006, 0.008, 0.03, respectively.) n ≥10 (a= anterior, defined here as 0°, p = posterior of the embryo).

significant difference between the groups. Additionally, all Pairwise Multiple Comparison Procedures (Tukey Test) was used to test the differences within the groups.

Heat Stressed Experiment

Additionally, at 72 hpf, the heat stressed wildtype larvae zebrafish exhibited also normal progress in looping, with an average looping angle of 4.2°. In contrast, singly mutant *flncb* (-/-) exon 14 embryos averaged 18.5°, which indicates a significant difference in morphology (P=0.004, n=12) (Fig 3.9E). This result suggests that *flncb* exon 14 (-/-) hearts were delayed or restricted in their transition from a linear heart tube (~26 hpf) to a normally looped heart tube. The T-test analysis was used the test the differences between groups.

Heart Rate

To evaluate cardiac function, heart rate was counted in beats per minute (bpm) in 53hpf embryos.

Genetic lines

Wildtype embryos demonstrated an average heart rate of 123.4 bpm. Relative to the wildtype, the average heart rates of single mutant *flnca* exon 1(-/-), single mutant *flncb* exon14(-/-), double mutant *flnca* exon1; *flncb* exon14 (mild) averaged 127bpm, 113bpm, 126bpm, and 113 bpm respectively; these values were not significantly different from wildtype, n=12. In contrast, relative to wildtype the heart rates of stringy embryos were significantly reduced with an average 106.5bpm with P<0.05, n=12 (Fig 3.9A). Next, we found the heart rate of the single mutant *flncb* exon14 (-/-) was significantly reduced compared to *flnca* exon1 (-/-) and *flncb* exon35 (-/-) with P<0.05, n=12 (Fig3.9F). Since the variable data not normally distributed, the Kruskal-Wallis One Way Analysis of Variance on Ranks was used to test whether significant difference between the

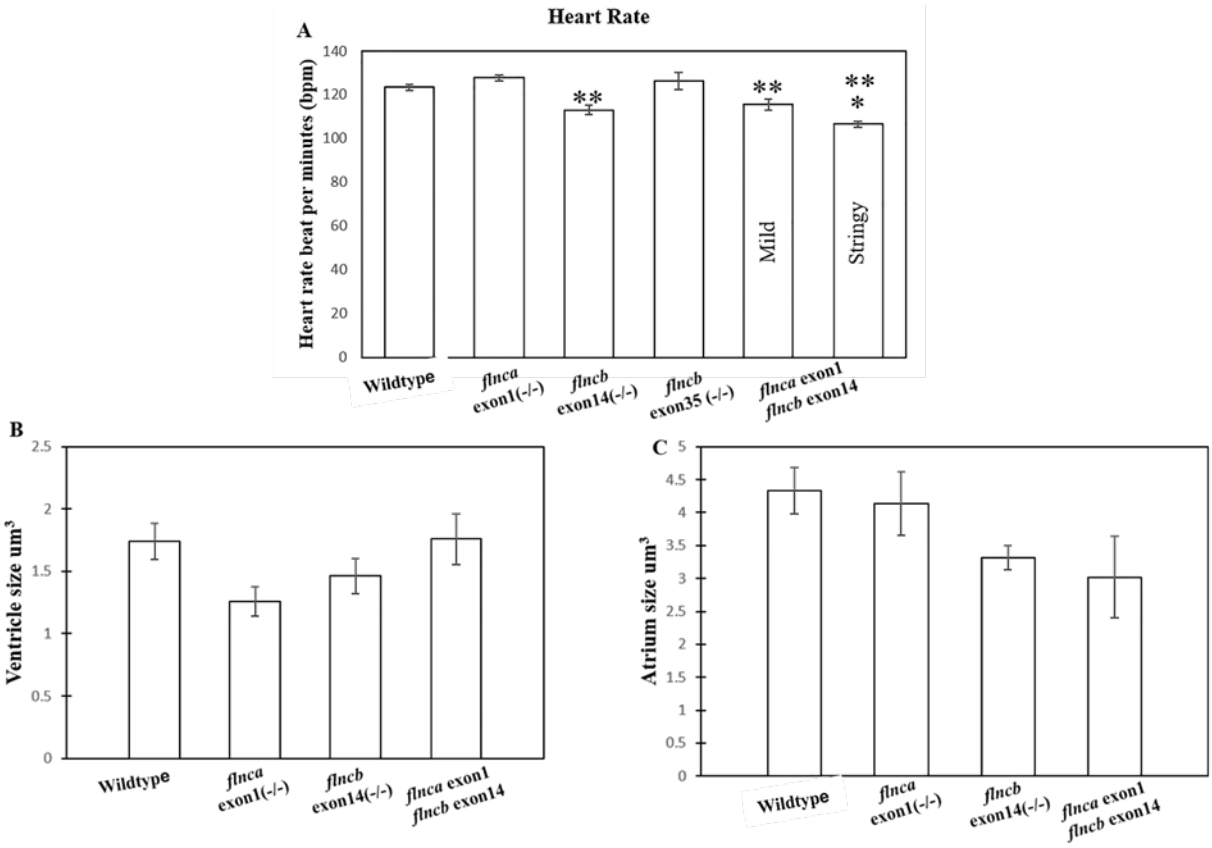

Figure 3.9 *flnca* and *flncb* displayed cardiac defect at an early stage of development. (A) Heart rate was measured in beats per minutes (BPM) at 53hpf. Relative to the wildtype, the double *flnca+b* mutants (stringy) had a significant decrease in heart rate. (Tukey **P*<0.05, n=12). The heart rate of the single *flncb* exon14 (-/-) and double *flnca* +b (mild) were significantly reduced. Tukey ***P*<0.05 in a comparison to *flnca* exon1 (-/-) and *flncb* exon35 (-/-) (n=12). **(B-C)** The ventricle and atrium size was determined by measuring chamber volume with the formula ((4/3) *3.14*a*b^2), where a is the middle of the anterior and posterior axis and b is the widest part of the chamber. **(B)**Relative to the wildtype, the average ventricle size of *flnca* exon1 (-/-), *flncb* exon14, and double *flnca+b*(mild) mutants were not significantly different (ANOVA *P*=0.38, n≥10). **(C)** There were no significant differences between wildtype, *flnca*, *flncb,* and mild double *flnca+b* mutant embryos (ANOVA*P*=0.67, n≥9).

groups. Additionally, all Pairwise Multiple Comparison Procedures (Tukey Test) was used to test the differences within the groups.

Heat Stressed Experiment

By 72hpf, compared to the wildtype embryos (162.5bpm), *flncb* exon14 (-/-) embryos showed a statistically lower heart rate (132.5 bpm) with *P*= 0.00001, n=12. (Fig 3.9D). When the embryos were exposed to heat stressed for 24 hours, the heart rates of *flncb* exon14 (-/-) likewise showed a significantly 101.8 bpm compared to 112.4 in wildtype with *P*=0.00007, n=12 (Fig 3.9E). The magnitude of the difference at 72hpf was thus 30bpm while after heat stress the difference was 11bpm. T-test analysis was used the test the differences between groups.

Morpholino Experiment

The average heart rates of wildtype, wildtype injected with low dose of *flncb* MO, and *flnca* exon1 (-/-) embryos did not significantly differ (120.4bpm, 114.8bpm, and 121bpm) (Fig 3.6E). In contrast, the heart rates of *flnca* exon1 (-/-) embryos injected with low dose of *flncb* MO were significantly reduced, averaging 95 bpm with *P* =1.059E-15, n=12(Fig 3.6E). The P value was calculated by using ANOVA and Tukey tests.

Based on above result, single *flncb* exon14 (-/-), double *flnca* exon1; *flncb* exon 14 mutant, and double *flnca* exon1 (-/-) injected with *flncb* MO embryos exhibited weak contractility. Moreover, single *flncb* exon 35 (-/-) showed higher in heart rate compared to wildtype suggesting disrupting in contractility mechanism and each *flncb* alleles variant have specific cardiac function.

Chamber Size

Genetic lines

The size of the atrial and ventricular chambers were measured at 48hpf. The average ventricle size for wildtype was 1.7 um^3 while single homozygous *flnca* exon1 and *flncb* exon14, and mild double

mutant exhibited average chamber sizes of 1.2 um^3, 1.4 um^3, and 1.7 um^3 respectively, which are not significantly different from controls (Fig 3.9B-C). The size of the atrium in wildtype, single and double *flnca* exon1; *flncb* exon14 mutant embryos was similarly measured. The average atrium size of wildtype was 4.3 while *flnca*, *flncb*, and double *flnca+b* were 4.1um^3, 4.1um^3, 3.3um^3, and 3um^3. Although a trend exists towards smaller size in the double mutants, no significant differences were noted (P=0.6, n≥9) (Fig 3.9J).

Morpholino Experiment

The size of the atrium was not significantly different in wildtype, single *flnca* (-/-) exon1, and wildtype injected with *flncb* MO, which averaged 2.9um^3, 3.4um^3 and 3.1um^3 respectively. In contrast, *flnca* exon1 mutant embryos injected with *flncb* MO developed a dilated atrial chamber, with significantly increased average size of 6.9um^3 (P= 0.0057, n≥7) (Fig 3.6F).

Heat Stressed Experiment

By 72hpf, the ventricle size in wildtype heat stressed hearts was 1.8um^3 while *flncb* exon14 (-/-) heat stressed hearts exhibited significant larger values, with an average 2.4um^3 (P= 0.01. n≥10). Relative to the atrium size for wildtype (2.6um^3), *flncb* exon14 (-/-) atria were significantly larger with an average 2.8um^3 (P= 0.004, n≥7) (Fig3.10 F, G).

Taken together, the results on looping angle and chamber size provide evidence that Flnc is required for normal heart morphology and indicates that *flnca* and *flncb* function is required in both cardiac chambers. Moreover, both *flnca* and *flncb* are redundant because double mutant embryos displayed more severe phenotypes than single mutants did.

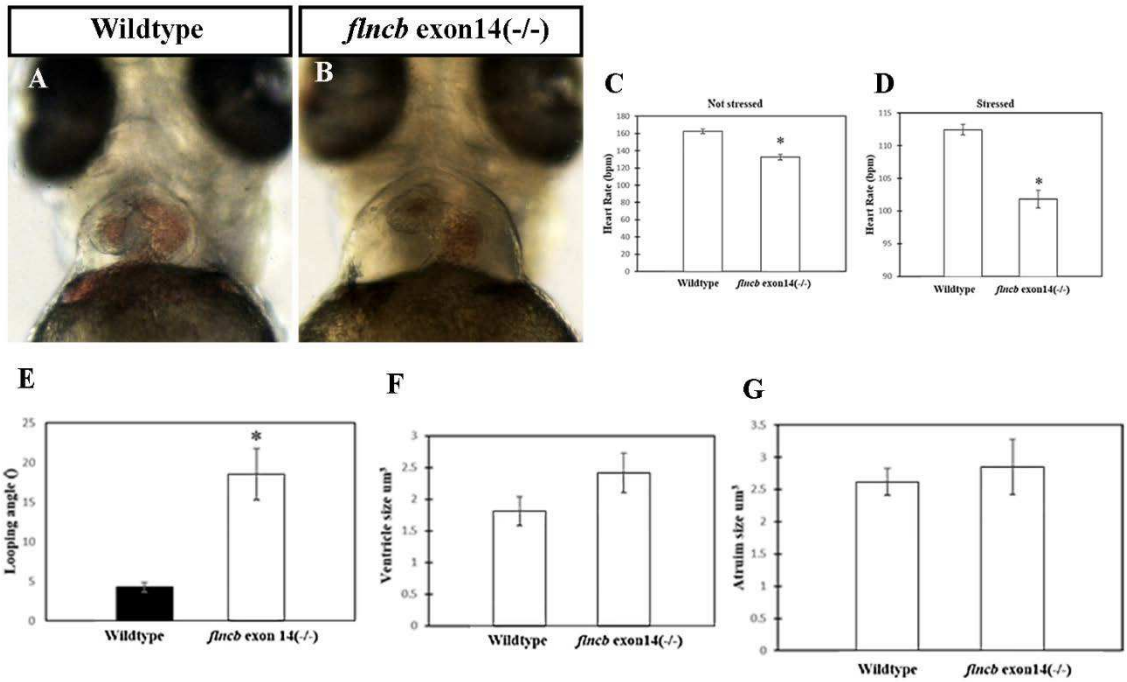

Figure 3.10 Exposure of homozygous *flncb* exon14 mutants to heat stress led to altered cardiac morphology. (A-B) Ventral view of wildtype and *flncb* heat-stressed embryos at 72hpf. **(B) The** *flncb* mutants have pericardial edema and looping defects after exposure to high temperature. **(C)** Heart rate was measured as beats per minute (BPM) for both wildtype embryos and *flncb* mutants at 72hpf. *flncb* mutant embryos had a significant decrease in heart rate (T-test**P*= 0.00001, n=12). **(D)** Heart rate of *flncb* mutants significantly decreased as compared to the wildtype after heat stress (T-test **P*= 0.00007, n=12). **(E)** Looping angle was measured as described in Figure 3.8. Relative to heat-stressed wildtype embryos, heat-stressed *flncb* mutant embryos had a significant difference in heart rate (T-test **P*= 0.0004, n=12). **(F-G)** Ventricle and atrium size were measured as described in the previous figure. The ventricles and atria of heat-stressed *flncb* mutant embryos were significantly larger than those of heat-stressed wildtype embryos (T-test **P*= 0.01 for ventricle, **P*= 0.004 for atrium, n ≥7).

Touch-evoked escape assay

To determine whether *flnca* and, or *flncb* genes have a role in touch response and skeletal muscle development, we performed a previously described touch-evoked escape assay. The speed of swimming (cm/sec) were calculated for embryos stimulated by a light touch on their dorsal side with a metal probe (Smith, Beggs et al. 2013). At 48hpf, wildtype and *flnca* exon1 (-/-) embryos responded normally to touch stimulation with immediate movement, with average speeds of 2.6 cm/s and 2.5 cm/s, respectively. However, the single *flncb* exon14 (-/-) mutant embryos, single *flncb* exon 35 (-/-) mutant embryos, and double *flnca* exon 1; *flncb* exon14 mutant embryos exhibited highly compromised abilities to respond in the touch assay. Their average escape speed were 0.34 cm/s, 0.19 cm/s, and 0.03 cm/s respectively (P=0.0001, n=≥15)(Fig 3.11B). One Way ANOVA and Tukey tests was used to calculate P value. This data indicates that *flncb* exon14 (-/-), and *flncb* exon35 (-/-) alleles have affect in skeletal muscle development. As in heart assays, double *flnca+b* mutant embryos had stronger skeletal muscle defects than did singly mutant embyors, which supports redundant functions in muscle as well as heart.

Comparative analysis of *flnca* and *flncb* expression on various Flnc alleles.

In zebrafish, previously reported in situ hybridization experiments showed that by 34hpf the expression of *flnca* and *flncb* was present in skeletal muscle (Fig 2.7) (Ruparelia, Zhao et al. 2012). To determine whether *flnca* and *flncb* are expressed in the cardiac muscle, we performed RT-PCR using RNA extracted from 72hpf hearts (Fig 3.12A). Assays using gene-specific primers confirmed that *flnca* and *flncb* are both expressed in zebrafish cardiac muscle at 72hpf. This expression is consistent with the noted effects of *flnca* and *flncb* depletion on zebrafish heart development.

Phenotypic analysis of Flnc alleles demonstrated that the doubly mutant *flnca* exon1; *flncb* exon14 embryos exhibited more severe phenotypes than single mutants. To determine if depletion of one paralog spurred compensatory transcriptional up-regulation of the alternate paralog, we compared the *flnca* and *flncb* expression levels in singly mutant *flnca* exon1 (-/-) hearts and singly mutant *flncb* exon14 (-/-) hearts at 72hpf using RT-PCR technique. We found no difference in expression levels of the *ef1a* control gene in hearts of the wildtype, *flnca* exon 1 (-/-), or *flncb* exon 14(-/-) mutant embryos at 72hpf by ANOVA analysis indicating persistent high levels of mRNA quantity and integrity in all reactions. In the homozygous *flnca* exon1 hearts, the expression of *flnca* mRNA was significantly decreased. Also, the expression of the paralog *flncb* was significantly increased (Fig 3.12b,c). In the homozygous *flncb* exon14 hearts, the expression level of *flncb* mRNA significantly decreased, while expression of the paralog *flnca* mRNA increased but not significant (Fig 3.12D,E). These results support a compensatory upregulation of the *flncb* and *flnca* paralogs in *flnca* and *flncb* mutant embryonic hearts, respectively.

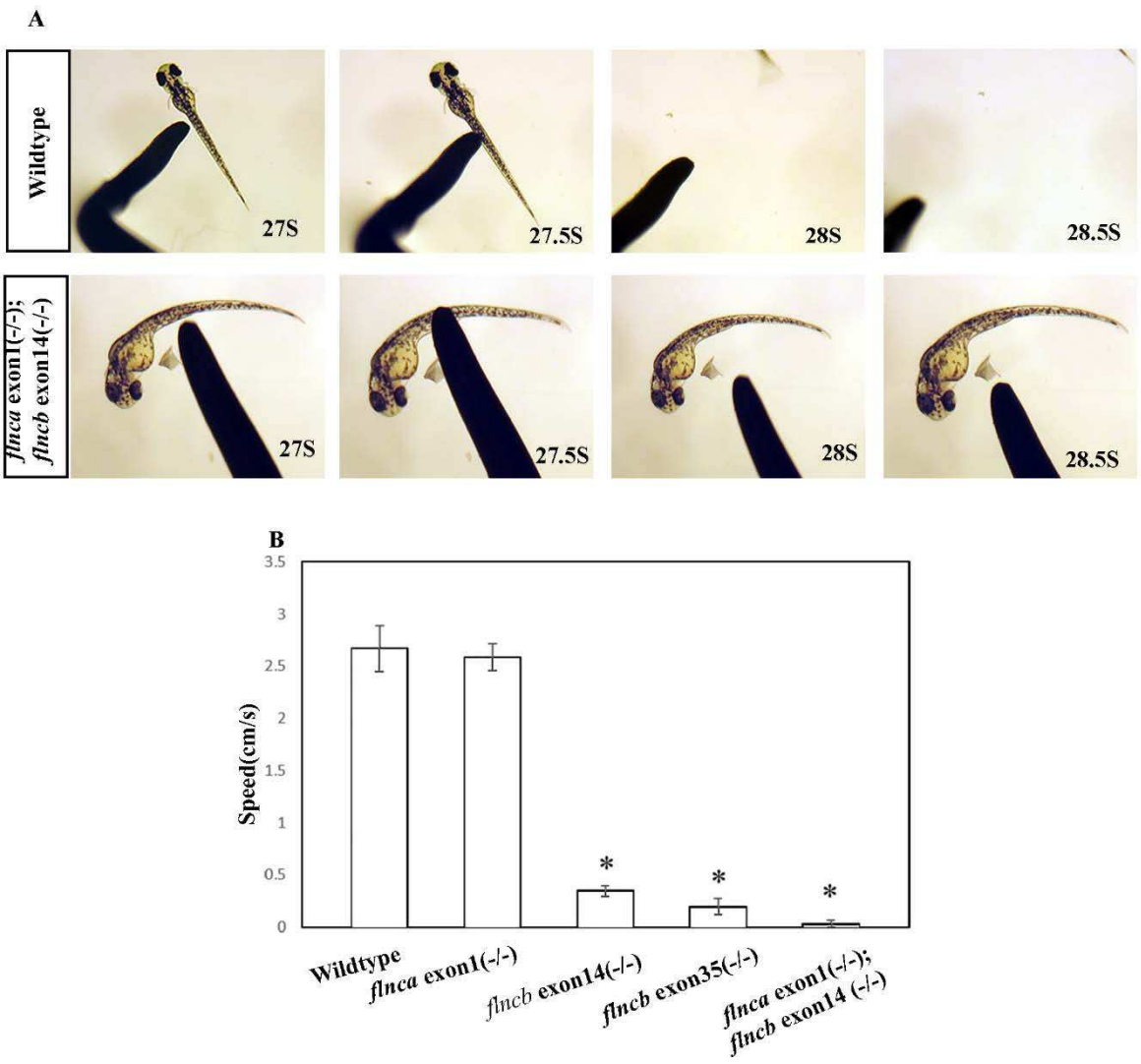

Figure 3.11 *flnca* and/or *flncb* mutants displayed swimming defects at 48hpf. (A, B) Time-lapse images illustrating zebrafish embryo responses to a light touch applied to the tail at 48hpf. **(A)** Wildtype embryo, **(B)** double *flnca+b* mutant embryo**. (D)** Average swimming speeds for *flncb* exon14, *flncb* exon35, and double *flnca+b* embryos were significantly different as compared to both the wildtype and *flnca* exon1 embryos ANOVA **P*=0.0001, $n \geq 15$).

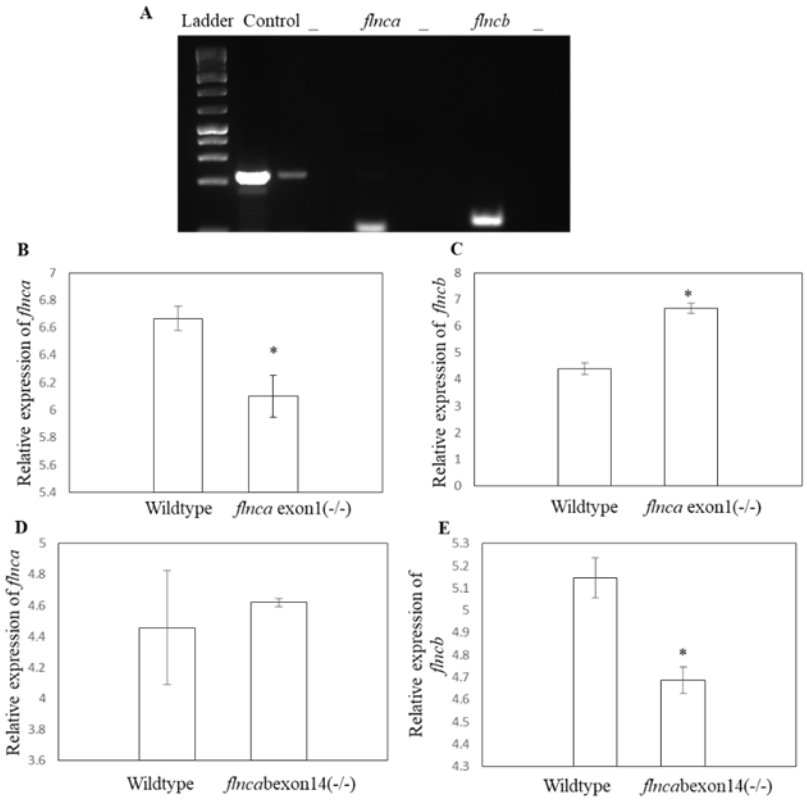

Figure 3.12 Mutations in *flnca* or *flncb* affect their expression in the zebrafish heart. (A) RT-PCR of dissected hearts at 72hpf. Elongation factor 1α (ef1α) was used as a positive control. **(B,C)** Comparison of *flnca* and *flncb* expression patterns in *flnca* exon1(-/-) hearts and **(D,E)** *flncb* exon14 (-/-) heart. *flnca* and *flncb* expression increased when these genes were mutated**.**

Discussion

In this chapter, we examined the function of the Flnca and Flncb proteins in zebrafish heart development. We used a series of *flnc* alleles, including *flnca* exon1 and *flncb* exon1 alleles, which contain nonsense mutations encoding stop codons in their actin binding domains, as well as *flncb* exon14 and 35 alleles, which contain nonsense mutations encoding stop codons in the immunoglobulin (Ig) repeat regions (Fig 3.1a,b). No clear heart phenotype was observed in putative null homozygous *flnca* exon1 or *flncb* exon1 embryos at 24, 48, or 72 hpf (Fig 3.3, 4C)). Putative truncation mutants *flncb* exon14 and *flncb* exon35 mutants did show cardiac phenotypes but in a smaller fraction of embryos less than the genotype would predict gain of function. The majority of single *flnca* exon1 and *flncb* exon14 embryos survived until the adult stage. This result suggests two possibilities: 1) *flnca* and *flncb* function redundantly, as they are highly conserved at the amino acid level; thus, a single functional *flnc* gene is sufficient for development [and/or,] 2) Although the mutant embryos survived until the adult stage, the mutation of a single *flnc* gene may affect the heart and skeletal muscle in the period between the larval and adult stages, an idea supported by the low percentage of mutant embryos that survived. More data are needed to confirm this finding.

Double *flnca* exon1 and *flncb* exon14 mutant embryos exhibited heart and skeletal muscle phenotypes characterized by abnormal or stringy heart tubes and swimming defects (Fig 3.5b). The conclusion from this result is that the *flnca* and *flncb* paralogs have redundant functions in zebrafish heart and skeletal muscle development. Several lines of evidence support this conclusion. First, the single *flnca* exon1 and *flncb* exon14 mutants had minor heart morphology phenotypes, such as an increased looping angle and decreased heart rate. Contrastingly, the double homozygote embryos displayed stronger heart morphology phenotypes, including the increased looping angle

and decreased heart rate phenotypes, as well as decreased ventricle size, poor contractility and mild or severe cardiac edema. In addition, the cardiac phenotype of the double mutant embryos was lethal. Second, knock-down of either *flnca* or *flncb* via morpholino injection resulted in defects in cardiac morphogenesis, which eventually affected looping morphogenesis, contractility, chamber size, and heart rate. However, double *flnca* and *flncb* morphant embryos exhibited more severe phenotypes, in greater percentages, than single knock-down embryos (Fig 2. 4; this result was discussed in chapter 2). Third, homozygous *flnca* exon1 embryos injected with a low dose of *flncb* morpholino showed a cardiac phenotype not observed in single *flnca* exon1 mutant embryos, again indicating that depletion of both genes had synergistic effects (Fig 3.6). Fourth, *flnca* exon1 or *flncb* exon1 homozygous embryos had no skeletal muscle phenotype, and homozygous *flncb* exon14 embryos had minor skeletal muscle defects (Fig 3.11), compared to much stronger skeletal muscle phenotypes observed in the doubly homozygous *flnca* and *flncb* embryos (Fig 3.11).

In a prior report focused on roles for *flnc* in skeletal muscle function, Ruparelia and colleagues support our finding (Ruparelia, Zhao et al. 2012). They found that the double *flnca* and *flncb* morphant embryos showed stronger skeletal muscle defects than either single *flnca* morphant embryos, *flncb* morphant embryos, or *flncb* (*Sot*) mutant embryos. The *Sot* zebrafish mutant has a nonsense mutation in *flncb* that encodes a stop codon in exon30. The skeletal muscle defect includes broken fibers of skeletal muscle and protein aggregation (Ruparelia, Zhao et al. 2012). In contrast, the *Zac* medaka mutant has a nonsense mutation encoding a stop codon at the 15th Ig repeat of *flnca*. This mutation caused myocardial rupture of the ventricle and skeletal muscle degeneration. More data are needed to test whether that the *flnca* and *flncb* paralogs function independently in medaka. In humans, heart and skeletal muscle cells express FLNC, but zebrafish heart and skeletal muscle express both Flnca and Flncb, which makes studying gene function more

complicated. The conclusion from the *flnca* exon1 (+/-), *flncb* exon14 (-/-) mutant is that the absence of three or four copies of *flnca* and *flncb* leads to the more severe heart and skeletal muscle phenotypes observed in zebrafish. This result demonstrates that the function of Flnc in the zebrafish heart and skeletal muscle development is dose-sensitive. Collectively, our results provide an allelic series: no or mild phenotypes occur for genetic combinations deleting one or two copies, whereas moderate or severe phenotypes occur for genetic combinations deleting three or four copies of *flnca* and *flncb*. Our prior study on *flncb* knockdown by morpholino suggested a mechanism of haploinsufficiency accounted for the observed phenotype (Begay, Tharp et al. 2016). The current study extends that work with analysis of genetic mutants, and provides additional support for a haploinsufficiency contribution to these phenotypes. Many studies on human subjects support a similar conclusion. Particularly, reduction in FLNC levels may cause distal myopathy, dilated cardiomyopathy, or arrythmogenic dilated cardiomyopathy (Guergueltcheva, Peeters et al. 2011, Begay, Tharp et al. 2016, Begay, Graw et al. 2018).

Remarkably, when compared to the phenotypes of the two presumed null alleles (*flnca* exon1 and *flncb* exon1) two other alleles studied here appeared to have stronger (more severe) phenotypes. First, the single *flncb* exon14 allele, which has a nonsense mutation encoding a stop codon in the Ig domain, shows mild swimming defects and a minor heart phenotype (Fig 3.8, 10). Moreover, when the single *flncb* exon14 embryos were exposed to heat stress, they exhibited a cardiac phenotype characterized by cardiac edema and abnormal dilated chambers (Fig 3.7). Continuing this theme, the *flncb* exon 35 mutation, which has a nonsense mutation at exon35 encoding a stop codon at the C-terminus, caused heart and skeletal muscle phenotypes at 48hpf (although with variable expressivity and penetrance). This phenotype is characterized by either cardiac edema or stringy chambers, or mild edema and abnormal chambers, as well as swimming defect. This

finding suggests two primary conclusions. First, these two alleles have a dominant negative? Gain-of-function effect that may derive from a truncated protein which interferes with the wild type protein in cardiac and skeletal muscle cells. A gain-of-function (dominant negative?) phenotype may arise if the truncated protein is misfolded and leads to protein aggregation, which becomes toxic to the cell. In the zebrafish *sot* model, skeletal muscle fibers that has lost their normal myosin striation patterns were observed to develop protein aggregations that were positive in immunohistochemistry assays for myosin and desmin (Ruparelia, Zhao et al. 2012). Second, different *flncb* alleles exhibit different severities of heart and skeletal muscle phenotypes, but our data suggest that skeletal muscle phenotypes are either easier to detect, or occur more readily than cardiac phenotypes in an allelic series depleting increasing amounts of *flnc*. Consistent with this, the zebrafish sot model exhibited skeletal muscle fiber degeneration but no cardiac phenotypes were recorded (Ruparelia, Zhao et al. 2012). We will investigate in chapter 4 whether these the *flncb* exon14 and exon35 alleles lead to abnormal protein aggregation.

Interestingly, we found that the phenotypes resulting from full (double) loss of function of *flnca* and *flncb* and the single gain of function of *flncb* exon35 phenotypes have variable expressivity and incomplete penetrance. Penetrance is the proportion of individuals with a particular genotype that display the expected phenotype. Incomplete penetrance is when the genotype is observed, but the expected phenotype is not present in some individuals. Several lines of evidence support that the phenotypes of double and single mutant are incompletely penetrant. First, in double *flnca* exon1, *flncb* exon14 and single *flncb* exon35 mutant embryos, the percentage of embryos with the phenotype expected from their genotype is not consistent with (and less than the predictions of) Mendelian inheritance. Second, in some individuals who were confirmed by genotyping to be single or double mutants, the expected phenotypes were not observable.

Alternatively, variable expressivity occurs when individuals who have the same genotype display the phenotype in varying degrees. In the case of double and single *flnc* mutant embryos, the phenotypes have variable expressivity for a few reasons. The full (double) loss of function embryos display variable heart and skeletal muscle phenotypes. The heart phenotype can include severe edema and stringy chambers, or mild edema and abnormal chambers. Contrastingly, the skeletal muscle phenotype is characterized by a curved tail and slow swimming, versus outright paralysis. Singly homozygous *flncb* exon35 mutant embryos exhibited heart and skeletal phenotypes to different degrees. The heart phenotypes varied similarly to the double mutant embryos, with the addition of a skeletal phenotype characterized by slow swimming and either curved or normal tails.

Several studies in human parallel the zebrafish genetic model in that Flnc, which is a Z-disc protein, shows variable expressivity and penetrance phenotype. Several mutant loci have been identified and studied in human Flnc ever (Shatunov, Olivé et al. 2009, Duff, Tay et al. 2011, Valdés-Mas, Gutiérrez-Fernández et al. 2014, Begay, Graw et al. 2018), In sum, these studies indicate that individuals may suffer from either HCM or skeletal muscle myopathy or both. In a study that examined patients who suffer from MFM due to one particular mutation in Flnc (p.W2710X), one third of patients had abnormal heart function, although only two individuals out of 25 were reported to have cardiomyopathy characterized by left ventricular dysfunction (Kley, Hellenbroich et al. 2007). In contrast, other mutant loci in FLNC appear only to associate with HCM and no skeletal muscle phenotypes were observed (Valdés-Mas, Gutiérrez-Fernández et al. 2014). In general, the disease of HCM relates to genes that encode sarcomeric proteins and some individuals have heart phenotype and/or skeletal muscle phenotype. Moreover, HCM can cause sudden death in around 20% of patients who have HCM with atrial fibrillation after 30 years of

age. (Maron and Maron 2013, Maron, Ommen et al. 2014, Maron, Udelson et al. 2015). Interestingly, some individuals have the genotype of several mutant genes that causes HCM but the phenotype is not present (Maron, Udelson et al. 2015). In conclusion, FLNC-mediated HCM associated with different morphological features such as cardiac muscle disarray, and protein aggregation. These features are not observed in all patients who suffer from HCM. Additionally, HCM occur in various ages and/or correlated with skeletal muscle defect (Valdés-Mas, Gutiérrez-Fernández et al. 2014, Maron, Udelson et al. 2015). This conclusion suggests that different sites of mutations causes the disease differently.

Additionally, human FLNC mutations have been linked to DCM and/or arrhythmogenic phenotypes (Begay, Tharp et al. 2016, Ortiz-Genga, Cuenca et al. 2016, Begay, Graw et al. 2018, Nozari, Aghaei-Moghadam et al. 2018). Among 28 families >97% of individuals who are older than 40 years and had inherited truncating mutations in FLNC, suffer from dilated and arrhythmogenic cardiomyopathies and 40 cases of 21 families had sudden cardiac death (Ortiz-Genga, Cuenca et al. 2016). Truncating mutations in FLNC variants were found to cause an arrhythmia/DCM phenotype. 85% and 38% of individuals who carry the mutations had DCM and ventricular arrhythmias phenotype respectively (Begay, Graw et al. 2018). The conclusion from these studies is that the FLNC is associated with different classes of cardiomyopathies and these, in some cases, overlapped with skeletal muscle defects. The phenotypes are variable in percentage and characters which suggest the variable and incomplete penetrance phenotypes. Of note, the zebrafish model described here encompasses many of these same aspects.

Materials and methods

Zebrafish husbandry

Adult zebrafish and larvae were maintained, raised, and staged according to standard protocols as previously described (Westerfield 1993, Nusslein-Volhard and Dahm 2002). All fish work and protocols were approved by the Colorado State University Animal Care and Use committee (IACUC). Larvae were stored at 28°C in E3 media and raised at 28°C, which is the appropriate temperature for normal development as described by (Kimmel, Ballard et al. 1995). To overcome growth of mold, the E3 medium was supplemented with 10−5% methylene blue.

Mutant alleles and establishment of mutant crosses

All mutant alleles were obtained from the Zebrafish International Resource Center (ZIRC). They include *flnca* sa24724, *flncb* sa15601, *flncb* sa11171, and *flncb* sa20217, which are referred to in the text and figures as *flnca* exon1, *flncb* exon1, *flncb* exon14, *flncb* exon35 respectively, based on the site of the mutation in the allele. All alleles encode nonsense mutations. Alignments between wildtype human FLNC, zebrafish *flnca,* zebrafish *flncb* and mouse FLNC were performed using ClustalW (Larkin, Blackshields et al. 2007). The F_0 adult heterozygous mutant fish were outcrossed with wildtype fish (WIKs) to reduce the prevalence of any background phenotype due to secondary mutations, and only the offspring of F_1 or later generations were analyzed. Adult fish heterozygous for single alleles [*flnca* exon1 (+/-), *flncb* exon1 (+/-), *flncb* exon14 (+/-), and *flncb* exon35 (+/-)] were mated to sibling heterozygous to generate homozygous mutant fish. Additionally, heterozygous *flnca* exon1 (+/-) and *flncb* exon14 (+/-) adults were crossed to create double mutant [*flnca* exon1 (+/-); *flncb* exon14 (+/-)] compound heterozygous mutant embryos,

which were subsequently raised and adults inter-crossed to obtain [*flnca* exon1 (-/-); *flncb* exon14 (-/-)] compound homozygous mutants along with siblings of various genotypic combinations.

Genotyping of filamin C various alleles mutant zebrafish.

Adult fish, 2 to 4 months old, were fin clipped and genomic DNA was extracted using the protocol described by (Meeker, Hutchinson et al. 2007). Then, genotyping was performed by PCR. PCR primers were designed using Primer3 software https://primer3plus.com/cgi-bin/dev/primer3plus.cgi to amplify the DNA locus spanning the mutation. Primer sequences are listed in table (3.1). PCR products were run on a 0.8% agarose gel and bands extracted by using (QIAquick Gel Extraction Kit Cat No. /ID: 28706) from Qiagene. The purified DNA samples were submitted to Quintarabio for sequencing following their instructions on following link https://www.quintarabio.com/service/dna_sequencing.

Table 3.1: PCR primer sequences for genotyping mutant lines.

Primer name	**Number in primer file**	**Primer sequence**
flnca sa24724 Fwd	484 Fwd	5'-GGCACAGACCTTGGAGAAGA-'3
flnca sa24724 Rev	485 Rev	5'-CCCTGTCCAGAAACTCCAGC-'3
flncb sa15601 Fwd	482 Fwd	5'-AAAGGGGGCACGAAAACATC-'3
flncb sa15601 Rev	483 Rev	5'-AAACCAGTTTGATGTGTTCCCT-'3
flncb sa11171 Fwd	470 Fwd	5'-GTGGAGCTGGAAGAGGACAG'-3
flncb sa11171 Rev	471 Rev	5-TTGATGGGCTTGATGGGTAT-3
flncb sa20217 Fwd	548 Fwd	5'-CTCCCAGGTGGTCTGTCATT-'3
flncb sa20217 Rev	549 Rev	5'-TTGCCCTCTCTTGTTCATCC-'3

Morpholino injection

The antisense morpholino oligonucleotides were synthesized by Gene Tools (California). The single splice *flncb* MO (*flncb* MO: GAGTTTTCTAATGGCCCTTACCTGC) was used. This morpholino was designed by (Ruparelia, Zhao et al. 2012). 1-4 cell wildtype and *flnca* exon1 (-/-) embryos were injected with a low dose of *flncb* MO (200 uM) and coinjected with 150 uM P53MO to reduce off target defects related to ectopic upregulation of the P53 pathway, and consequent non-specific cell death (Campbell, Sinagra et al. 2013). To identify well-injected embryos a 1:10 dilution of 10x rhodamine was incorporated with the morpholino mix and 0.3x Danieaus buffer was used. Before injection, the embryos were transferred using a fire-polished Pasteur pipette from a petri dish to an injection plate. 1-2 cell embryos were injected with morpholino using a Femtojet (Eppendorf). Injection needles were created from 0.75mm inner diameter borosilicate capillary tubes (World Precision Instruments, Sarasota, FL) and pulled on a Sutter P97 Flaming/Brown Micropipette puller using the following program: Heat: 715, Pull: 60, Velocity: 80, Time: 200.

Assessing phenotype

The embryos from the above mutant lines were scored during three consecutive time points (the second, third and sixth day after fertilization (dpf)), equivalent to the pharyngula, hatching, or swimming larva periods (Kimmel, Ballard et al. 1995). The scoring was performed under a dissecting microscope to detect visible abnormalities. Embryos of the pharyngula and hatching period (48-72hpf) were examined for abnormalities in the shape and morphology of the cardiovascular system and developing somites. The larvae received tactile stimulation to assay the embryo motility. The response to touch was tested by briefly contacting the embryos with an insect pin (see below). During each observation the general morphology appearance of

cardiovascular system and skeletal muscle of mutant embryos was recorded in a score sheet for defects in cardiac looping, chamber size (dilated), presence of cardiac edema or arrhythmia and blood circulation, straightness of the body axis, and swimming ability. Some embryos that showed relevant phenotypes were sequenced to confirm the genotype.

Imaging

48 and 72 hpf live larvae were anesthetized using 5ml of 1mg/ml tricaine (i.e. MESAB) per petri dish and placed on 2% low melt agarose (in liquid form) for imaging. All samples were viewed using an Olympus SZX12 stereo-dissecting microscope and microscope-mounted Qimaging Retiga R1 CCD camera, then photographed using Ocular® image acquisition software. Post processing was done by using Adobe Photoshop software to resize images and adjust the white balance.

Cardiac Morphology

48hpf wildtype, mutant and morpholino-injected mutant embryos were anesthetized using MESAB and mounted into a petri dish containing 2% low melt agarose. All samples were imaged by using Olympus SZX12 t stereo-microscope and Spot Insight IN1120 digital camera. Cardiac looping angles were determined by measuring the angle formed between the atrioventricular junction [AVJ] of the heart and the anteroposterior [A/P] axis of the embryos using ImageJ software (Parrie, Renfrew et al. 2013). The chamber size was determined by measuring chamber volume through the following formula ((4/3) *3.14*a*b^2) (a is the middle of the anterior and posterior axes, b is the widest part of the chamber). The heart rate was recorded by counting the heart rate beat per minute for 30 seconds. Three replicates were averaged per fish.

Quantitative Real-time PCR

RNA Extraction

The hearts of 72hpf embryos were dissected by using fine forceps and transferred to 1.5ml Eppendorf tubes containing LB15 medium in 10% fetal bovine serum (FBS) for the following groups: wildtype (WIK), *flnca* exon1(-/-), *flncb* exon14(-/-). Around 10-15 hearts from each group were dissected and homogenized using 250ul TRIzol reagent for each mix (Invitrogen, Carlsbad, CA, USA). Total RNA was isolated according to the manufacturer's protocol. In brief, total RNA was extracted by adding phenol: chloroform, followed by precipitation of RNA with 1 volume of isopropanol to remove salts. After the precipitation step, a washing step with 75% ETOH was applied and the RNA resuspended in 13µl of nuclease-free water. Then, DNase treatment was applied by using 1ul DNase I (Invitrogen) to remove genomic DNA.

cDNA Synthesis

To determine RNA quality and concentration an aliquot of each extract was used for spectrophotometry. RNA samples with a 260/280 ratio between 1.8–2.0 and a 260/230 ratio > 1 and < 3 were used in this study. Next, 1-2µg of RNA; (in 20µl final reaction volume) along with Oligo(dT)$_{12-18}$ primer (Invitrogen) were used for cDNA synthesis reactions using 1ul AMV reverse transcriptase (Fisher Scientific) according to the manufacturer's instructions.

Oligonucleotides

All oligonucleotide primers were synthesized by IDTA. Gene-specific oligonucleotide primers for *flnca, flncb* were developed using Primer-Blast https://www.ncbi.nlm.nih.gov/tools/primer-blast/. Primer sets were verified for specificity using standard RT-PCR and cDNA from wildtype embryonic zebrafish hearts as a template to verify the production of a single band of the predicted size. The following primers were used.

Table 3.2: Quantitative PCR primer sequences.

Primer name	Number in primer file	Primer sequence
flnca	525 Fwd.	5'-AGTTTCTGGACAGGGAGAGA-'3
flnca	526 Rev.	3'-CCCAGAATCAGCTTCAGGTT-'5
flncb	533 Fwd.	5'-ACGATGAAGACGCCAGAAAG-'3
flncb	534 Rev.	5'-CAGTCCCTGTGGAAGTTGTT-'3
Elongation factor 1-alpha *(efa1)*	546 Fwd.	5'-CGGTGACAACATGCTGGAGG-'3
efa1	547 Rev.	5'-ACC AGT CTCCACACGACCCA-'3

Quantitative Analysis

Quantitative reverse transcription polymerase chain reaction (qRT-PCR) was performed with the Light Cycler Fast Start DNA Master Plus SYBR Green I reaction mix and a Light Cycler 480 thermal cycler (Roche Applied Science, Indianapolis, IN, USA). Samples contained 5ul 2× SYBR green master mix, 2ul of each forward and reverse primers (5μM each, sequences in Table above) and 1μl RT reaction for a final volume of 10 μl. Samples were run in triplicate in optically clear 384-well plates (2 biological replicates × 2 RT reactions × 2 PCR runs × 3 reactions per PCR run). PCR cycling parameters included an initial denaturation at 95°C for 5 min, followed by 45 cycles of denaturation at 95°C for 20 seconds, annealing at 55°C for 20seconds, and extension at 72°C for 15 seconds. At the end of each run, an analysis of the PCR product melting temperature was performed.

Data Analysis

Data generated by real-time PCR were compiled and the PCR amplification efficiency (E) for each primer pair was determined. The value of E = 10(-1/slope) was determined by linear regression analysis of a dilution series of reactions (Muller, Janovjak et al. 2002). The PCR efficiency value of all acceptable amplifications was between 1.9 and 2.2. The efficiency of each primer pair (E), together with the Ct values, was used to determine a relative gene expression value for each transcript following the equation

$$RQ = \frac{(E_{target})^{\Delta Ct\,(target)}}{(E_{reference})^{\Delta Ct\,(reference)}}$$

(Tang, Dodd et al. 2007). The Ct value (cycle threshold) is described as the number of cycles required for the fluorescence to cross a specific threshold level of detection and is associated with the amount of template present in the reaction (Walker 2002). The Student's t-test was used to determine significant differences in expression of *flnca* and *flncb* between wild type and *flnca* exon1 (-/-), or *flncb* exon14 (-/-).

Touch-evoked Escape Behavior Assay

Swimming behavior was quantified by assaying the touch-evoked response in multiple embryos of wild type and mutant genotypes according to the protocol (Smith, Beggs et al. 2013). Briefly, 48hpf embryos of wildtype, *flnca* exon1 (-/-), *flncb* exon14 (-/-), and double *flnca* exon1 (-/-); *flncb* exon14 (-/-) were dechorionated and placed individually into a deep petri dish marked with a grid, and centered in the camera field of view. Videos were recorded using a Canon digital camera (Power Shot S119) and the same frequency of imaging was used for both wild-type and mutant fish. Mechanosensory stimuli were applied to the embryos by briefly touching the tail with an

insect pin. Videos were then analyzed frame by frame and the average distance (cm) embryos were able to swim was measured, and swimming speed (cm/sec) was calculated.

Means of swimming speeds were compared between wildtype, *flnca* exon1 (-/-), *flncb* exon14 (-/-), and double *flnca* exon1 (-/-) + *flncb* exon14 (-/-) embryos using analysis of variance (ANOVA). Post-hoc multiple comparisons were applied using Tukey–Kramer HSD tests.

Chapter4: Cell morphology in embryonic zebrafish hearts lacking Flnca and Flncb

Introduction

Embryonic zebrafish heart morphogenesis at a glance

The heart is the first organ to function in the vertebrate (Stainier 2001, Bakkers 2011). The embryonic heart of the zebrafish is a simple tube comprised of three cellular layers: the endocardium, myocardium and pericardium. The endocardium is an endothelial lining that is connected with the rest of the vasculature. On the other hand, the myocardium is the muscle of the heart that undergoes rhythmic contractions to cause circulation of blood. The pericardium covers the outside of myocardial layer. This three-layered tube is divided into two main chambers, the atrium and ventricle. The blood flow proceeds from the posterior atrium to the anterior ventricle (Glickman and Yelon 2002, Brown, Samsa et al. 2016).

Heart formation passes through many major events that happen in chronological order, including cardiac cell specification, migration, proliferation, and organ growth. A complex series of morphogenetic events occurs to form the heart tube at the embryonic midline. After formation of the endocardium and myocardium, myofibrils and differentiation the chambers and valves proceed. The initial heart tube will be remodeled through several events including: heart looping, chamber ballooning, valve development, ventricular wall thickening, and ventricular trabeculae formation (Yelon 2001, Glickman and Yelon 2002, Bartman, Walsh et al. 2004). Three regulatory factors affect cardiac size development: 1) regulation of cardiac cell specification through a well-regulated spatially and temporally coordinated processes, 2) regulation of cell division rate, and 3)

regulation of the number and volume of individual cardiomyocytes (Bryant and Simpson 1984, Day and Lawrence 2000).

The early heart tube starts to contract around 24hpf (Warren and Fishman 1998, Glickman and Yelon 2002). Cardiac contraction involves coordinated muscle constriction which occurs in response to the conduction signals. The network of cardiomyocytes maintain the conduction system which controls the heart beat in both larvae and adult zebrafish (Staudt and Stainier 2012). The conduction system modulates the blood flow through contractions that lead blood cells to move through the heart. Therefore, the formation of normal contractile sarcomeres and heart morphology influences the correct contractile pattern (Staudt and Stainier 2012). Additionally, the heartbeat, blood flow, and contraction help to maintain other heart development processed (Glickman and Yelon 2002). As a consequence, the blood flow disruption affect both morphological features of the heart, leading to defective chamber shape and size, abnormal looping, and valve formation defects, and may affect the myofibrillar content (Hove, Köster et al. 2003, Lin, Swinburne et al. 2012).

Cardiogenesis is an important developmental process for life for humans and complex animals. Thus, analysis of pathways and genes involved in cardiac morphogenesis remains an important trend in the field of developmental biology ,and contribute knowledge to our understanding of heart morphogenesis (Glickman and Yelon 2002, Fahed, Gelb et al. 2013). On the other hand, the biomechanical factor such as stretch, contraction and blood flow have a substantial impact on the correct heart morphogenesis (Lin, Swinburne et al. 2012). Mutation in genes that have a role in cardiac morphogenesis may change the way cells respond to biomechanical factors, thereby disrupting normal heart development. These genes can be responsible for developing disease such as cardiomyopathies and other heart malformations in adulthood (Srivastava 2004, Srivastava

2006). Therefore, knowing the identity of key genes and the mechanisms by which mutations lead to cardiomyopathy disease is required for therapeutic goals to prevent cardiac disease in adults.

Cardiomyopathy definition

Cardiomyopathies can be defined as a heterogeneous class of diseases of the myocardium linked to medical and/or electrical dysfunction that normally exhibit inappropriate ventricular hypertrophy or dilation as a result of different etiologies, which are hereditary in most cases (Maron, Towbin et al. 2006). While cardiomyopathies can either be restricted to the heart, they can also be part of generalized systemic disorders. Often, they result in cardiovascular death or a progressive heart failure-related disability (Maron, Towbin et al. 2006). Cardiomyopathies consist of different types including: dilated cardiomyopathy (DCM), hypertrophic cardiomyopathy (HCM), and restrictive cardiomyopathy (RCM) arrhythmogenic right ventricular cardiomyopathy (ARVC) (Hughes and McKenna 2005, Arbustini, Narula et al. 2013, Braunwald 2017, Corrado, Basso et al. 2017).

Inherited cardiomyopathy is a major cause of heart disease in every age group. These disorders normally manifests upon the onset of adolescence or early adult life (Watkins, Ashrafian et al. 2011).

Common genetic cause myocardium disease

Mutations in different genes encoding cardiac proteins are responsible for familial cardiomyopathy disease. However, most of genetic variations that cause familial cardiomyopathies are still unknown (Dellefave and McNally 2010, Jefferies and Towbin 2010, Valdés-Mas, Gutiérrez-Fernández et al. 2014, McNally and Mestroni 2017).

Inherited DCM varies genetically; causal mutations have been identified in more than 50 genes. Most of these mutations are in genomic regions encoding costamere, the boundaries of the sarcomere (Z-discs), mitochondrial, desmosomal, nuclear membrane, or RNA-binding proteins. Therefore, various pathological mechanisms result in DCM (Davies 2000, Hughes and McKenna 2005, McNally, Golbus et al. 2013, McNally and Mestroni 2017). Costamere is a functional structure located sub-sarcolemma of cardiac and skeletal muscles, which connects the sarcomere to the cell membrane(Srivastava and Yu 2006). Sarcoglycan, which encodes a transmembrane protein and links the cortical actin fibers to the extracellular matrix, and dystrophin, which expresses in cardiac and skeletal muscles, are a costamere genes. Mutations in either sarcoglycan or dystrophin genes produce cardiomyopathy, that on most occasions is linked to muscular dystrophy (Tsubata, Bowles et al. 2000) (Watkins, Ashrafian et al. 2011, McNally and Mestroni 2017). Moreover, many genes connected to DCM encode proteins that assemble into the sarcomere, which is the basic contraction unit of muscle. Titin (*TTN*), myosin heavy chain 7 (*MYH7)*, cardiac troponin 2 (*TNNT2),* and tropomyosin 1 (*TPM1)* are the most commonly mutated sarcomere genes associated with DCM, based on the latest data from clinical genetic testing (Kamisago, Sharma et al. 2000, Pugh, Kelly et al. 2014, McNally and Mestroni 2017).

HCM is a common genetic disease with variable expression characters and is associated with more than 1500 mutations in 11 genes (Maron, Towbin et al. 2006, Maron, Udelson et al. 2015). Mutations in one or more of the nine sarcomere genes cause 60% of HCM cases. These genes encode for components of the heart's contractile apparatus. Of these nine, the majority of known mutations occur in four: the β-myosin heavy chain gene *MYH7* (20–30%), the myosin-binding protein C gene *MYBPC3* (30–40%), the cardiac troponin T gene *TNNT2* (10%), and the cardiac

troponin I *TNNI3* (7%). In other sarcomere genes, mutations are very uncommon (Richard, Charron et al. 2003, Hughes and McKenna 2005, Kimura 2008, Hensley, Dietrich et al. 2015).

Although researchers have identified thousands of human gene mutations that cause myocardium disorders, many gene mutations are still unknown, or need more data to significantly correlate them to cardiomyopathies. An example is FLNC, which is a sarcomeric protein that links the cortical actin to transmembrane proteins such as integrin through costamere (Dalkilic, Schienda et al. 2006, Fürst, Goldfarb et al. 2013).

Filamin C (FLNC)

The *FLNC* gene encode a protein of high molecular weight (291 kDa) which forms homodimers (van der Flier and Sonnenberg 2001). FLNC structure be composed of two calponin homology (CH) domains at N terminal (CH1, CH2), followed by a series of 24 immunoglobulin (Ig) like-repeats and the C terminal domain (van der Flier and Sonnenberg 2001, Nakamura, Stossel et al. 2011). The expression of FLNC is restricted to the skeletal and cardiac muscle and is required for normal myogenesis (KOTELIANSKY, GLUKHOVA et al. 1986) (Dalkilic, Schienda et al. 2006, Lad, Kiema et al. 2007). Within the cell, FLNC localizes at the Z-discs (a structure which joins sarcomeres) and intercalated discs (a structure which joins adjacent myocytes of heart muscle). In addition, FLNC protein localizes within the costamere in small amounts (Ruparelia, Zhao et al. 2012). Consistent with this subcellular distribution, FLNC plays an important role in organizing the sarcomeric components, and in linking the Z-disc components and cortical actin fibers to the sarcolemma. Through its function in the costamere, FLNC helps to anchor the mechanical system (sarcomere, and cytoskeleton) to cell membrane proteins as integrin. Therefore, FLNC functions as a scaffolding protein (Zhou, Hartwig et al. 2010, Tucker, McLellan et al. 2017).

A few previous studies investigated the role of filaminC in heart development. Fujita and his colleagues used medaka as a model, and our prior report with Begay and her colleagues used zebrafish as a model to test the role of filaminC in heart muscle development (Fujita, Mitsuhashi et al. 2012, Begay, Tharp et al. 2016). Additionally, other studies have linked the FLNC mutation to various cardiomyopathies: two to DCM (Begay, Tharp et al. 2016, Nozari, Aghaei-Moghadam et al. 2018), two to ARC (Begay, Graw et al. 2018), one to RCM (Brodehl, Ferrier et al. 2016), and one to HCM (Valdés-Mas, Gutiérrez-Fernández et al. 2014). Despite these prior studies, the mechanism by which FLNC mutation can lead to cardiomyopathies is poorly understood.

Myofibrillar myopathies (MFMs) are a group of progressive inherited muscle disorders that usually result in severe disability and early death. MFMs are caused by mutations in genes located at or associated with Z-disc proteins, including desmin, filamin C, plectin, VCP, FHL1, ZASP, myotilin, αB-crystallin, BAG3, and DNAJB6 (Claeys and Fardeau 2013, Latham and Lopez 2015). MFM is characterized by disintegration of myofibrils at the Z-disc, dysfunction of the mitochondria, and accumulation of intramyoplasmic protein aggregates (Maerkens, Olivé et al. 2014, Latham and Lopez 2015, Winter and Goldmann 2015, Vincent, Grady et al. 2016). Some human FLNC alleles cause MFM and/or HCM show protein aggregations whereas others do not. It remains unknown whether protein aggregates are toxic to the cell or affect the cell in a different way, or at all.

Over the years, zebrafish has developed as a powerful model to study human cardiovascular diseases and to elucidate the mechanisms incorporated in this disease (Bakkers 2011, Bournele and Beis 2016, Gut, Reischauer et al. 2017, Yalcin, Amindari et al. 2017). In this study, I extended the initial zebrafish FLNC morpholino studies to investigate for the contributions of various FLNC alleles to cardiac muscle disease. Additionally, I addressed several outstanding

questions and gaps in our knowledge about how FLNC leads to myocardium diseases. First, does FLNC has a role in z-disc formation and organization? Second, does FLNC mutant affect the sarcomere and myofibril development and assembly? Third, how does FLNC depletion impact the actin fibers network organization? Fourth, do presumed null and truncation mutant FLNC alleles develop equivalent heart defects and/or skeletal muscle defects? To date, the correlation between the site of *FLNC* mutation in the gene and the prevalence of heart versus skeletal myopathy(ies) still unclear. Fifth, how the FLNC deficiency influence how the heart responds to biomechanical factors as arising from blood flow and contraction and how in turn does this affect the heart development. Additionaly, I investigated whether the severity of the phenotype correlate with the FLNC dosage. Lastly, this project identify which FLNC alleles produce truncated protein and develop protein aggregation.

Results

Flnc is required for sarcomere arrangement and Z-disc assembly of zebrafish heart

The sarcomere is the repeating segment between two Z-discs and delimits the basic unit of contractility (Krans 2010). To examine the assembly of the Z-disc, which outlines the border of the sarcomere and links thin filaments via proteins, we performed two different experiments: 1) using a transgenic line, *TG (Cmlc2: Cypher-EGFP),* that marks the location of the Z-discs in the zebrafish heart to assess the global organization of sarcomeres (Fig 4.1), 2) transmission electronic microscopy (TEM) to discern the ultrastructure of the myofibril organization (Fig 4.3).

Cypher transgenic line experiment at 53hpf

The length of Z-discs from side to side, and the distance between two Z-disc (i.e., the length of sarcomere), were measured at 53hpf for several groups including: wildtype, *flnca* MO, *flncb* MO, *flnca*+*b*MO, *flnca* exon1 (-/-) + *flncb* MO, *flnca* exon1 (-/-), *flncb* exon14 (-/-), and double mutant *flnca* exon1 +*flncb* exon14. In the morpholino group, the average length of Z-discs significantly decreased for the *flnca* MO, double *flnca*+b MO, and *flnca* exon1 (-/-) + *flncb* MO embryos, to 0.9μm, 0.9μm, and 0.9μm respectively. In contrast, the wildtype averaged 1.2μm and *flncb* Mo averaged 1.2μm, (*P* value = 0.001; Fig 4.1J). The length of Z-discs was also significantly shorter in *flncb* exon14 (-/-), and double *flnca* exon1 + *flncb* exon14 mutants, with averaged 1.0μm, and 0.9μm, compared to wildtype and *flnca* exon1 which averaged 1.2μm, and 1.1μm respectively (Fig 4.1K). In contrast, no significant differences were observed in the length of the sarcomere among all groups measured,

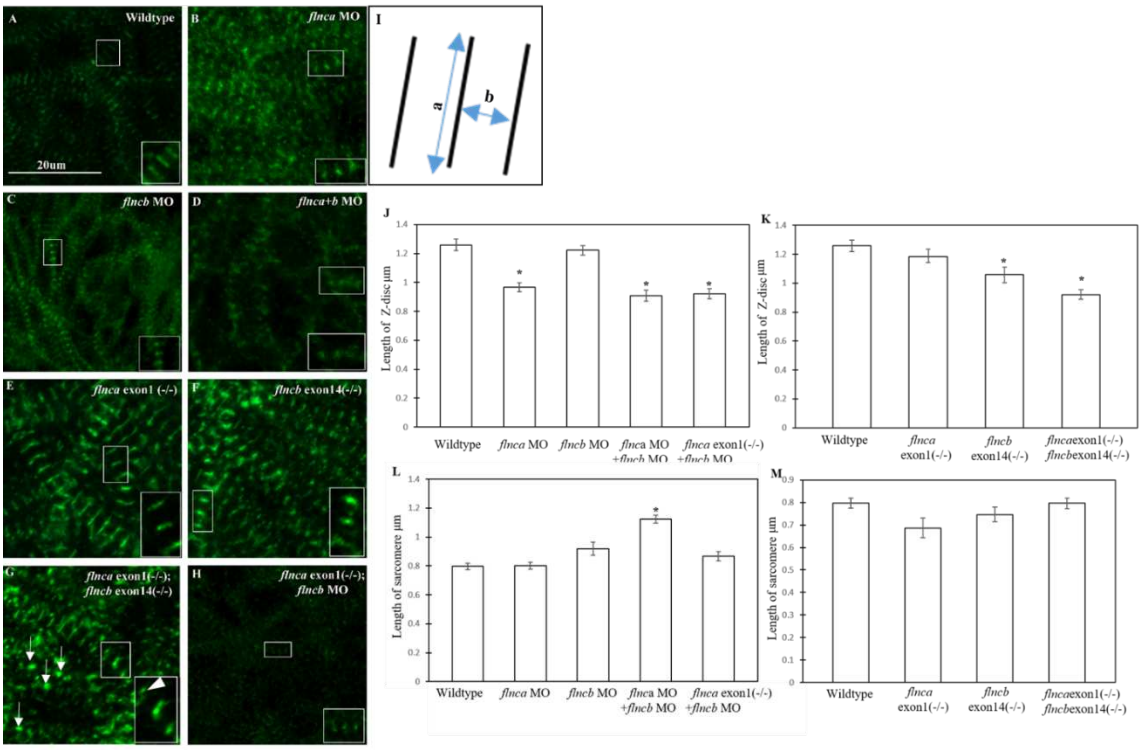

Figure 4.1 Flnc mutant and deficient lead to Z-disc deforming and disruption. (A-H) *Tg (cmlc2: cypher-egfp*) fish, in which the transgene marks the location of Z-discs. Images of dissected ventricle at 53hpf from (A) wildtype, (B) *flnca* MO, (C) *flncb* MO, (D) *flnca+b* MO, (E) *flnca* exon1 (-/-), (F) *flncb* exon14 (-/-), (G) double *flnca+b* mutant, and (H) double *flnca* mutant + *flncb*MO. Boxed areas were zoomed at the right bottom each image. Wildtype hearts exhibit a striated pattern, with fully formed and well-aligned Z-discs. In some cases (B, D, G,) Z-discs are deformed and arrested. (H) Z-discs appears as two dots not fully joined (arrows) or misaligned (arrowheads) (I) Diagram of the dimensions measured, blue arrows indicates length of Z-disc (a), and the length of sarcomeres (b). (J, K) Measurements of the length of Cypher- EGFP bands (J) for MOs experiments and (K) for genetic lines. Relative to the wildtype, the length of Z-discs is significantly decreased in *flnca* MO, *flnca+b*MO, *flnca* exon1 (-/-); *flncb*MO, and double *flnca+b* mutant. ANOVA **P*<0.001. (L, M) the measurement of sarcomere length, distance between two Z-bands,. Relative to wildtype, the single *flncb* exon14 (-/-) and double *flnca+b* MOs heart exhibit a significant increase in sarcomere length. Sarcomeres, ANOVA *P*<0.001. n≥30 bands for length of Z-disc measurment, n=30 sarcomeres for length of sarcomere measurement.

including wildtype, *flnca* MO, *flncb* MO, *flnca* exon1 (-/-) + *flncb* MO, *flncb* exon 14 (-/-), double *flnca* exon1+ *flncb* exon14 mutant with an average 0.8±0.2μm for all genotype. However, the sarcomere length of double *flnca*+*b*MO embryos was significantly larger compared to wildtype with an average of 1.1μm (*P* value<0.001; Fig. 4.1).

Sarcomere assembly proceeds through several stages in the process of becoming fully formed. These include: 1) By the 12 somite stage, actin filaments form as perimembrane network, while myosin (thick filaments) form as a rodlet structure. 2) by the 18 somite stage, actin and myosin filaments are joined to Z-bodies, which form as irregular dots (Dabiri, Turnacioglu et al. 1997). 3) By the 21 somite stage, Z-bodies are arranged as pairs of dots separated laterally by a short distance, and appearing at regular intervals between forming sarcomeres. Then, once the heart tube starts to contract, the space between the two dots gradually decreases and the Z-bodies are fused. 4) By24hpf, the Z-bodies have transitions to elongated Z-discs. Lastly, at 48hpf myofibrils are bundled and full-length Z-discs align with each other to form mature Z-disc (Huang, Zhang et al. 2009, Yang, Shih et al. 2014) (Fig 4.2).

At 48 hpf, wildtype hearts exhibited a striated pattern of fully formed and well-aligned Z-discs (Fig4.1A). In contrast, the heart of morpholino group resemble wt heart of 26 somite stage suggesting the Z-disc had not fully formed or had arrested in hearts of all morpholino groups. In the single homozygous *flnca* exon1 (-/-) mutants, and *flncb* exon14 (-/-) mutants, the majority of Z-discs resembled those of wildtype. The development of most of the Z-discs in the double *flnca* exon1+ *flncb*exon14 mutant appeared to have developed to the status typical of the 26 somite stage (Huang, Zhang et al. 2009). Whereas by 48 hpf, the wildtype Z-discs had grown laterally to form the mature Z-disc visible as a short line, Z-discs in the double mutant appeared as two dots that were not fully joined into a solid line, suggesting that Z-disc formation was delayed or arrested.

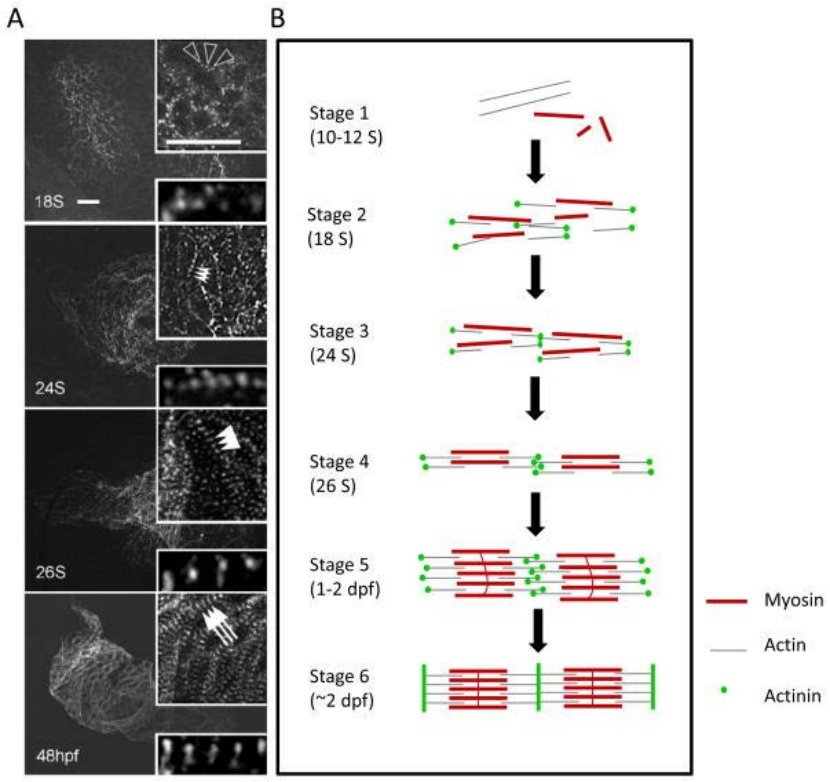

Figure 4.2 Sarcomere assembly stages. **(A)** Images for zebrafish heart from 18 somite stages to 48hpf, the Z-disc marked with αactinine antibody by performing ICC. **(B)** schematic representation describes sarcomere assembly. By the 12 somite stage, actin (thin filaments) form as perimembrane network, while myosin (thick filaments) form as a rodlet structure. 2) by the 18 somite stage, actin and myosin filaments are joined to Z-bodies, which form as irregular dots (Dabiri, Turnacioglu et al. 1997). 3) By the 21 somite stage, Z-bodies are arranged as pairs of dots separated laterally by a short distance, and appearing at regular intervals between forming sarcomeres. Then, once the heart tube starts to contract, the space between the two dots gradually decreases and the Z-bodies are fused. 4) By24hpf, the Z-bodies have transitions to elongated Z-discs. Lastly, at 48hpf myofibrils are bundled and full-length Z-discs align with each other to form mature Z-disc (Huang, Zhang et al. 2009, Yang, Shih et al. 2014)

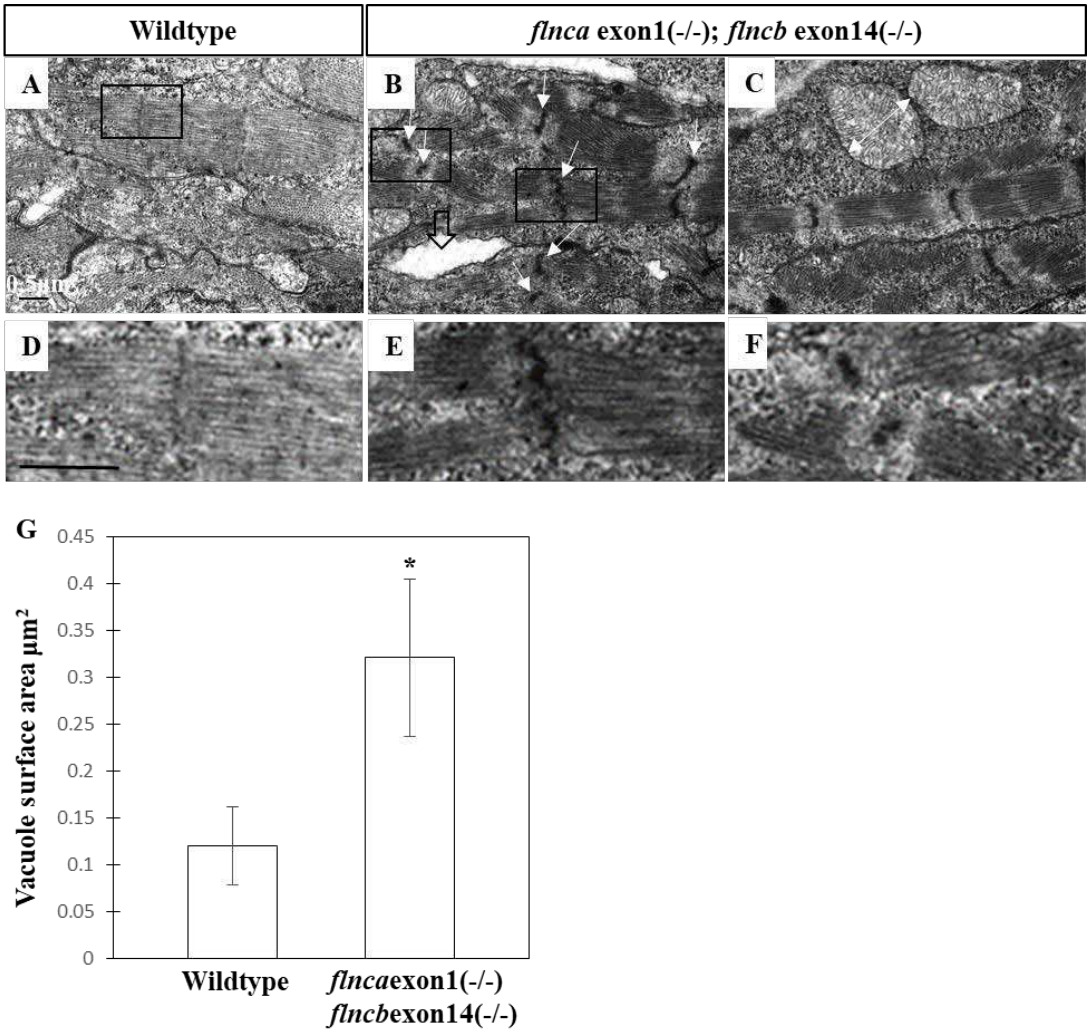

Figure 4.3 Flnc mutant affects sarcomere assembly and Z-disc alignment. (A-C) Transmission electron micrographs of CMs at 72 hpf embryos. (D-F) Images with high-magnification of boxed regions panels A, B. (A, D) wild-type heart exhibits organized several consecutive sarcomeres with clearly distinct Z-discs. (B,C,E,F) Double *flnca+b* mutant exhibits abnormal Z-disc (arrows in panel B). Most of Z discs in double *flnca+b* mutant are misaligned, displaying as either zigzagged lines (E) or detached dots (F). Sarcomere arrangement in myofibrils was often nonconsecutive. Large extracellular space located near the cell membrane, creating a gap between adjacent cardiomyocytes (white arrow). (C) Large and abnormally shaped mitochondria (arrow). G) Measurement of vacuoles area on electron microscope data. Double *flnca+b* mutant CMs had significant larger vacuoles compared to wildtype. T-test **P*=0.001. n≥19

Among hearts of the double mutants, Z-discs failed to assemble into a regular consecutive pattern, but instead were misaligned (Fig 4.1). These results indicate that, collectively, Flnc function is important for Z-disc growth and maturation, and for regular arrangement within the cardiac muscle.

TEM experiment

In order to examine sarcomere assembly in Flnc mutant hearts, we performed a TEM study on hearts of 72hpf wildtype and double *flnca* exon1+*flncb* exon14 mutant embryos (Fig 4.3) At 72hpf the heart of zebrafish completely form myofibrils with mature Z-disc (Huang, Zhang et al. 2009). By 72hpf, hearts of wildtype embryos had bundles of myofibrils regularly arranged in repeated sarcomere units (Fig. 4.3A). Sarcomeres were linked by distinctly-stained Z-discs of constant thickness and width (Fig 4.3B). In contrast, in hearts of double mutant embryos, myofibrils were not uniformly aligned in successive and parallel sarcomeres, but rather branched irregularly (Fig 4.3B). Bundles were of variable width and length. The Z-discs were irregular in shape (many were zigzagged rather than flat as in wildtype) (Fig 4.3E). Some Z-discs of mutants showed thicker regions of electron density than controls, yet in other cases the Z-disc material was reduced or absent (Fig 4.3F). We conclude that in Flnc-depleted embryos, the early sarcomerogenesis was initiated but did not proceed normally and the myofibril growth was diminished.

We also noted the presence of electron-sparse regions, termed ‘vacuoles’ in the literature (Dunn 1990, Reggiori 2006). In our samples, vacuoles were larger and more frequent in the cardiomyocytes of doubly mutant embryos. The area of vacuoles was measured by tracking the circumference in Image J. Vacuole area in doubly mutant hearts was increased, averaging 0.3 μm^2 compared to the wildtype, which averaged 0.12 μm^2 (Fig. 4.3G). In many cases, large vacuoles formed in close association with the cell membranes of two adjacent cardiomyocytes, or occurred

between them (Fig. 4.3B), suggesting the possibility that intercellular attachments were disrupted, and that cells had begun to separate, or that the cytoskeleton (or costamere) had detached from the cell periphery. Taken together, these data support an important role for Flnc in the maturation or maintenance of sarcomere structure and cardiomyocyte architecture or intercellular attachment.

Cardiomyocyte surface area and shape change in Flnc mutant embryos

To examine whether Flnc plays a role in development and differentiation of individual cardiomyocytes, we measured the cross-sectional area and shape of double Flnc mutant cardiomyocytes of dissected ventricles at 53hpf, during the chamber ballooning stage. Cell growth and modulation of cardiomyocytes cell shape is important in controlling the development of general heart tube morphology (Auman, Coleman et al. 2007). To measure cell cross-sectional area and shape of cardiomyocytes in the embryonic zebrafish heart, we performed immunohistochemistry to mark the location of the cell membrane via zn8 immunogenicity. Then, we used ImageJ software to calculate the cell area and degree of circularity in cardiomyocytes in the outer curvature (OC) and inner curvature (IC) of the ventricle, as well as cells residing in the middle region of each chamber. A circularity value of 1.0 represents a perfectly round cell, whereas smaller values indicate elongated polygons. The average IC and OC cell surface area and shape displayed no significant differences between wildtype and double mutant hearts; (P= 0.3, and 0.4) for OC surface areas and shape and (P= 0.1, and 0.1) for IC cell surface area and shape (Fig 4.4C, D). In contrast, the average cell cross-sectional area of cardiomyocytes in the middle region of the ventricular chamber increased for double mutant hearts compared to the wildtype (P=0.004) (Fig 4.4C). The average circularity value for cells in the middle region was significantly reduced, indicating these cells are elongated compared to similar wildtype cardiomyocytes (P=0.03) (Fig. 4.4D). In sum, these data suggest that a limited degree of change occurs in cell size and shape in

Flnc mutant ventricles. Such changes would be expected to lead to abnormal chamber ballooning and development, without severely affecting cardiac looping, which relies heavily on changes in OC cells.

Actin filaments assembly in Flnc mutant embryos

The FLNC protein contains an actin binding domain which links cortical actin to the cell membrane as part of the costamere structure, and connects the actin filaments in the sarcomere to the actin cytoskeleton (Stossel, Condeelis et al. 2001). To examine the effect of Flnc in the assembly of actin filaments, we performed IHC for double *flnca* exon1 (-/-); *flncb* exon14 (-/-) hearts at 53hpf by using Phalloidin tagged with Alexa Fluor to label actin filaments of zebrafish cardiac muscle. In the wildtype cardiac muscle, actin filaments were assembled in parallel, and tightly packed into stiff, thick bundles. Actin present in sarcomere is detectable as periodic units consecutively arranged (Fig 4.5A). In contrast, actin filaments at the cell periphery of double *flnca+b* mutants assembled into thinner, longer collections of filaments which overall appeared more curved and loosely compacted (Fig 4.5B,C). In double *flnca+b* mutant hearts, the presence of periodic units denoting sarcomeric actin filaments were markedly more difficult to detect (Fig 4.5B,C). The atrium of wildtype hearts showed a pattern of actin filaments characterized by loose but parallel arrangements of fibers across the width of the cell. In contrast, the double *flnca+b* exhibited a disorganized collection of microfilaments. While local regions of parallel fibers were detectable, these were oriented in multiple different directions across the cell. This data suggests that FLNC is an important actin cross linker and contributes to the overall organization of the microfilament network.

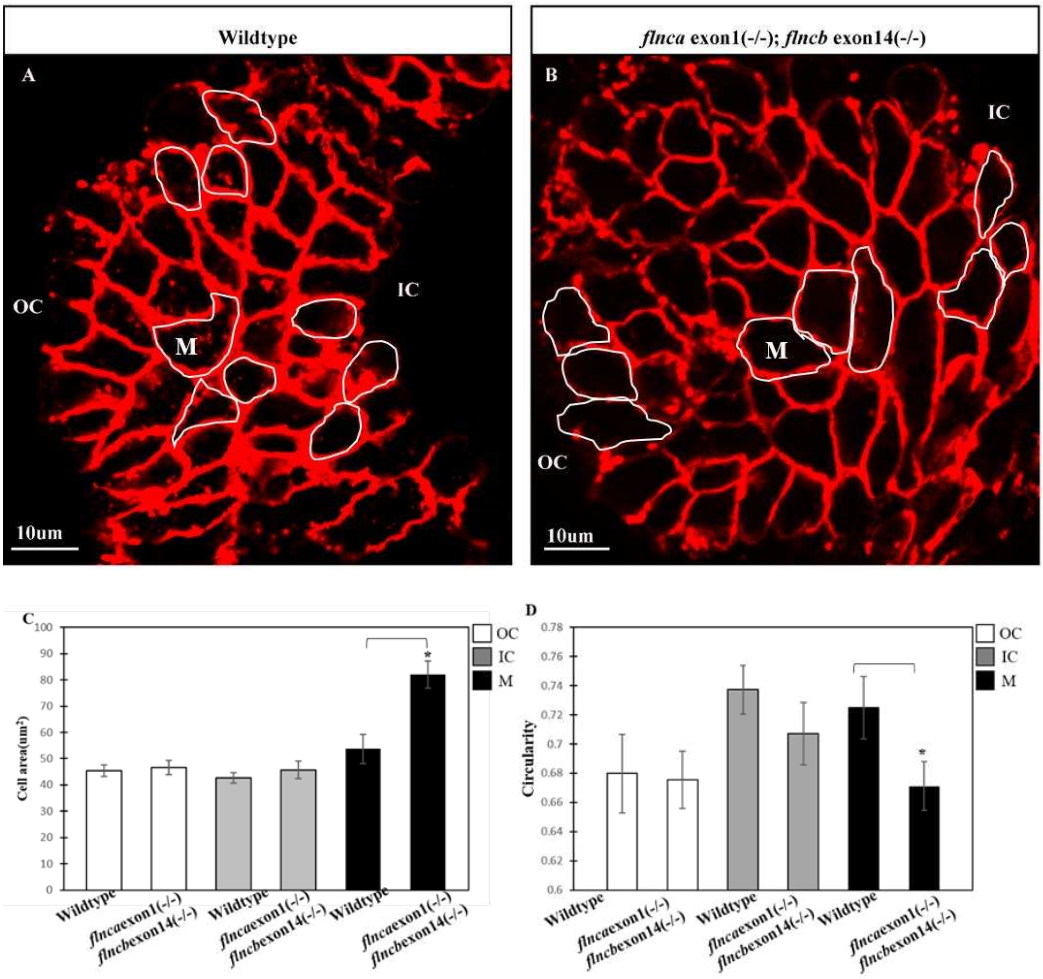

Figure 4.4 Cardiomyocytes are enlarged in 53hpf Flnc mutant embryos. (A-B) 3D Images of dissected ventricles from wildtype and double *flnca+b* mutant embryos at 53 hpf with zn8 immunostaining, which labels cell membrane. IC and OC were identified as defined in Auman *et al* (2007). Measured IC, OC, and M were outlined with white lines. **(C)** Quantification of cardiomyocyte surface area in the ventricle of individual cells. The double *flnca+b* mutant hearts exhibit significant larger surface area relative to wildtype. T-test **P*=0.004 n=27**(D)** Quantification of cardiomyocyte shape for ventricular chambers, in which higher numbers represents a more circular shape. The double *flnca+b* mutant hearts displayed significant elongated cardiomyocytes of the middle area. T-test **P*=0.03. n=27. 4 hearts for wildtype, 5 hearts for double *flnca+b* mutant. IC = Inner Curvature, OC = Outer Curvature cells, M=middle.

Since FLNC forms a part of the costamere, which links actin and a variety of other large molecules to the cell periphery, we hypothesized that FLNC actin-binding properties are necessary to for extensive co-localization of actin filaments with the cell periphery. Therefore, we examined double *flnca+b* mutant hearts processed for immunohistochemistry with zn8 antibody, which marks cell membrane, and labeled with Alexa-Fluor Phalloidin to mark actin filaments. Using merged images, the extent of co-localization between the cell membrane and actin filaments was quantified. We found no significant differences between mutant or wildtype cardiomyocytes by Pearson's coefficient in a T-test. This data indicates that the actin filaments displayed high correlation with cell membrane in both wildtype and double *flnca+b* mutant ventricles.

Measurement the biomechanical factors of double Flnc mutant zebrafish heart

FLNC is a sarcomeric protein which contributes to the basic function of contractility and ability of the cell to withstand mechanical stress during cardiac contraction. We measured the biomechanical behavior of wildtype and double mutant *flnca+b* hearts at 53hpf by analysis of high speed videos (Video1, 2). We note that cardiac output (13.4 nl/min) and stroke volume (0.9 nl) were significantly decreased in double *flnc*a+b mutant embryos relative to the wildtype embryos (cardiac output 20.9nl/min, stroke volume 0.1nl) P=0.05 and 0.03 for cardiac output and stork volume respectively (Fig 4.6B,C). In double *flnc*a+b mutant embryos, the heart rate (124.1 bpm) and reverse flow fraction (0.1) trended toward higher values than wildtype hearts, but these were not significant (heart rate 132.6 bpm, reverse flow fraction 0.05) (Fig 4.6A, D). These data determined that double *flnca+b* embryos were not able to maintain normal cardiac output and stroke volume. Thus, double *flnca+b* hearts exhibited reduced function.

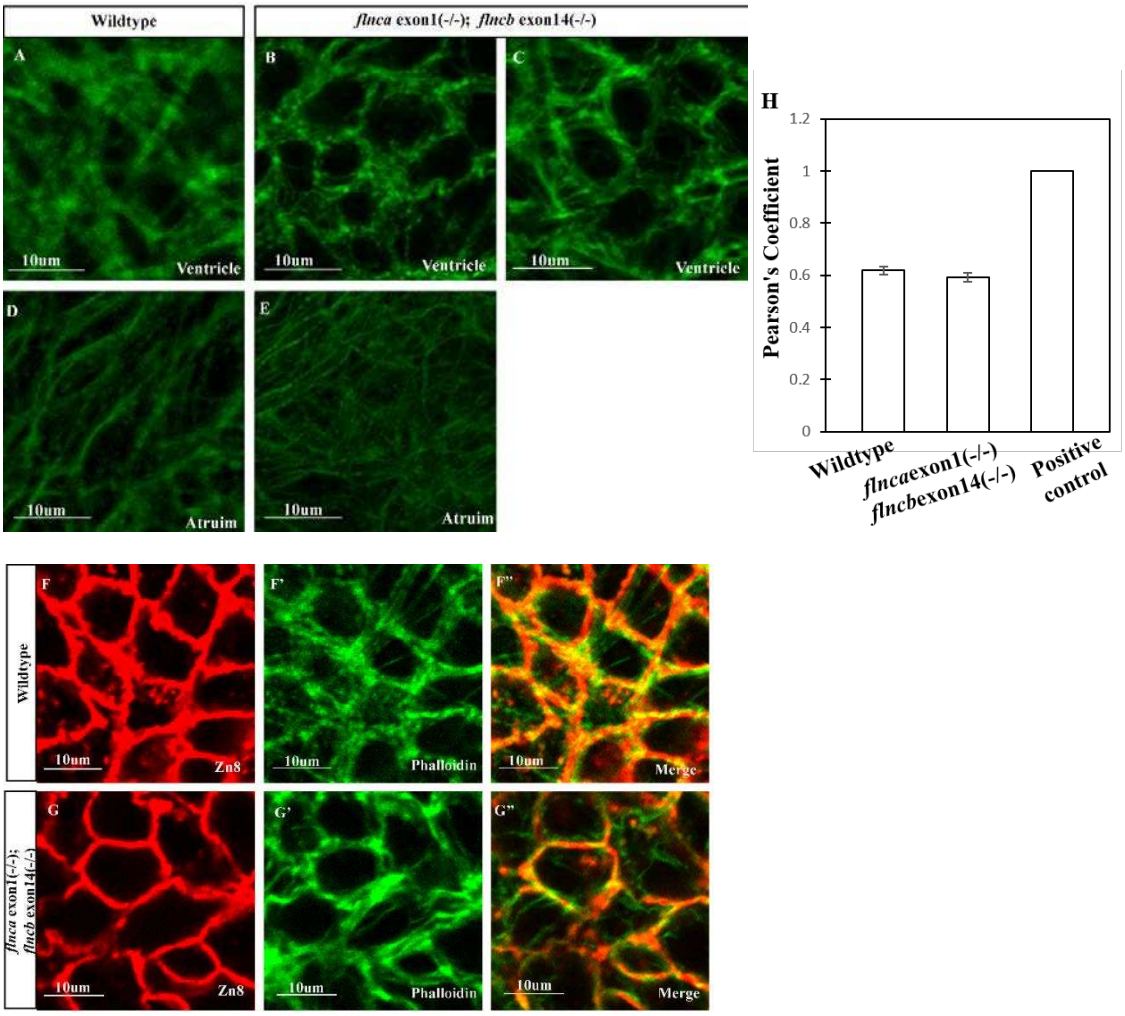

Figure 4.5 Actin filaments assembly disrupted in double Flnc mutant hearts at53hpf. (A-E) 3D images of dissected hearts at 53hpf with Alexa-Fluor Phalloidin labeling to mark actin filaments. **(A, D)** Wildtype ventricle and atrium; actin filaments are assembled in parallel and tightly packed into stiff, thick bundles. **(B, C, E)** double *flnca+b* ventricle and atrium. The actin filaments appear thin, less compacted and curved (arrow), dots or brighter signal are noted (arrowhead). (D) Wildtype actin filaments of the atrium assembled in parallel bundles. (E) Double *flnca+b* were disorganized and less parallel. (F'', G'') 3D images of isolated hearts at 53hpf with two color immunostaining using the zn8 antibodies to mark cell membrane (red) (F,G) and Alexa-Fluor Phalloidin to mark actin filaments (green)(F',G'). The actin filaments are associated with cell membrane at 53hpf. (H) Pearson's coefficient test describes the degree of co-locaization between cell membrane (green) and actin filaments (red). Perfect overlap scores as 1.0 (positive control).

Histological cardiac analysis of *flncb* exon35 allele at 48hpf

The *flncb* exon35 allele is a nonsense mutation in exon 35 out of 48 total exons. We hypothesize that the *flncb* exon 35 allele encodes a truncated protein, which combines with other large costamere molecules to generate protein aggregates in cardiomyocytes of homozygous mutant hearts. In order to examine this hypothesis, we performed histological analysis by using trichrome gomori staining. Sections of cardiac muscle were stained with hematoxylin and eosin followed by trichrome staining. The nucleus, collagen and muscle fibers appear in black/blue, red, and blue color respectively after staining. By 48hpf, the myocardium is present as a single layer. Wildtype cardiac muscle stained with red and the nucleus of the red blood cells appear in purple color (Fig 4.7A). The *flncb* exon35 mutant cardiac muscle appeared thinner (Fig 4.7B). Sections were examined with 200x magnification for the best possible resolution. Using this method, we did not observe any protein aggregation in mutant cardiac muscle.

Flnc mutant embryos exhibit skeletal muscle defect

FLNC is expressed also in skeletal muscle, where, like heart muscle, it specifically localizes to the Z-discs and costameres (Xie, Xu et al. 1998, Thompson, Chan et al. 2000). The large FLNC protein interacts with numerous Z-disc proteins such as actin and myotilin and connects the sarcomere to the sarcolemma via transmembrane proteins such as integrin or sarcoglycan. Thus, FLNC helps to scaffold the structural integrity of the muscle cell. We examined the role of several alleles of *flnc* in maintaining consistent skeletal muscle development of zebrafish, by processing embryos for IHC using Alexa-Fluor phalloidin to mark F-actin. By 24hpf, actin in the wildtype skeletal muscle is arranged in consecutive, tight, and parallel bundles (Fig 4.8A).

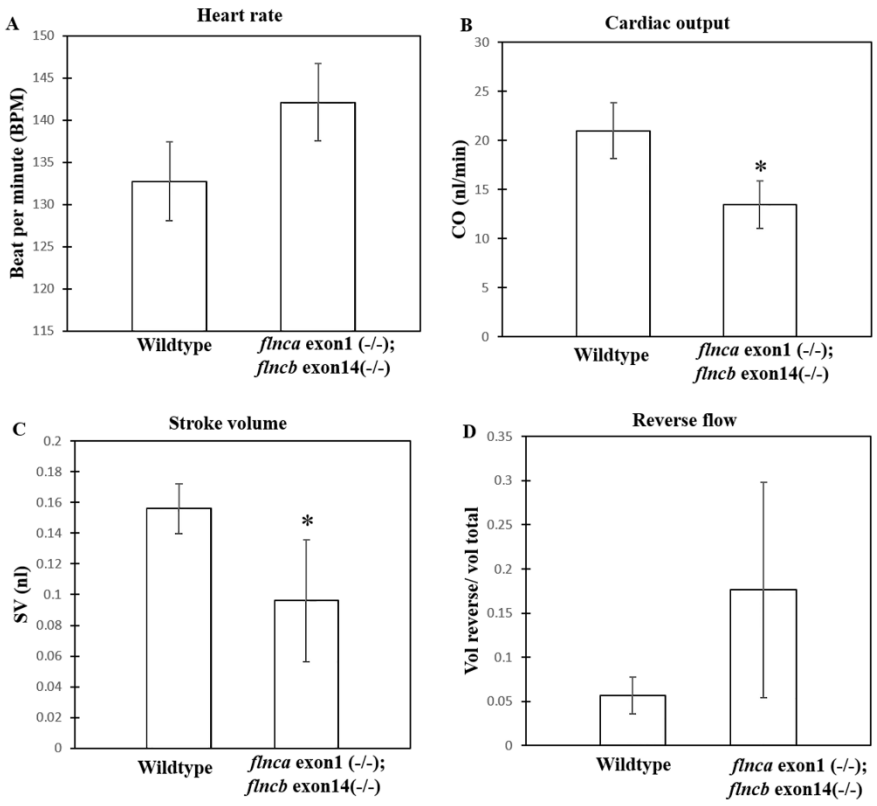

Figure 4.6 Double *flnca+b* mutants exhibit morphological cardiac defects at 53hpf. The impact of phenotypes on heart function and biomechanical factors (CO, HR, RV, and SV) of embryonic zebrafish heart at 53hpf were analyzed using high speed videos and MATLAB software. Morphology of double *flnca* exon1 (-/-); *flncb* exon14 (-/-) hearts was compared to wildtype hearts. (A) Relative to the wildtype average HR (132.6bpm), double *flnca+b* displayed a higher (but not significant) average HR (142.1bpm). (B) CO of double *flnca+b* mutant embryos was significantly decreased compare to wildtype. T-test **P*=0.05. (C) SV of double mutant embryos was decreased relative to wildtype. T-test**P*=0.03. (D) RF fraction of double flnca+b mutant heart was increased but not significantly compared to wildtype. n=5. HR=heart rate, CO= cardiac output, SV=stroke volume,RF, reverse flow, bpm= beats per minute

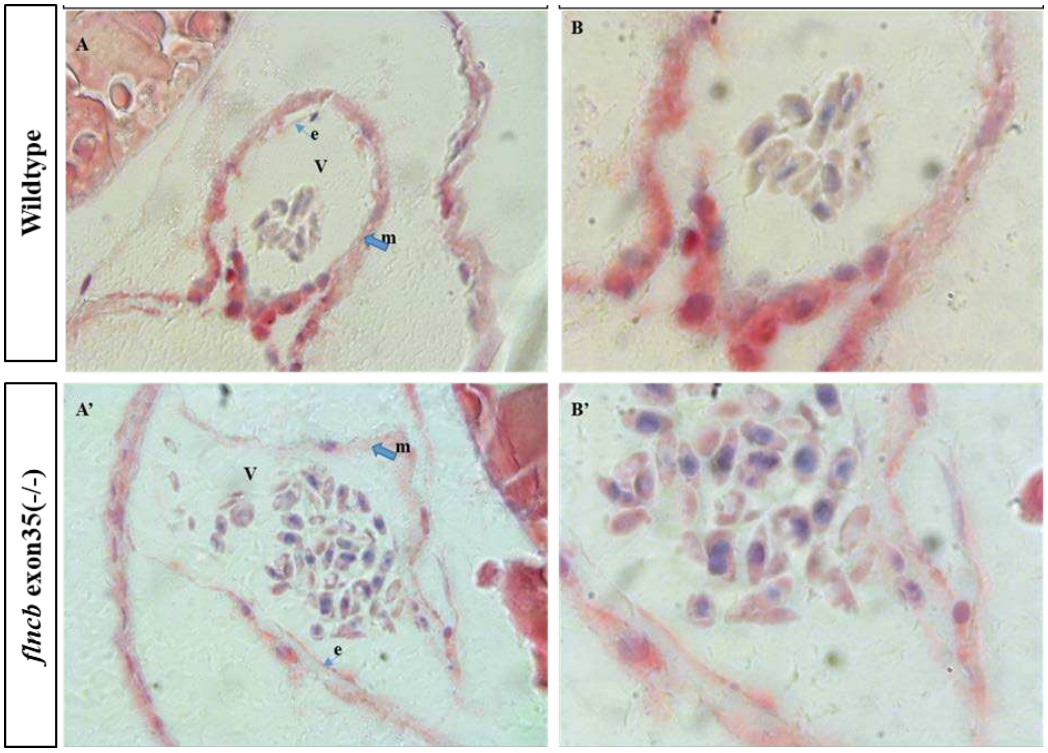

Figure 4.7 Histological analysis for *flncb* exon35 mutant heart at 48hpf. (A-B) Bright field images for ventral sectioned stained with modified trichrome of the ventricle at 48hpf. **(A'-B')** Images were taken under 200X magnification. **(V)** Ventricle, (m) myocardium, **(e)** endocardium**.**

The arrangement of skeletal muscle fibers in homozygous *flnca* exon1 (-/-) somatic muscle strongly resembled those of wildtype (Fig 4.8B), suggesting that *flncb* function is sufficient for muscle fiber arrangement in the absence of *flnca*. In contrast, fibers in somatic muscle of the homozygous *flncb* exon 14 (-/-), *flncb* exon 35 (-/-), or double mutant *flnca+b* embryos exhibited an abnormal phenotype characterized by a less ordered, less streamlined arrangement of actin fibers, and fibers degeneration(Fig. 4.8C, D). Thus, in contrast to the heart, mutant phenotypes could be readily detected in the majority of singly mutant *flncb* exon14 (-/-), and *flncb* exon35 (-/-) embryos. In addition, the single *flncb* exon14 (-/-), and double *flnc*a+b mutant muscles appeared to form fewer actin fibers across the somatic muscles compared to the wildtype or singly mutant *flnca* muscles (Fig 4.8C, E). We predict that*flncb* exon1 (-/-) embyros show no disruption compared to *flncb* exon14 (-/-) and *flncb* exon35 (-/-) phenotypes, we conclude the latter two alleles have gain-of-function affects in skeletal muscle development of zebrafish embryos.

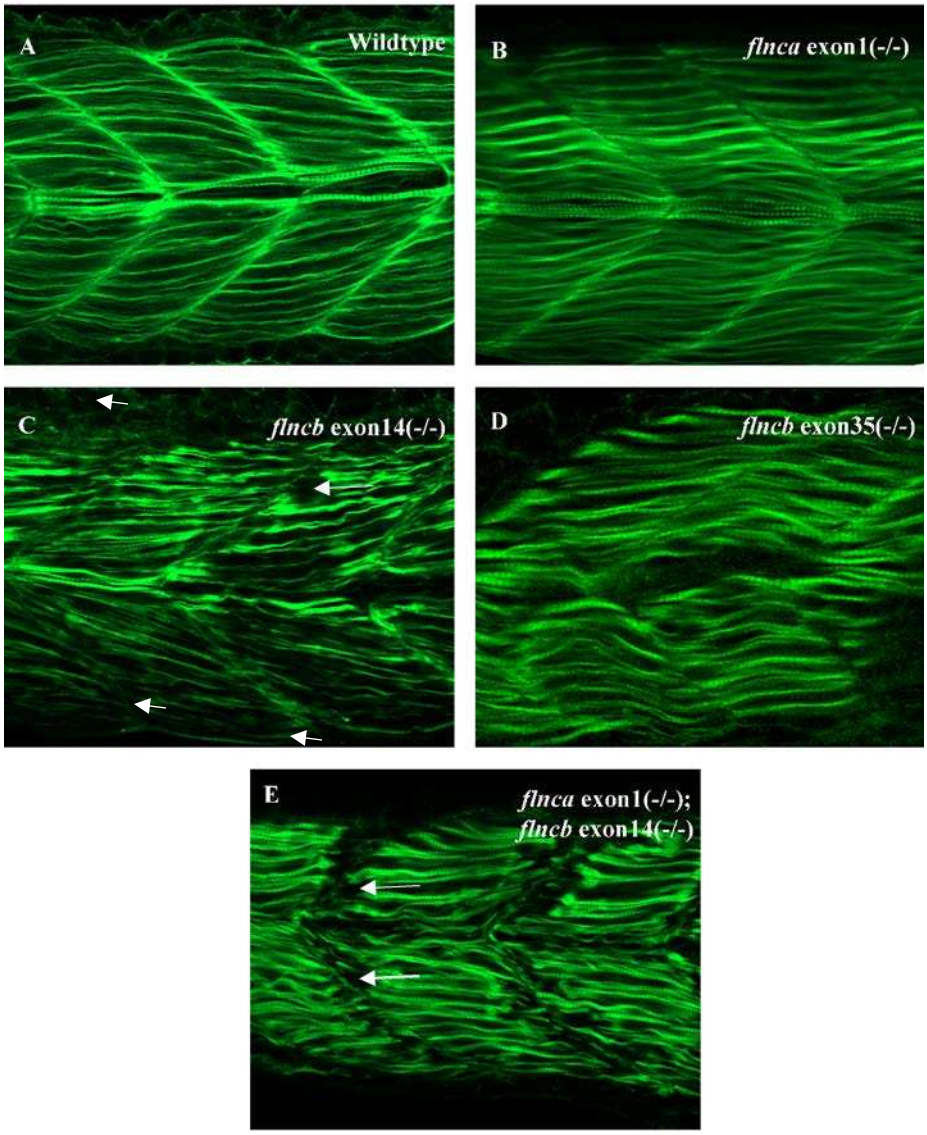

Figure 4.8 Flnc mutants display skeletal muscle defects. (A-E) Images of zebrafish skeletal muscle at 24hpf with Alexa-Fluor Phalloidin labeling actin filaments. **(A)**Wildtype muscle exhibits actin fibers arranged in consecutive, tight, and parallel bundles. **(B)** *flnca* exon1(-/-) skeletal muscle show an arrangement of fibers that resemble wildtype. **(C-E)** *flncb* exon14 (-/-), *flncb* exon35 (-/-), and double *flnca+b* display a less ordered, less streamlined arrangement of fibers, Arrows indicate fibers degeneration. n≥4

Discussion

In this chapter I used zebrafish as a model to investigate how Flnc mutations affect in myofibril and sarcomere assembly. In addition, I examined some mechanisms that cause cardiac muscle disease.

Flnc is required for Z-disc and sarcomere assembly

Based on data from the *Tg (Cmlc2: Cypher: Egfp)* and TEM studies, we conclude that Flnc is required for Z disc formation and arrangement based on several lines of evidence. First, disruption of *flnca* and/or *flncb* by morpholino injection leads to disorder, misalignment and decrease in length of cardiac Z-discs. Second, in many cases the Z-disc formation was delayed or possibly arrested at an earlier stage of development. Third, the length of cardiac sarcomeres was increased in double morphant embryos, which suggests that abnormal Z-disc formation is associated with abnormal sarcomere formation. Morpholino knockdown of *flnca* alone or double knockdown of *flnca+b* produced embryos exhibiting more severe phenotypes in the Z-disc than did morpholino knockdown of *flncb* alone. Two explanations may contribute to this data: 1) the *flnca* morpholino blocks the translation start site, which shields the initiation site and blocks the RNA translation whereas the *flncb* MO targets a conserved splice site and facilitates aberrant splicing of the pre-mRNA. So part of the gene will be translated and partially function. 2) The double knockdown disrupted the two genes which are at least partially redundant.

Using the same approach to analyze genetic mutants, we observed that double mutant *flnca+b* embryos showed phenotypes similar to double morpholino knockdown embryos, including irregular Z-disc organization and alignment and delay of Z-disc maturation. The single *flncb* exon14 (-/-) mutant exhibited a mild Z-disc phenotype which suggests that the single *flncb* exon

14 (-/-) allele has gain of function effects. We are planning to examine the Z-disc assembly of *flncb* exon35 (-/-) allele to determine whether this allele likewise exhibits gain-of-function effects. Fourth, double *flnca+b* mutant exhibits abnormal Z-disc defects such as thickened, missing, or zigzag shapes, which causes myofibrils to deform.

Flnc links actin cytoskeleton to transmembrane proteins such as integrin and sarcoglycan through the costamere (Stossel, Condeelis et al. 2001, Fujita, Mitsuhashi et al. 2012). Interestingly, large extracellular spaces were observed in the cardiac muscle of double *flnca+b* mutant hearts. We could explain this observation due to FLNC interactions. FLNC is a dimer and binds actin filament through its N-terminus and different transmembrane proteins through the two c-terminal domains. This observation suggests that Flnc has an indirect role in cell-cell adhesion. More studies are needed to investigate this hypothesis such as performing dual IHC to mark transmembrane proteins that interact with Flnc to examine whether the juxtaposition in double Flnc mutant hearts differs from wildtype.

Several studies demonstrate that Z-disc proteins are essential for Z-disc assembly and sarcomere formation. Mutations in Titin and Talin disrupt cardiac Z-disc and sarcomere assembly of zebrafish. Talin is a cytoskeleton protein that functions as a linker between cortical actin and integrin, a transmembrane protein (Critchley and Gingras 2008). Titin is a sarcomeric protein that gives muscle cells elasticity and controls the contraction of cardiac muscle (Itoh-Satoh, Hayashi et al. 2002, Seeley, Huang et al. 2007, Wu, Zhang et al. 2015). As another example, knockdown of the cytoskeletal heart-enriched actin-associated proteins (CHAP), which is a Z-disc protein, lead to morphological defects in the embryonic heart of zebrafish and disorganization of Z-discs of zebrafish skeletal muscle at 72 hpf (Beqqali, Monshouwer-Kloots et al. 2010). Based on our

TEM and Cypher transgenic data, we conclude that Flnc functions in Z-disc and sarcomere assembly.

Cardiomyocytes surface area and shape are changed in double mutant Flnc embryos

The Flnc heart phenotypes observed in the double mutants support the hypothesis that Flnc is required for cardiomyocyte morphogenesis. Compared to wildtype, the ventricular OC and IC cells of double Flnc mutant embryos exhibited normal cell surface area and normal cell shape in the chamber ballooning stage. As expected, the shape of ventricular OC cells was more elongated than IC cells for both wildtype and double Flnc mutant embryos. This result is similar to previous studies which examined the shape of OC and IC cells of the wildtype ventricle in the chamber ballooning period (Auman, Coleman et al. 2007). In contrast, we note that in double mutants, cells located in the middle of the ventricular chamber exhibited greater cell cross-sectional area and were elongated more than wildtype. We have not yet explored whether atrial cells show differences in size or shape relative to wildtype hearts. Based on this result Flnc plays a role in ventricular cardiomyocyte size and shape, but contributes more strongly to some cells than others. The IC and OC data for the double mutant group are variable (a few cells exhibit a smaller size) which affects the average.

Analysis of TEM data indicated the presence of large extracellular gaps. Based on this observation, we suggest this space leads to enlargement of the middle cell and several OC, and IC cells.

Flnc controls actin filaments assembly

Actin is an abundant protein that plays a key role in muscle cell contraction. Actin is composed of globular monomers that polymerize to form long filaments. Several actin binding proteins can serve as actin cross linkers and control the stability and length of actin filaments (Fowler 1996).

Several cross linker proteins bind to actin filaments through Calponin homology domain (CH) or immunoglobulin domains (Ig) such as Titin (Puius, Mahoney et al. 1998, Jin 2000). FLNC cross links actin cytoskeleton to transmembrane proteins such as integrin and also interact with actin filaments at Z-disc(Zhou, Borén et al. 2007). We determined that Flnc plays a role in actin filament arrangement. The actin filament bundles of double Flnc mutant embryos appeared thinner, less dense, and in some cases, curved. Additionally, the organization of actin filaments of ventricle and atrium appeared abnormal (distributed in many direction). Actin microfilamts are associated to cell membrane of zebrafish cardiac muscle at 48hpf (Huang, Zhang et al. 2009, Yang, Shih et al. 2014). We performed double IHC staining with phalloidin to mark actin filaments and zn8 to label cell membrane. Although we did not detect an altered quantity of actin filaments overall nor changes in actin and cell membrane colocalization at the cell periphery in Flnc mutant embryos, we did note that the actin filaments network distribution was abnormal; specifically, bundles were not uniformly arranged in parallel but rather, were distributed in all direction.

The high ratio of the frequent interaction of filamin (FLN) to actin microfilaments leads to tighter networks of actin microfilaments (Wang and Singer 1977, Cunningham, Gorlin et al. 1992, Tseng, An et al. 2004). For example in an in vitro study using rabbit skeletal muscle F-actin, a molar ratio of 1:50 ABP filamin :actin leads to the formation of parallel bundles of actin filaments, while an orthogonal network of actin is promoted when the stoichiometry is 1:150-740 (Brotschi, Hartwig et al. 1978, van der Flier and Sonnenberg 2001). Moreover, the type of actin cross-linking proteins present influences the type of actin network built. For example, an *in vitro* mixture of FLN and α-actinin results in the formation of dense actin fibers, while the presence of FLN alone in the mixture leads to orthogonal networks (Schollmeyer, Rao et al. 1978). Myotilin is Z-disc protein and cross linker that interacts directly with FLNC and actin filaments. Myotilin controls

stability of actin assembly and prevents actin disassembly (Salmikangas, van der Ven et al. 2003). Since myotilin interacts directly with FLNC, it's possible that FLNC reinforces the actin cytoskeleton in a way similar to myotilin. More studies are needed to confirm the role of Flnc in assembly of actin microfilaments. These may include: 1) Performing immunoblots to determine whether actin abundance is altered in the absence of FLNC.2) Examine actin microfilaments distribution by using TEM technique.

Histological cardiac analysis of *flncb* exon35 allele at 48hpf

Extensive formation of protein aggregates may produce toxic effects that lead to muscle degeneration. The protein aggregation related to FLNC in cardiac muscle have been found in patients with MFM as well as HCM, or RCM (Valdés-Mas, Gutiérrez-Fernández et al. 2014, Brodehl, Ferrier et al. 2016). The disruption of interaction sites and dimerization domains of FLNC results in the accumulation of many muscle proteins in insoluble cytoplasmic aggregates, which then may produce disease. Several different FLNC mutations generate aggregates, which are proposed to exert toxic effects on the cell (Dalkilic, Schienda et al. 2006, Ruparelia, Zhao et al. 2012). Our histological study did not show protein aggregate in the cardiac muscle. However, a major limitation of this study is that the age of cardiac muscle examined was 48hpf and by this point the heart has developed only a single layer of myocardium. The small size of the cells and the limited tissue made it difficult to observe with confidence that no aggregates were present. To overcome this obstacle, we are performing the histological analysis using sections for 5 dpf hearts. In addition, we plan to perform immunocytochemistry (ICC) with two Z-disc antibodies including Desmin and FLNC to test for colocalization of these two proteins and determine whether they combine to produce aggregate.

Skeletal muscle phenotype vary between different *flnc* alleles

Myofibrillar myopathies (MFMs) are a group of progressive inherited muscle disorders that usually result in severe disability and early death (Latham and Lopez 2015). Mutations in the *FLNC* gene are associated with MFM in human populations across the world. To examine how different zebrafish *flnc* alleles affect skeletal muscle development, F-actin was labelled with Alexa-Fluor-phalloidin. We noted a variable skeletal muscle phenotypes among different *flnc* alleles. Single mutant *flnca* exon1 (-/-) embryos showed normal skeletal muscle. However, single mutant *flncb* exon14 (-/-) or *flncb* exon35 (-/-) embryos, and double mutant *flnca* exon1; *flncb* exon14 embryos exhibited disorder among actin filaments in skeletal muscle of the somites. In addition, single mutant *flncb* exon35 (-/-) embryos had a slightly milder phenotype compared to *flncb* exon14 and double *flnca+b*. If we link the heart phenotype with skeletal muscle phenotype, we find that *flncb* exon14 embryos had a mild-heart, severe-skeletal muscle phenotype whereas *flncb* exon35 (-/-) embryos had a severe-heart, milder-skeletal muscle) phenotype. Interestingly, *flncb* exon14 (-/-) embryos and double *flnca+b* (-/-) embryos exhibited minor degeneration of actin fibers at 24 hpf. Quantification of actin filaments signal of IHC data could confirm our finding. The *sot* mutant, which is a nonsense mutation in *flncb* exon30 of zebrafish, displayed a skeletal muscle phenotype between the 24-somite and 32-somite stages characterized by occasional fibers being lost, which appears as a black gap in the labeled specimen (Ruparelia, Zhao et al. 2012). Although our specimens were labeled with phalloidin instead or myosin, we observed similar black gaps in *flncb* exon14 and double *flnca+b* mutant skeletal muscle marked actin fibers. In addition *sot* mutant displays formation of aggregates positive for myosin immunomarkers (Ruparelia, Zhao et al. 2012).

The cardiac biomechanical factors change in Flnc mutant embryos.

To better understand how mutations in *flnc* alter the heart muscle's response to biomechanical factors, we used a high speed camera to capture and analyze cardiac function in mutant embryos. By 53hpf, the cardiac muscle of double mutant *flnca+b* embryos displayed significantly lower stroke volume and cardiac output, as was observed in human cardiomyopathy (Garfinkel, Seidman et al. 2018). The heart rate and extent of flow retrograde are variable and tended to be greater in double *flnca+b* mutant embryos at 53hpf, although these differences did not reach significance. Changes in these functional factors can lead to changes in cardiac morphology during development that may ultimately lead to heart failure (Begay, Tharp et al. 2016). In contrast to the double mutant embryos, Begay et al found that *flncb* MO injected embryos displayed normal the cardiac output and stroke volume, but the heart rate and flow retrograde were significantly increased (Begay, Tharp et al. 2016). The explanation of these different results may reflect that the double mutant embryos lack all *flnc* function, leading to more severe contractile deficiencies that reduce stroke volume and cardiac output. In contrast, *flncb* morphant embryos are expected to retain function for the *flnca* paralog. *flncb* morphant embryos may experience weaker contractile defects which are insufficient to depress stroke volume and cardiac output, but nevertheless affect patterns of contraction in the heart tube in ways that lead to less efficient forward-propulsion of blood. Further analysis such as flow rate and velocity and more samples may serve to confirm this hypothesis. In conclusion, the significant parallels of cardiac phenotypes in zebrafish *flnca* and *flncb* mutants and progression of human FLNC cardiomyopathies establish zebrafish as an amenable model for mechanistic studies for FLNC function or amelioration of phenotype.

Material and methods

Zebrafish husbandry

All zebrafish (*Danio rerio*) used in this study were obtained from protocols approved by the Colorado State University Animal Care and Use committee (IACUC). Adult zebrafish and larvae were maintained, raised, and staged according to standard protocol as previously described (Westerfield 1993, Nusslein-Volhard and Dahm 2002). Larvae were stored at 28°C in E3 media and developed at 28℃, which is the appropriate temperature for normal development as described by (Kimmel, Ballard et al. 1995). The E3 medium was supplemented with 10−5% methylene blue to overcome growth of mold,

Establishment of mutant crosses

The single *flnca* exon1 (+/-), and *flncb* exon14 (+/-) lines were crossed with transgenic line: *Tg(cmlc2-Cypher: egfp)* (Yang and Xu 2012) marks Z-disc of cardiac muscle with green fluorescent. First, the single heterozygous mutant adult fish of *flnca* exon1 and *flncb* exon 14 were crossed with *Tg(cmlc2-Cypher: egfp)* fish to obtain heterozygous mutant fish of *flnca* exon1 and *flncb* exon 14 fish that express cmlc2-Cypher:EGFP. Then, the single heterozygous mutant fish of *flnca* exon1 and *flncb* exon 14 that express Cypher:EGFP were crossed with single homozygous *flnca* exon1 or *flncb* exon 14 mutant adults respectively to obtain single *flnca* exon1 (-/-)*Tg(cmlc2-Cypher: egfp)*, or *flncb* exon14 (-/-)*Tg(cmlc2-Cypher: egfp)* embryos for experimental analysis. Moreover, to create double mutant embryos that express Cypher EGFP, I crossed *flnca* exon1 (-/-) X *flncb* exon14 (+/-)-*Tg(cmlc2-Cypher: egfp)* and *flncb* exon14 (-/-) X *flnca* exon1 (+/-)-*Tg(cmlc2-Cypher: egfp).*

Genotyping of filamin C various alleles mutant zebrafish that express cmlc2-Cypher-EGFP. Adult fish, 2 to 4 months old, were fin clipped and genomic DNA was extracted using the protocol as described by (Meeker, Hutchinson et al. 2007). Then, PCR was performed. All primers were designed using Primer3 software https://primer3plus.com/cgi-bin/dev/primer3plus.cgi to amplify the DNA locus spanning the mutation. Primer sequence is listed in table (3.1). This PCR product was run on a 0.8% agarose gel and extracted by using QIAquick Gel Extraction Kit (Cat No. /ID: 28706 from Qiagene). The purified DNA samples were submitted to Quintarabio for sequencing following their instructions on following link https://www.quintarabio.com/service/dna_sequencing.

Table 3.1: PCR primer sequences for genotyping mutant lines.

Primer name	**Number in primer file**	**Primer sequance**
flnca sa24724 Fwd	484 Fwd	5'-GGCACAGACCTTGGAGAAGA-'3
flnca sa24724 Rev	485 Rev	5'-CCCTGTCCAGAAACTCCAGC-'3
flncb sa15601 Fwd	482 Fwd	5'-AAAGGGGGCACGAAAACATC-'3
flncb sa15601 Rev	483 Rev	5'-AAACCAGTTTGATGTGTTCCCT-'3
flncb sa11171 Fwd	470 Fwd	5'-GTGGAGCTGGAAGAGGACAG'-3
flncb sa11171 Rev	471 Rev	5-TTGATGGGCTTGATGGGTAT-3
flncb sa20217 Fwd	548 Fwd	5'-CTCCCAGGTGGTCTGTCATT-'3
flncb sa20217 Rev	549 Rev	5'-TTGCCCTCTCTTGTTCATCC-'3

Morpholino injection

The antisense morpholino oligonucleotides were synthesized by Gene Tools (California). The single splice *flncb* MO (*flncb* MO: GAGTTTTCTAATGGCCCTTACCTGC) was used. This

morpholino was designed and verified by (Ruparelia, Zhao et al. 2012). 1-4 cell wildtype and *flnca* exon1 (+/-); *Tg*(*cmlc2-Cypher:EGFP)* embryos were injected with a low dose of *flncb* MO (200 µM) and coinjected with 150 µM P53MO to reduce off-target defects related to ectopic upregulation of the P53 pathway, and consequent non-specific cell death (Campbell, Sinagra et al. 2013). To identify well-injected embryos 1:10 10x rhodamine was included in the morpholino mix as well as 0.3x Danieaus buffer. Before injection, the embryos were transferred using a fire-polished Pasteur pipette from a petri dish to an injection plate. 1-2 cell embryos were injected with morpholino using a Femtojet (Eppendorf). Injection needles were created from 0.75mm inner diameter borosilicate capillary tubes (World Precision Instruments, Sarasota, FL) and pulled on a Sutter P97 Flaming/Brown Micropipette puller using the following program: Heat: 715, Pull: 60, Velocity: 80, Time: 200. After injection, the well injected embryos were scored for positive rhodamine signal at 5hpf

Imaging embryonic heart express cmlc2-Cypher: EGFP

The 48hp embryonic zebrafish hearts were dissected by pulling the heart with forceps as following described protocol (Yang and Xu 2012). All dissected embryo hearts expressed green fluorescent protein from the transgene *Tg(cmlc2-Cypher: EGFP).* The genotypes examined included: 1) wildtype, 2) *flnca* exon1 (-/-), 3) *flncb* exon14 (-/-), 4) *flnca* exon1 (+/-); *flncb* exon14 (+/-), and 5) *flnca* exon1 (-/-) embryos injected with *flncb* MO. Next, the all dissected hearts were transferred to polylysine-coated slides and fixed with 4%paraformaldhyde (PFA) in 1x PBS for 40 min. The fixed hearts were washed with 1xPBS for 3X, for 5 mins each. Lastly, the hearts were mounted with 70% glycerol and gently covered with a coverslip. Images were taken by using a Zeiss LSM 800 laser scanning confocal microscope located in room W5 of the A/Z building.

The post imaging process was performed using Zen blue, image J, and Photoshop software.

Transmission electron microscopy (TEM)

Wildtype, and double mutant *flnca* exon1(-/-); *flncb* exon 14 (-/-) embryos were fixed and processed for TEM based on the procedure of (Ebert, Hume et al. 2005). Samples were sectioned to Silver to pale-gold sections (60nm-90nm) using a diamond knife on a Reichert Ultracut E ultramicrotome (Leica Microsystems AG, Wetzlar, Germany). Then, sections were mounted on formvar-coated slot grids and stained with uranyl acetate and lead citrate. Lastly, the JEOL JEM-1400 TEM (Peabody, Massachusetts) operated at 100 kV and was used to observe all samples.

Immunocytochemistry (ICC)

The 53hpf embryonic zebrafish hearts of wildtype, single mutant *flnca* exon1 (-/-), single mutant *flncb* exon14, and doubly mutant *flnca* exon1 (-/-); *flncb* exon14 (-/-) embryos were dissected by pulling the heart with forceps. Then, the heart samples were transferred to polylysine coated slides. Samples were encircled with the immEdge pen to make a well and placed in the humidified chamber. 20ul LB15 media in 10% fetal bovine serum (FBS) was added to each well. All hearts were then fixed using 4% PFA for 40 mins at room temperature. Next, hearts were rinsed with phosphate buffered saline Triton (PBST, defined as PBS supplemented with 2% Triton), blocked 3x for 5mins, then blocked with 10% sheep serum in PBST for 1 hour at room temperature. After that, the heart samples were incubated with primary antibody and washed, secondary then secondary antibody. The following primary antibodies were used: anti-Alcam at 1:10 dilution and Alexa Fluor 488 phalloidin 1:20 dilution, in 10% sheep serum/PBST for 1 hour at room temperature. The secondary antibody was Alexa Fluor-conjugated anti-mouse antibody at 1:350 dilution in in PBST for 1 hour. Lastly, 10 µl of 70% glycerol was added to each well to mount the heart which were covered with a cover slip. Heart samples were imaged using a Zeiss LSM 800 laser scanning confocal microscope located in room W5 of the A/Z building.

Zebrafish heart structure analysis

Z-disc

Z-disc length and sarcomere length (distance between two Z-discs) of wildtype or mutant hearts were measured at 53hpf. Three Z-lines were measured then averaged per sample. One way ANOVA analysis was used to compare the different between the groups and all pairwise (Tukey test) was performed to test the different among groups. The statistical analysis was applied with Sigma Plot software (version 12.0, Systat Software, San Jose, California), and $P < 0.05$ was considered to be significant.

Cell area

To assess cell area of wildtype and mutant heart samples at 53hpf, cell membranes were labeled by immunocytochemistry using with anti-Alcam antibody (as described above). The encompassed cell area calculated, using image J software. The area of three cells were averaged and counted as one sample. Differences among groups was analyzed using one way ANOVA followed by Tukey tests with SigmaPlot software (version 12.0, Systat Software, San Jose, California), and $P < 0.05$ was considered to be significant.

Zebrafish heart function analysis

The hearts of wildtype or doubly mutant *flnca* exon1 (-/-); *flncb* exon 14(-/-) zebrafish embryos were embedded in 1.5% low melting agarose gel, the ventral side up. Then, the embryo hearts were imaged using a high-speed camera connected to a bright field stereomicroscope. All videos were recorded at 1,600 frames/s with a resolution of 1,310 pixels/mm. Heart rate, blood velocity, and the diameter of the atrioventricular junction orifice were measured using a spatiotemporal plot extracted from the video sequence. Stroke volume (SV) is defined as the net volume of blood

pumped to the body per cardiac cycle, and was created by integrating the instantaneous flow rate curve over an entire cardiac cycle. Cardiac output is obtained from multiplying the SV times by the heart rate. The retrograde (reverse) fraction or flow (RF) is known as the portion of total blood that moves in the reverse path through the AVG over the course of 1 cardiac cycle. The RF was measured as a ratio of the volume of retrograde-moving blood divided by the volume of forward-moving blood. Multiple comparisons were performed using one way ANOVA and Tukey test with SigmaPlot software (version 12.0, Systat Software, San Jose, California), and $P < 0.05$ was considered to be significant.

Histology study

Wildtype, doubly mutant *flnca* exon1 (-/-); *flncb* exon14 (-/-), and *flncb* exon 35 (-/-) zebrafish embryos were fixed with 4% PFA at 72hpf for 4 hours at room temperature or overnight at 4°C. Fixed embryos were passed through dehydration and resin infiltration processes as follows:

50% EtOH/50% water	-	15 min
70% EtOH/30% water	-	15 min
90% EtOH/10% water	-	10 min
100% EtOH	-	10 min
1:1 EtOH:Resin	-	1hour
100% Resin	-	1 hours

Then, the embryos were embedded in an embedding mold containing 100% LR White resin. Aclar film was placed on top of the resin-filled molds to exclude oxygen, and the embedded embryos were incubated at 65°C oven for overnight to allow the resin to polymerize. The hardened LR White blocks were sectioned by using a Sorvall Porter Blum Ultra-Microtome Model MT-2 with sections having the thickness of 4um. All sections were placed on charged slides and process using the Trichrome Stain Kit (Modified Gomori's) from ScyTek followed protocol manufacture.

Lastly, the sectioned samples were imaged by the Zeiss LSM 800 laser scanning confocal microscope located in room W5 of the A/Z building.

Chapter5: Overall summary and future directions

Cardiomyopathies can be defined as a heterogeneous class of diseases of the myocardium linked to medical and/or electrical dysfunction that normally exhibit inappropriate ventricular hypertrophy or dilation as a result of different etiologies, which are hereditary in most cases (Maron, Towbin et al. 2006). While cardiomyopathies can either be restricted to the heart, they can also be part of generalized systemic disorders. Often, they result in cardiovascular death or a progressive heart failure-related disability (Maron, Towbin et al. 2006).

Mutations in different genes encoding cardiac proteins are responsible for familial cardiomyopathy disease. However, most of the genetic alterations that cause inherited cardiomyopathies are still unknown (Dellefave and McNally 2010, Jefferies and Towbin 2010, Valdés-Mas, Gutiérrez-Fernández et al. 2014, McNally and Mestroni 2017). We reported recently a novel splicing variant of the filaminC (*FLNC*) gene in three unrelated families who suffer cardiomyopathy. This finding supports the hypothesis that mutations in the *FLNC* gene are linked to heritable cardiomyopathy in humans (Begay, Tharp et al. 2016).

The FLN genes encode large homodimer proteins of 240-260 kDa, which are essential for cellular differentiation (Gorlin, Yamin et al. 1990, Razinia, Mäkelä et al. 2012, Sethi, Seppälä et al. 2014). Developmental expression of *FLNC* occurs in skeletal muscles and in cardiac muscle. The FLNC protein interacts with many z-disc proteins and also links many cell membrane proteins to cortical actin fibers, which underlies its fundamental role in the organization of z-disc architecture and actin fibers network (van der Ven, Obermann et al. 2000). Moreover, filaminC links the costameric complexes with z-disc proteins. Thus, filaminC has a role in force transmission from the sarcomere to the sarcolemma (Peter, Cheng et al. 2011).

To date, few studies have investigated the relationship between cardiomyopathy and FLNC (Begay, Tharp et al. 2016, Begay, Graw et al. 2018, Nozari, Aghaei-Moghadam et al. 2018) Interestingly, alteration in *FLNC* genes have been linked to myofibrillar myopathy (MFM), a type of muscular dystrophy that affects muscle function and causes muscle weakness (Selcen and Engel 2011, Bührdel, Hirth et al. 2015). Some patients suffer from both MFM and cardiomyopathy and some develop either MFM or cardiomyopathy.

To comprehend in detail the contribution of FLNC to cardiac phenotypes, we used zebrafish as an animal model in this project. Zebrafish are a useful model to study cardiovascular disease, due to the unique features of embryos that allow researchers to study heart development, even when defects are severe. Zebrafish have two *flnc* paralogous genes (*flnca* and *flncb*), which are around 82% identical at the amino acid level. However, the zebrafish *flncb* paralog is most closely related to the human FLNC, as it is ~ 84% identical at the amino acid level compared to *flnca* with ~80% identity. Our studies were implemented with the aim of determining FLNC`s functional role in development of cardiac defect in zebrafish.

Overall conclusions

Aim1

To better understand how mutations in FLNC contribute to cardiac phenotypes, we created zebrafish loss-of-function models for two *flnca* and *flncb* paralogous genes using a MO knockdown approach.

Knock-down of *flnca* or *flncb* via MO injection resulted in abnormal heart and skeletal muscle development. The *flnca* MO targeted the region of *flnca* encoding the translation start site, with the expectation that mRNA could be transcribed but not translated. The *flncb* MO targeted the

splice site region of *flncb* (Ruparelia, Zhao et al. 2012). A deficiency of either Flnca or Flncb disrupted cardiac morphogenesis, affecting looping morphogenesis, contractility, and blood flow. These phenotypes were somewhat stronger in *flnca* knockdown embryos than in *flncb* knockdown embryos, especially with regard to the looping angle and decrease in ventricle size. Cardiac defects in zebrafish *flnca* and *flncb* knockdowns share some phenotypic features with some patients who suffer from dilated cardiomyopathy, such as poor systolic function which alters the pattern of blood flow, and low cardiac output (Begay, Tharp et al. 2016).

Aim2

In this aim, we tested the function of the Flnca and Flncb proteins in zebrafish heart development. We used a series of *flnc* alleles, including *flnca* exon1 and *flncb* exon1 alleles, which contain nonsense mutations encoding stop codons in their actin binding domains, as well as *flncb* exon14 and 35 alleles, which contain nonsense mutations encoding stop codons in the immunoglobulin (Ig) repeat regions (Fig 3.1a,b). No clear heart phenotype was observed in putative null homozygous *flnca* exon1 or *flncb* exon1 embryos at 24, 48, or 72 hpf (Fig 3.3, 4C)).

Double *flnca* exon1 and *flncb* exon14 mutant embryos exhibited heart and skeletal muscle phenotypes characterized by abnormal or stringy heart tubes as well as swimming defects or even paralysis (Fig 3.5b). I conclude that the *flnca* and *flncb* paralogs have redundant functions in zebrafish heart and skeletal muscle development, based on several lines of evidence. The single *flnca* exon1 and *flncb* exon14 mutants had minor heart morphology phenotypes, such as an increased looping angle and decreased heart rate. Contrastingly, the double homozygote embryos displayed stronger heart morphology phenotypes, including the increased looping angle and decreased heart rate phenotypes, as well as decreased ventricle size, poor contractility and mild or severe cardiac edema. In addition, the cardiac phenotype of the double mutant embryos was lethal.

Putative truncation mutant *flncb* exon14 and *flncb* exon35 mutants did show cardiac phenotypes but in a smaller fraction of embryos than expected based on genotype. Although these phenotypes are not dominant, we consider them to constitute gain of function phenotypes since they are more severe than those of the null mutants. Moreover, the *flncb* exon 35 mutation, which has a nonsense mutation at exon35 encoding a stop codon at the C-terminus, caused heart and skeletal muscle phenotypes at 48hpf (although with variable expressivity and penetrance). This phenotype is characterized by either cardiac edema or stringy chambers, or mild edema and abnormal chambers, as well as swimming defects. This finding suggests two primary conclusions. First, these two alleles have a gain-of-function effect that may derive from a truncated protein which interferes with the wild type protein in cardiac and skeletal muscle cells. Although this type of effect is frequently described as "dominant negative" in this case heterozygous individuals do not display any abnormal phenotypes. However, to verify this conclusion, it will be necessary to confirm by Western blot that the null alleles actually are null (do not encode any protein) and that the truncated alleles do encode transcripts that are translated.

Aim3

In this aim I used zebrafish as a model to investigate how Flnc mutations affect myofibril architecture and sarcomere assembly. Based on data from the *Tg (Cmlc2: Cypher: Egfp)* transgenic line, and TEM studies of cardiac tissue, we conclude that Flnc is required for z disc formation and arrangement (Fig4.1; 4.3).

The Flnc heart phenotypes observed in the double mutants support the hypothesis that Flnc is required for cardiomyocyte morphogenesis. I note that in double mutants, cells located in the middle of the ventricular chamber exhibited greater cell cross-sectional area and were elongated

more than wildtype. Based on this result Flnc plays a role in ventricular cardiomyocyte size and shape.

FLNC protein cross links the actin cytoskeleton to transmembrane proteins such as integrin and also interact with actin filaments at the z-disc (Zhou, Borén et al. 2007). I determined that Flnc plays a role in actin filament arrangement. The actin filament bundles of double Flnc mutant embryos appeared thinner, less dense, and in some cases, curved. Additionally, the organization of actin filaments of ventricle and atrium appeared abnormal (distributed in many directions).

In conclusion, based on this study, zebrafish is a good model to study Flnc function and disease mechanism. Additionally, Flnc plays an important role in zebrafish heart development. Specifically, Flnc is required for normal z disc assembly and actin cytoskeleton arrangement.

Future directions

Zebrafish have two *flnc* paralogous genes (*flnca* and *flncb*), which are around 82% identical at the amino acid level. However, the zebrafish *flncb* paralog is most closely related to the human FLNC, as it is ~ 84% identical at the amino acid level compared to *flnca* with ~80% identity. Although this project shows that indeed, *flnca* and *flncb* genes have essential roles in cardiac morphogenesis, many research questions and technical challenges need to be elucidated.

In chapter 2, the MO data demonstrate that Flnc is required for normal zebrafish heart development and indicate that the loss of *flnca* and/or *flncb* leads to cardiac dysgenesis through defects in cardiac morphology, ultrastructure, and biomechanical dynamics. However, a limitation of this study is that MO reagents may cause off-target effects, and may not achieve 100% efficacy in gene knockdown, although we attempted to mitigate this potential problem by coinjecting the embryos with p53 MO to reduce off-target effects. To better interpret the efficacy of MO knockdown, a Western blot procedure using antibodies specific to Flnca and

Flncb could be used to determine whether any translated protein is present in knockdown animals. Zebrafish-specific Flnca and Flncb antibodies are not available yet but we could use human FLNC antibody.

In chapter 3, mutation of *flnca* or *flncb* genes that generate a stop codon in exon 1 exhibited no clear phenotype in zebrafish heart and skeletal muscle development. Alternatively, the *flncb* exon 35 mutation, which has a nonsense mutation at exon35 encoding a stop codon at the C-terminus, caused heart and skeletal muscle phenotypes at 48hpf (although with variable expressivity and penetrance). This finding suggests two primary conclusions. First, the *flncb* exon 35 allele may have a dominant negative (gain-of-function) effect that may derive from a truncated protein which interferes with the wild type protein in cardiac and skeletal muscle cells. A gain-of-function (dominant negative) phenotype may arise if the truncated protein is misfolded and leads to protein aggregation, which becomes toxic to the cell. We started investigating whether mutation of *flncb* exon35 produces cytoplasmic protein aggregates by staining sectioned embryo hearts with trichrome gomori, which labels the nuclei in black, cytoplasm and muscle in red, and collagen in blue. However we were not able to confidently assess whether aggregates were present since to the cardiomyocyte layer area is comprised only of a single layer of small cells in hearts of 48 hpf embryos. Alternatively, we suggest performing immunocytochemistry (ICC) experiments to label candidate proteins that may aggregate along with aberrant FLNC protein. These candidate proteins are normally located within the sarcomere or Z-disc, and include Desmin, Myosin, and Actin (Brodehl, Hedde et al. 2012, Ruparelia, Zhao et al. 2012, Guglielmi, Tomelleri et al. 2018). We anticipate that this experiment will provide us more readily visible data on aggregation while also informing us of the co-aggregation of other proteins anticipated to be present. Moreover, by studying the effect of different *flnc* alleles on the

heart and skeletal muscle development we hope to determine why different mutations in Flnc cause cardiomyopathy and/ or MFM.

In chapter 4, we discussed how Flnc mutations affect myofibril and sarcomere assembly. According to TEM data, we found that homozygous mutations in doubly mutant *flnca* and *flncb* hearts leads to delays in Z-disc formation and disrupts sarcomere assembly. Interestingly, large extracellular spaces were observed in the cardiac muscle of doubly mutant *flnca* and *flncb* homozygous mutant hearts. We hypothesize that this observation is due to disrupted FLNC interactions with costamere proteins important in the cardiac intercalated discs. A weakened intercalated disc may lead to separation of cardiomyocytes. FLNC is a dimer and binds actin filaments through its N-terminus and different transmembrane proteins through the two C-terminal domains. This observation suggests that Flnc has an indirect role in cell-cell adhesion. More studies are needed to investigate this hypothesis such as performing dual IHC to mark transmembrane proteins that interact with Flnc to examine whether the juxtaposition of intercalated discs in doubly mutant Flnc mutant hearts differs from wildtype.

References

Abelmann, W. H. (1984). "Classification and natural history of primary myocardial disease." Progress in cardiovascular diseases **27**(2): 73-94.

Aguzzi, A. and T. O'connor (2010). "Protein aggregation diseases: pathogenicity and therapeutic perspectives." Nature reviews Drug discovery **9**(3): 237.

Arbustini, E., et al. (2013). "The MOGE (S) classification for a phenotype–genotype nomenclature of cardiomyopathy: endorsed by the World Heart Federation." Journal of the American College of Cardiology **62**(22): 2046-2072.

Arbustini, E., et al. (2014). "The MOGE (S) classification of cardiomyopathy for clinicians." Journal of the American College of Cardiology **64**(3): 304-318.

Arunachalam, M., et al. (2013). "Natural history of zebrafish (Danio rerio) in India." Zebrafish **10**(1): 1-14.

Auman, H. J., et al. (2007). "Functional modulation of cardiac form through regionally confined cell shape changes." PLoS biology **5**(3): e53.

Avila-Smirnow, D., et al. (2010). "P2. 18 A novel missense FLNC mutation causes arrhythmia and late onset myofibrillar myopathy with particular histopathology features." Neuromuscular Disorders **20**(9): 623-624.

Baker, K., et al. (1997). "Defective "pacemaker" current (Ih) in a zebrafish mutant with a slow heart rate." Proceedings of the National Academy of Sciences **94**(9): 4554-4559.

Bakkers, J. (2011). "Zebrafish as a model to study cardiac development and human cardiac disease." Cardiovascular research **91**(2): 279-288.

Bartman, T., et al. (2004). "Early myocardial function affects endocardial cushion development in zebrafish." PLoS biology **2**(5): e129.

Beatham, J., et al. (2004). "Filamin C interacts with the muscular dystrophy KY protein and is abnormally distributed in mouse KY deficient muscle fibres." Human molecular genetics **13**(22): 2863-2874.

Bedell, V. M., et al. (2011). "Lessons from morpholino-based screening in zebrafish." Briefings in functional genomics **10**(4): 181-188.

Beffagna, G., et al. (2005). "Regulatory mutations in transforming growth factor-β3 gene cause arrhythmogenic right ventricular cardiomyopathy type 1." Cardiovascular research **65**(2): 366-373.

Begay, R. L., et al. (2018). "Filamin C Truncation Mutations Are Associated With Arrhythmogenic Dilated Cardiomyopathy and Changes in the Cell–Cell Adhesion Structures." JACC: Clinical Electrophysiology **4**(4): 504-514.

Begay, R. L., et al. (2016). "FLNC gene splice mutations cause dilated cardiomyopathy." JACC: Basic to Translational Science: 37.

Beis, D., et al. (2005). "Genetic and cellular analyses of zebrafish atrioventricular cushion and valve development." Development **132**(18): 4193-4204.

Beqqali, A., et al. (2010). "CHAP is a newly identified Z-disc protein essential for heart and skeletal muscle function." Journal of cell science: jcs. 063859.

Boffa, G. M., et al. (1991). "Cardiomyopathy: a necessary revision of the WHO classification." International journal of cardiology **30**(1): 1-7.

Bournele, D. and D. Beis (2016). "Zebrafish models of cardiovascular disease." Heart failure reviews **21**(6): 803-813.

Braunwald, E. (2017). "Cardiomyopathies: An Overview." Circulation research **121**(7): 711-721.

Brigden, W. (1957). "Uncommon myocardial diseases: the non-coronary cardiomyopathies." The Lancet **270**(7008): 1243-1249.

Brodehl, A., et al. (2016). "Mutations in FLNC are associated with familial restrictive cardiomyopathy." Human mutation **37**(3): 269-279.

Brodehl, A., et al. (2017). FLNC (Filamin-C): A New (er) Player in the Field of Genetic Cardiomyopathies, Am Heart Assoc.

Brotschi, E. A., et al. (1978). "The gelation of actin by actin-binding protein." Journal of Biological Chemistry **253**(24): 8988-8993.

Brown, D. R., et al. (2016). "Advances in the study of heart development and disease using zebrafish." Journal of cardiovascular development and disease **3**(2): 13.

Bryant, P. J. and P. Simpson (1984). "Intrinsic and extrinsic control of growth in developing organs." The Quarterly Review of Biology **59**(4): 387-415.

Bührdel, J. B., et al. (2015). "In vivo characterization of human myofibrillar myopathy genes in zebrafish." Biochemical and biophysical research communications **461**(2): 217-223.

Burke, M. A., et al. (2016). "Clinical and mechanistic insights into the genetics of cardiomyopathy." Journal of the American College of Cardiology **68**(25): 2871-2886.

Campbell, N., et al. (2013). "Whole exome sequencing identifies a troponin T mutation hot spot in familial dilated cardiomyopathy." PLoS One **8**(10): e78104.

Chakarova, C., et al. (2000). "Genomic structure and fine mapping of the two human filamin gene paralogues FLNB and FLNC and comparative analysis of the filamin gene family." Human genetics **107**(6): 597.

Chernyavskaya, Y., et al. (2012). "Voltage-gated calcium channel CACNB2 (β2. 1) protein is required in the heart for control of cell proliferation and heart tube integrity." Developmental Dynamics **241**(4): 648-662.

Chiang, W., et al. (2000). "Filamin isogene expression during mouse myogenesis." Developmental Dynamics **217**(1): 99-108.

Christoffels, V. M., et al. (2000). "Chamber formation and morphogenesis in the developing mammalian heart." Developmental biology **223**(2): 266-278.

Claeys, K. G. and M. Fardeau (2013). Myofibrillar myopathies. Handbook of clinical neurology, Elsevier. **113:** 1337-1342.

Corrado, D., et al. (2017). "Arrhythmogenic cardiomyopathy." Circulation research **121**(7): 784-802.

Critchley, D. R. and A. R. Gingras (2008). "Talin at a glance." Journal of cell science **121**(9): 1345-1347.

Cunningham, C. C., et al. (1992). "Actin-binding protein requirement for cortical stability and efficient locomotion." Science **255**(5042): 325-327.

Dabiri, G. A., et al. (1997). "Myofibrillogenesis visualized in living embryonic cardiomyocytes." Proceedings of the National Academy of Sciences **94**(17): 9493-9498.

Dabrowska, R., et al. (1985). "Dual effect of filamin on actomyosin ATPase activity." Journal of Muscle Research & Cell Motility **6**(1): 29-42.

Dalkilic, I., et al. (2006). "Loss of FilaminC (FLNc) results in severe defects in myogenesis and myotube structure." Molecular and cellular biology **26**(17): 6522-6534.

Davies, M. (1984). "The cardiomyopathies: a review of terminology, pathology and pathogenesis." Histopathology **8**(3): 363-393.

Davies, M. (2000). "The cardiomyopathies: an overview." Heart **83**(4): 469-474.

Day, S. J. and P. A. Lawrence (2000). "Measuring dimensions: the regulation of size and shape." Development **127**(14): 2977-2987.

Dellefave, L. and E. M. McNally (2010). "The genetics of dilated cardiomyopathy." Current opinion in cardiology **25**(3): 198.

Duff, R. M., et al. (2011). "Mutations in the N-terminal actin-binding domain of filamin C cause a distal myopathy." The American Journal of Human Genetics **88**(6): 729-740.

Dunn, W. (1990). "Studies on the mechanisms of autophagy: formation of the autophagic vacuole." The Journal of cell biology **110**(6): 1923-1933.

Ebert, A., et al. (2005). "Calcium extrusion is critical for cardiac morphogenesis and rhythm in embryonic zebrafish hearts." Proceedings of the National Academy of Sciences **102**(49): 17705-17710.

Elliott, P. M. (2013). "Classification of cardiomyopathies: evolution or revolution?" Journal of the American College of Cardiology **62**(22): 2073-2074.

Engeszer, R. E., et al. (2007). "Zebrafish in the wild: a review of natural history and new notes from the field." Zebrafish **4**(1): 21-40.

Fahed, A. C., et al. (2013). "Genetics of congenital heart disease: the glass half empty." Circulation research **112**(4): 707-720.

Faulkner, G., et al. (2000). "FATZ, a filamin-, actinin-, and telethonin-binding protein of the Z-disc of skeletal muscle." Journal of Biological Chemistry **275**(52): 41234-41242.
Feng, J., et al. (2002). "Mutations in the dystrophin gene are associated with sporadic dilated cardiomyopathy." Molecular genetics and metabolism **77**(1): 119-126.

Feng, Y., et al. (2006). "Filamin A (FLNA) is required for cell–cell contact in vascular development and cardiac morphogenesis." Proceedings of the National Academy of Sciences **103**(52): 19836-19841.

Forouhar, A. S., et al. (2006). "The embryonic vertebrate heart tube is a dynamic suction pump." Science **312**(5774): 751-753.

Fowler, V. M. (1996). "Regulation of actin filament length in erythrocytes and striated muscle." Current opinion in cell biology **8**(1): 86-96.

Fox, J. W., et al. (1998). "Mutations in filamin 1 prevent migration of cerebral cortical neurons in human periventricular heterotopia." Neuron **21**(6): 1315-1325.

Franzini-Armstrong, C. and K. R. Porter (1963). "The Z disc of skeletal muscle fibrils." Zeitschrift für Zellforschung und mikroskopische Anatomie **61**(5): 661-672.

Frey, N. and E. N. Olson (2002). "Calsarcin-3, a novel skeletal muscle-specific member of the calsarcin family, interacts with multiple Z-disc proteins." Journal of Biological Chemistry.

Fucini, P., et al. (1999). "Molecular architecture of the rod domain of the Dictyostelium gelation factor (ABP120) 1." Journal of molecular biology **291**(5): 1017-1023.

Fujita, M., et al. (2012). "Filamin C plays an essential role in the maintenance of the structural integrity of cardiac and skeletal muscles, revealed by the medaka mutant zacro." Developmental biology **361**(1): 79-89.

Fürst, D. O., et al. (2013). "Filamin C-related myopathies: pathology and mechanisms." Acta neuropathologica **125**(1): 33-46.

Garfinkel, A. C., et al. (2018). "Genetic pathogenesis of hypertrophic and dilated cardiomyopathy." Heart failure clinics **14**(2): 139-146.

Garrity, D. M., et al. (2002). "The heartstrings mutation in zebrafish causes heart/fin Tbx5 deficiency syndrome." Development **129**(19): 4635-4645.

Gehmlich, K., et al. (2010). "Ponsin interacts with Nck adapter proteins: implications for a role in cytoskeletal remodelling during differentiation of skeletal muscle cells." European journal of cell biology **89**(5): 351-364.
Gerhard, G. S., et al. (2002). "Life spans and senescent phenotypes in two strains of Zebrafish (Danio rerio)." Experimental gerontology **37**(8-9): 1055-1068.

Glasauer, S. M. and S. C. Neuhauss (2014). "Whole-genome duplication in teleost fishes and its evolutionary consequences." Molecular genetics and genomics **289**(6): 1045-1060.

Glick, D., et al. (2010). "Autophagy: cellular and molecular mechanisms." The Journal of pathology **221**(1): 3-12.

Glickman, N. S. and D. Yelon (2002). Cardiac development in zebrafish: coordination of form and function. Seminars in cell & developmental biology, Elsevier.

Go, A. S., et al. (2013). "Heart disease and stroke statistics—2013 update." Circulation **127**(1): e6-e245.

Golbus, J. R., et al. (2014). "Targeted analysis of whole genome sequence data to diagnose genetic cardiomyopathy." Circulation: Genomic and Precision Medicine: CIRCGENETICS. 113.000578.

Gomer, R. H. and E. Lazarides (1981). "The synthesis and deployment of filamin in chicken skeletal muscle." Cell **23**(2): 524-532.

Gomer, R. H. and E. Lazarides (1983). "Highly homologous filamin polypeptides have different distributions in avian slow and fast muscle fibers." The Journal of cell biology **97**(3): 818-823.

Gómez, J., et al. (2017). "Screening of the Filamin C Gene in a Large Cohort of Hypertrophic Cardiomyopathy PatientsCLINICAL PERSPECTIVE." Circulation: Genomic and Precision Medicine **10**(2): e001584.

Gontier, Y., et al. (2005). "The Z-disc proteins myotilin and FATZ-1 interact with each other and are connected to the sarcolemma via muscle-specific filamins." J Cell Sci **118**(16): 3739-3749.

Goodwin, J. (1974). "Prospects and predictions for the cardiomyopathies." Circulation **50**(2): 210-219.

Goodwin, J., et al. (1961). "Clinical aspects of cardiomyopathy." British medical journal **1**(5219): 69.

Goodwin, J. and C. Oakley (1972). "The cardiomyopathies." British heart journal **34**(6): 545.

Gorlin, J. B., et al. (1990). "Human endothelial actin-binding protein (ABP-280, nonmuscle filamin): a molecular leaf spring." The Journal of cell biology **111**(3): 1089-1105.

Guergueltcheva, V., et al. (2011). "Distal myopathy with upper limb predominance caused by filamin C haploinsufficiency." Neurology **77**(24): 2105-2114.

Gut, P., et al. (2017). "Little Fish, Big Data: Zebrafish as a Model for Cardiovascular and Metabolic Disease." Physiological reviews **97**(3): 889-938.

Guyon, J. R., et al. (2003). "Calpain 3 cleaves filamin C and regulates its ability to interact with γ-and δ-sarcoglycans." Muscle & Nerve: Official Journal of the American Association of Electrodiagnostic Medicine **28**(4): 472-483.

Hall, C. L., et al. (2018). "Frequency of genetic variants associated with arrhythmogenic right ventricular cardiomyopathy in the genome aggregation database." European Journal Of Human Genetics: 1.

Hart, A. W., et al. (2006). "Cardiac malformations and midline skeletal defects in mice lacking filamin A." Human molecular genetics **15**(16): 2457-2467.

Harvey, P. A. and L. A. Leinwand (2011). "Cellular mechanisms of cardiomyopathy." The Journal of cell biology **194**(3): 355-365.

Hensley, N., et al. (2015). "Hypertrophic cardiomyopathy: a review." Anesthesia & Analgesia **120**(3): 554-569.

Herman, D. S., et al. (2012). "Truncations of titin causing dilated cardiomyopathy." New England Journal of Medicine **366**(7): 619-628.

Himmel, M., et al. (2003). "The limits of promiscuity: isoform-specific dimerization of filamins." Biochemistry **42**(2): 430-439.

Hock, R. S., et al. (1990). "Purification of human smooth muscle filamin and characterization of structural domains and functional sites." Biochemistry **29**(40): 9441-9451.

Holmes, W. B. and C. L. Moncman (2008). "Nebulette interacts with filamin C." Cell motility and the cytoskeleton **65**(2): 130-142.

Hove, J. R., et al. (2003). "Intracardiac fluid forces are an essential epigenetic factor for embryonic cardiogenesis." Nature **421**(6919): 172.

Howe, K., et al. (2013). "The zebrafish reference genome sequence and its relationship to the human genome." Nature **496**: 498.

Huang, W., et al. (2009). "Myofibrillogenesis in the developing zebrafish heart: A functional study of tnnt2." Developmental biology **331**(2): 237-249.

Hughes, S. E. and W. J. McKenna (2005). "New insights into the pathology of inherited cardiomyopathy." Heart **91**(2): 257-264.

Itoh-Satoh, M., et al. (2002). "Titin mutations as the molecular basis for dilated cardiomyopathy." Biochemical and biophysical research communications **291**(2): 385-393.
Jaillon, O., et al. (2004). "Genome duplication in the teleost fish Tetraodon nigroviridis reveals the early vertebrate proto-karyotype." Nature **431**(7011): 946.

Jefferies, J. L. and J. A. Towbin (2010). "Dilated cardiomyopathy." The Lancet **375**(9716): 752-762.

Jin, J.-P. (2000). Titin-thin filament interaction and potential role in muscle function. Elastic Filaments of the Cell, Springer**:** 319-335.

Kamisago, M., et al. (2000). "Mutations in sarcomere protein genes as a cause of dilated cardiomyopathy." New England Journal of Medicine **343**(23): 1688-1696.

Kawai, C. (1999). "From myocarditis to cardiomyopathy: mechanisms of inflammation and cell death: learning from the past for the future." Circulation **99**(8): 1091-1100.

Kimmel, C. B., et al. (1995). "Stages of embryonic development of the zebrafish." Developmental dynamics **203**(3): 253-310.

Kimura, A. (2008). "Molecular etiology and pathogenesis of hereditary cardiomyopathy." Circulation Journal **72**(SupplementA): A38-A48.

Kley, R. A., et al. (2007). "Clinical and morphological phenotype of the filamin myopathy: a study of 31 German patients." Brain **130**(12): 3250-3264.

Kley, R. A., et al. (2012). "Pathophysiology of protein aggregation and extended phenotyping in filaminopathy." Brain **135**(9): 2642-2660.

Koteliansky, V., et al. (1981). "Identification of a filamin-like protein in chicken heart muscle." FEBS letters **125**(1): 44-48.

KOTELIANSKY, V. E., et al. (1986). "Isolation and localization of filamin in heart muscle." The FEBS Journal **156**(3): 619-623.
Krakow, D., et al. (2004). "Mutations in the gene encoding filamin B disrupt vertebral segmentation, joint formation and skeletogenesis." Nature genetics **36**(4): 405.

Krans, J. (2010). "The sliding filament theory of muscle contraction." Nature Education **3**(9): 66.

Kupperman, E., et al. (2000). "A sphingosine-1-phosphate receptor regulates cell migration during vertebrate heart development." Nature **406**(6792): 192.

Kyndt, F., et al. (2007). "Mutations in the gene encoding filamin A as a cause for familial cardiac valvular dystrophy." Circulation **115**(1): 40-49.

Lad, Y., et al. (2007). "Structure of three tandem filamin domains reveals auto-inhibition of ligand binding." The EMBO journal **26**(17): 3993-4004.

Larkin, M. A., et al. (2007). "Clustal W and Clustal X version 2.0." bioinformatics **23**(21): 2947-2948.

Latham, G. J. and G. Lopez (2015). "Anesthetic considerations in myofibrillar myopathy." Pediatric Anesthesia **25**(3): 231-238.

Lazzarini, E., et al. (2015). "The ARVD/C genetic variants database: 2014 update." Human mutation **36**(4): 403-410.

Li, D., et al. (2010). "Identification of novel mutations in RBM20 in patients with dilated cardiomyopathy." Clinical and translational science **3**(3): 90-97.

Lin, Y.-F., et al. (2012). "Multiple influences of blood flow on cardiomyocyte hypertrophy in the embryonic zebrafish heart." Developmental biology **362**(2): 242-253.

Linnemann, A., et al. (2010). "The sarcomeric Z-disc component myopodin is a multiadapter protein that interacts with filamin and α-actinin." European journal of cell biology **89**(9): 681-692.

Liu, G.-S., et al. (2015). "A novel human R25C-phospholamban mutation is associated with super-inhibition of calcium cycling and ventricular arrhythmia." Cardiovascular research **107**(1): 164-174.

Loo, D. T., et al. (1998). "Filamin Binds to the Cytoplasmic Domain of the β1-Integrin IDENTIFICATION OF AMINO ACIDS RESPONSIBLE FOR THIS INTERACTION." Journal of Biological Chemistry **273**(36): 23304-23312.

Löwe, T., et al. (2007). "The pathomechanism of filaminopathy: altered biochemical properties explain the cellular phenotype of a protein aggregation myopathy." Human molecular genetics **16**(11): 1351-1358.

Lu, J. T., et al. (2011). "LMNA cardiomyopathy: cell biology and genetics meet clinical medicine." Disease models & mechanisms **4**(5): 562-568.

Lu, S., et al. (2003). "New N-RAP-binding partners α-actinin, filamin and Krp1 detected by yeast two-hybrid screening: implications for myofibril assembly." Journal of cell science **116**(11): 2169-2178.

Luan, X., et al. (2010). "A novel heterozygous deletion–insertion mutation (2695–2712 del/GTTTGT ins) in exon 18 of the filamin C gene causes filaminopathy in a large Chinese family." Neuromuscular disorders **20**(6): 390-396.

Luther, P. K. (2009). "The vertebrate muscle Z-disc: sarcomere anchor for structure and signalling." Journal of muscle research and cell motility **30**(5-6): 171-185.

Maerkens, A., et al. (2014). "A.P.1: Proteomic analysis in 72 myofibrillar myopathy (MFM) patients identifies new disease-relevant proteins accumulating in aggregates and reveals subtype-specific proteomic profiles." Neuromuscular Disorders **24**(9): 830.

Marian, A. J., et al. (2016). "Genetics and genomics of single-gene cardiovascular diseases: common hereditary cardiomyopathies as prototypes of single-gene disorders." Journal of the American College of Cardiology **68**(25): 2831-2849.

Maron, B. J. and M. S. Maron (2013). "Hypertrophic cardiomyopathy." The Lancet **381**(9862): 242-255.
Maron, B. J., et al. (2014). "Hypertrophic cardiomyopathy: present and future, with translation into contemporary cardiovascular medicine." Journal of the American College of Cardiology **64**(1): 83-99.

Maron, B. J., et al. (2006). "Contemporary definitions and classification of the cardiomyopathies: an American heart association scientific statement from the council on clinical cardiology, heart failure and transplantation committee; quality of care and outcomes research and functional genomics and translational biology interdisciplinary working groups; and council on epidemiology and prevention." Circulation **113**(14): 1807-1816.

Maron, B. J., et al. (2015). "Eligibility and disqualification recommendations for competitive athletes with cardiovascular abnormalities: task force 3: hypertrophic cardiomyopathy, arrhythmogenic right ventricular cardiomyopathy and other cardiomyopathies, and myocarditis:

a scientific statement from the American Heart Association and American College of Cardiology." Journal of the American College of Cardiology **66**(21): 2362-2371.
Mayosi, B. M. (2014). "Cardiomyopathies: MOGE (S): a standardized classification of cardiomyopathies?" Nature Reviews cardiology **11**(3): 134.

McNair, W. P., et al. (2011). "SCN5A mutations associate with arrhythmic dilated cardiomyopathy and commonly localize to the voltage-sensing mechanism." Journal of the American College of Cardiology **57**(21): 2160-2168.

McNally, E. M., et al. (2013). "Genetic mutations and mechanisms in dilated cardiomyopathy." The Journal of clinical investigation **123**(1): 19-26.

McNally, E. M. and L. Mestroni (2017). "Dilated cardiomyopathy: genetic determinants and mechanisms." Circulation research **121**(7): 731-748.

Meeker, N. D., et al. (2007). "Method for isolation of PCR-ready genomic DNA from zebrafish tissues." Biotechniques **43**(5): 610-614.

Merlo, M., et al. (2018). "Evolving concepts in dilated cardiomyopathy." European journal of heart failure **20**(2): 228-239.

Merner, N. D., et al. (2008). "Arrhythmogenic right ventricular cardiomyopathy type 5 is a fully penetrant, lethal arrhythmic disorder caused by a missense mutation in the TMEM43 gene." The American Journal of Human Genetics **82**(4): 809-821.

Miao, J., et al. (2018). "A case report: a heterozygous deletion (2791_2805 del) in exon 18 of the filamin C gene causing filamin C-related myofibrillar myopathies in a Chinese family." BMC neurology **18**(1): 79.

Morton, N. E. (1991). "Parameters of the human genome." Proceedings of the National Academy of Sciences **88**(17): 7474-7476.

Moulton, J. D. (2017). Making a morpholino experiment work: controls, favoring specificity, improving efficacy, storage, and dose. Morpholino Oligomers, Springer**:** 17-29.

Muller, P. Y., et al. (2002). "Short technical report processing of gene expression data generated by quantitative real-time RT-PCR." Biotechniques **32**(6): 1372-1379.
Nakamura, F., et al. (2007). "Structural basis of filamin A functions." The Journal of cell biology **179**(5): 1011-1025.

Nakamura, F., et al. (2011). "The filamins: organizers of cell structure and function." Cell adhesion & migration **5**(2): 160-169.
Noegel, A. A., et al. (1989). "The Dictyostelium gelation factor shares a putative actin binding site with alpha-actinins and dystrophin and also has a rod domain containing six 100-residue motifs that appear to have a cross-beta conformation." The Journal of cell biology **109**(2): 607-618.

Nolte, H., et al. (2015). "Dynamics of zebrafish fin regeneration using a pulsed SILAC approach." Proteomics **15**(4): 739-751.

Nozari, A., et al. (2018). "A novel splicing variant in FLNC gene responsible for a highly penetrant familial dilated cardiomyopathy in an extended Iranian family." Gene **659**: 160-167.

Nusslein-Volhard, C. and R. Dahm (2002). Zebrafish, Oxford University Press.

Ohta, Y., et al. (1999). "The small GTPase RalA targets filamin to induce filopodia." Proceedings of the National Academy of Sciences **96**(5): 2122-2128.

Ortiz-Genga, M. F., et al. (2016). "Truncating FLNC mutations are associated with high-risk dilated and arrhythmogenic cardiomyopathies." Journal of the American College of Cardiology **68**(22): 2440-2451.

Parks, S. B., et al. (2008). "Lamin A/C mutation analysis in a cohort of 324 unrelated patients with idiopathic or familial dilated cardiomyopathy." American heart journal **156**(1): 161-169.

Parrie, L. E., et al. (2013). "Zebrafish tbx5 paralogs demonstrate independent essential requirements in cardiac and pectoral fin development." Developmental Dynamics **242**(5): 485-502.

Patrosso, M., et al. (1994). "The exon-intron organization of the human X-linked gene (FLN1) encoding actin-binding protein 280." Genomics **21**(1): 71-76.

Pavalko, F. M., et al. (1989). "Identification of a filamin isoform enriched at the ends of stress fibers in chicken embryo fibroblasts." Journal of cell science **94**(1): 109-118.

Pelster, B. and W. W. Burggren (1996). "Disruption of Hemoglobin Oxygen Transport Does Not Impact Oxygen-Dependent Physiological Processes in Developing." transport **79**: 358-362.

Peter, A. K., et al. (2011). "The costamere bridges sarcomeres to the sarcolemma in striated muscle." Progress in pediatric cardiology **31**(2): 83-88.

Pfaff, M., et al. (1998). "Integrin β cytoplasmic domains differentially bind to cytoskeletal proteins." Journal of Biological Chemistry **273**(11): 6104-6109.

Postlethwait, J. H., et al. (1998). "Vertebrate genome evolution and the zebrafish gene map." Nature genetics **18**(4): 345.

Price, M. G., et al. (1994). "Different temporal patterns of expression result in the same type, amount, and distribution of filamin (ABP) in cardiac and skeletal myofibrils." Cell motility and the cytoskeleton **27**(3): 248-261.

Pudas, R., et al. (2005). "Structural basis for vertebrate filamin dimerization." Structure **13**(1): 111-119.

Pugh, T. J., et al. (2014). "The landscape of genetic variation in dilated cardiomyopathy as surveyed by clinical DNA sequencing." Genetics in Medicine **16**(8): 601.

Puius, Y. A., et al. (1998). "The modular structure of actin-regulatory proteins." Current opinion in cell biology **10**(1): 23-34.

Razinia, Z., et al. (2012). "Filamins in mechanosensing and signaling."

Reggiori, F. (2006). "Membrane origin for autophagy." Current topics in developmental biology **74**: 1-30.

Reinstein, E., et al. (2016). "Congenital dilated cardiomyopathy caused by biallelic mutations in Filamin C." European Journal of Human Genetics **24**(12): 1792.

Reinstein, E., et al. (2016). "Congenital dilated cardiomyopathy caused by biallelic mutations in Filamin C." European Journal Of Human Genetics **24**: 1792.

Reischauer, S., et al. (2016). "Cloche is a bHLH-PAS transcription factor that drives haemato-vascular specification." Nature **535**(7611): 294.

Richard, P., et al. (2003). "Hypertrophic cardiomyopathy: distribution of disease genes, spectrum of mutations, and implications for a molecular diagnosis strategy." Circulation **107**(17): 2227-2232.

Richardson, P. (1996). "Report of the WHO/ISFC task force on the definition and classification of cardiomyopathies." Circulation **93**: 840-842.

Richardson, P., et al. (1996). "O, Connell J, Olsen E, Thiene G, Goodwin J, Gyarfas I, Martin I, Nordet P: Report of the 1995 World Health Organization/International Society and Federation of Cardiology Task Force on the Definition and Classification of cardiomyopathies." Circulation **93**: 841-842.

Roger, V. L., et al. (2011). "Heart disease and stroke statistics—2011 update: a report from the American Heart Association." Circulation **123**(4): e18.

Ruparelia, A. A., et al. (2012). "Characterization and investigation of zebrafish models of filamin-related myofibrillar myopathy." Human molecular genetics **21**(18): 4073-4083.

Ruskamo, S. and J. Ylänne (2009). "Structure of the human filamin A actin-binding domain." Acta Crystallographica Section D: Biological Crystallography **65**(11): 1217-1221.

Salmikangas, P., et al. (2003). "Myotilin, the limb-girdle muscular dystrophy 1A (LGMD1A) protein, cross-links actin filaments and controls sarcomere assembly." Human molecular genetics **12**(2): 189-203.

Schollmeyer, J., et al. (1978). "An actin-binding protein in human platelets. Interactions with alpha-actinin on gelatin of actin and the influence of cytochalasin B." The American journal of pathology **93**(2): 433.

Schröder, R. and B. Schoser (2009). "Myofibrillar myopathies: a clinical and myopathological guide." Brain Pathology **19**(3): 483-492.

Schröder, R., et al. (2007). "Primary desminopathies." Journal of cellular and molecular medicine **11**(3): 416-426.

Schwerte, T. (2009). "Cardio-respiratory control during early development in the model animal zebrafish." Acta histochemica **111**(3): 230-243.

Seeley, M., et al. (2007). "Depletion of zebrafish titin reduces cardiac contractility by disrupting the assembly of Z-discs and A-bands." Circulation research **100**(2): 238-245.

Selcen, D. and A. G. Engel (2011). Myofibrillar myopathies. Handbook of clinical neurology, Elsevier. **101:** 143-154.

Sen-Chowdhry, S., et al. (2010). "Arrhythmogenic cardiomyopathy: etiology, diagnosis, and treatment." Annual review of medicine **61**: 233-253.

Sethi, R., et al. (2014). "A novel structural unit in the N-terminal region of filamins." Journal of Biological Chemistry **289**(12): 8588-8598.

Sharma, C. P., et al. (1995). "Direct interaction of filamin (ABP-280) with the beta 2-integrin subunit CD18." The Journal of Immunology **154**(7): 3461-3470.

Shatunov, A., et al. (2009). "In-frame deletion in the seventh immunoglobulin-like repeat of filamin C in a family with myofibrillar myopathy." European Journal Of Human Genetics **17**(5): 656.

Shi, X., et al. (2018). "Zebrafish heart failure models: opportunities and challenges." Amino acids: 1-12.

Sisakian, H. (2014). "Cardiomyopathies: evolution of pathogenesis concepts and potential for new therapies." World journal of cardiology **6**(6): 478.

Sjekloća, L., et al. (2007). "Crystal structure of human filamin C domain 23 and small angle scattering model for filamin C 23–24 dimer." Journal of molecular biology **368**(4): 1011-1023.

Smith, L. L., et al. (2013). "Analysis of skeletal muscle defects in larval zebrafish by birefringence and touch-evoke escape response assays." Journal of visualized experiments: JoVE(82).

Spence, R., et al. (2006). "The distribution and habitat preferences of the zebrafish in Bangladesh." Journal of Fish Biology **69**(5): 1435-1448.

Spence, R., et al. (2008). "The behaviour and ecology of the zebrafish, Danio rerio." Biological Reviews **83**(1): 13-34.

Sprague, J., et al. (2006). "The Zebrafish Information Network: the zebrafish model organism database." Nucleic acids research **34**(suppl_1): D581-D585.

Srivastava, D. (2004). "Heart disease: An ongoing genetic battle?" Nature **429**(6994): 819.

Srivastava, D. (2006). "Making or breaking the heart: from lineage determination to morphogenesis." Cell **126**(6): 1037-1048.

Srivastava, D. and S. Yu (2006). "Stretching to meet needs: integrin-linked kinase and the cardiac pump." Genes & development **20**(17): 2327-2331.

Stainier, D. Y. (2001). "Zebrafish genetics and vertebrate heart formation." Nature Reviews Genetics **2**(1): 39.

Staudt, D. and D. Stainier (2012). "Uncovering the molecular and cellular mechanisms of heart development using the zebrafish." Annual review of genetics **46**: 397-418.

Stossel, T. P., et al. (2001). "Filamins as integrators of cell mechanics and signalling." Nature reviews Molecular cell biology **2**(2): 138.
Takada, F., et al. (2001). "Myozenin: an α-actinin-and γ-filamin-binding protein of skeletal muscle Z lines." Proceedings of the National Academy of Sciences **98**(4): 1595-1600.

Takafuta, T., et al. (1998). "Human β-filamin is a new protein that interacts with the cytoplasmic tail of glycoprotein Ibα." Journal of Biological Chemistry **273**(28): 17531-17538.

Tang, R., et al. (2007). "Validation of zebrafish (Danio rerio) reference genes for quantitative real-time RT-PCR normalization." Acta biochimica et biophysica Sinica **39**(5): 384-390.

Tasca, G., et al. (2012). "Novel FLNC mutation in a patient with myofibrillar myopathy in combination with late-onset cerebellar ataxia." Muscle & nerve **46**(2): 275-282.

Thompson, T. G., et al. (2000). "Filamin 2 (FLN2): a muscle-specific sarcoglycan interacting protein." J Cell Biol **148**(1): 115-126.

Tseng, Y., et al. (2004). "The bimodal role of filamin in controlling the architecture and mechanics of F-actin networks." Journal of Biological Chemistry **279**(3): 1819-1826.

Tsubata, S., et al. (2000). "Mutations in the human δ-sarcoglycan gene in familial and sporadic dilated cardiomyopathy." The Journal of clinical investigation **106**(5): 655-662.

Tucker, N. R., et al. (2017). "Novel Mutation in FLNC (Filamin C) Causes Familial Restrictive CardiomyopathyCLINICAL PERSPECTIVE." Circulation: Genomic and Precision Medicine **10**(6): e001780.

Tyler, J. M., et al. (1980). "Structural comparison of several actin-binding macromolecules." The Journal of cell biology **85**(2): 489-495.

Ueda, K., et al. (2003). "The carboxy-terminal pleckstrin homology domain of ROCK interacts with filamin-A." Biochemical and biophysical research communications **301**(4): 886-890.
UEDA, M., et al. (1992). "Interaction of the low-molecular-mass, guanine-nucleotide-binding protein with the actin-binding protein and its modulation by the cAMP-dependent protein kinase in bovine platelets." The FEBS Journal **203**(3): 347-352.

Valdés-Mas, R., et al. (2014). "Mutations in filamin C cause a new form of familial hypertrophic cardiomyopathy." Nature communications **5**: 5326.

van der Flier, A. and A. Sonnenberg (2001). "Structural and functional aspects of filamins." Biochimica Et Biophysica Acta (BBA)-Molecular Cell Research **1538**(2-3): 99-117.

van der Ven, P. F., et al. (2006). "Unusual splicing events result in distinct Xin isoforms that associate differentially with filamin c and Mena/VASP." Experimental cell research **312**(11): 2154-2167.

van der Ven, P. F., et al. (2000). "Characterization of muscle filamin isoforms suggests a possible role of γ-filamin/ABP-L in sarcomeric Z-disc formation." Cytoskeleton **45**(2): 149-162.

van der Ven, P. F., et al. (2000). "Indications for a novel muscular dystrophy pathway: γ-filamin, the muscle-specific filamin isoform, interacts with myotilin." The Journal of cell biology **151**(2): 235-248.

Vargas, M., et al. (1996). "Identification and cellular localization of the actin-binding protein ABP-120 from Entamoeba histolytica." Molecular microbiology **22**(5): 849-857.

Vikhorev, P. G., et al. (2017). "Abnormal contractility in human heart myofibrils from patients with dilated cardiomyopathy due to mutations in TTN and contractile protein genes." Scientific Reports **7**(1): 14829.

Vincent, A. E., et al. (2016). "Mitochondrial dysfunction in myofibrillar myopathy." Neuromuscular Disorders **26**(10): 691-701.

Vorgerd, M., et al. (2005). "A mutation in the dimerization domain of filamin c causes a novel type of autosomal dominant myofibrillar myopathy." The American Journal of Human Genetics **77**(2): 297-304.

Walker, N. J. (2002). "A technique whose time has come." Science **296**(5567): 557-559.

Wang, K., et al. (1975). "Filamin, a new high-molecular-weight protein found in smooth muscle and non-muscle cells." Proceedings of the National Academy of Sciences **72**(11): 4483-4486.

Wang, K. and S. Singer (1977). "Interaction of filamin with F-actin in solution." Proceedings of the National Academy of Sciences **74**(5): 2021-2025.

Warren, K. S. and M. C. Fishman (1998). "“Physiological genomics”: mutant screens in zebrafish." American Journal of Physiology-Heart and Circulatory Physiology **275**(1): H1-H7.

Watkins, H., et al. (2011). "Inherited cardiomyopathies." New England Journal of Medicine **364**(17): 1643-1656.

Westerfield, M. (1993). The zebrafish: a guide for the laboratory use of zebrafish (Brachydanio reriro), Inst. of Neuroscience, University of Oregon.
Westerfield, M., et al. (1998). Zebrafish informatics and the ZFIN database. Methods in cell biology, Elsevier. **60:** 339-355.

Whiteley, A. R., et al. (2011). "Population genomics of wild and laboratory zebrafish (Danio rerio)." Molecular Ecology **20**(20): 4259-4276.

Williams, D., et al. (2005). "A new dominant distal myopathy affecting posterior leg and anterior upper limb muscles." Neurology **64**(7): 1245-1254.

Wilson, R., et al. (1994). "2.2 Mb of contiguous nucleotide sequence from chromosome III of C. elegans." Nature **368**(6466): 32.

Winter, L. and W. H. Goldmann (2015). "Biomechanical characterization of myofibrillar myopathies." Cell biology international **39**(4): 361-363.

Woods, I. G., et al. (2005). "The zebrafish gene map defines ancestral vertebrate chromosomes." Genome research **15**(9): 1307-1314.

Wu, Q., et al. (2015). "Talin1 is required for cardiac Z-disk stabilization and endothelial integrity in zebrafish." The FASEB Journal **29**(12): 4989-5005.

Xie, Z.-w., et al. (1998). "Molecular cloning of human ABPL, an actin-binding protein homologue." Biochemical and biophysical research communications **251**(3): 914-919.

Xu, W.-f., et al. (1998). "A Novel Human Actin-Binding Protein Homologue That Binds to Platelet Glycoprotein Ib□" Blood **92**(4): 1268-1276.

Yalcin, H. C., et al. (2017). "Heart Function and Hemodynamics Analysis for Zebrafish Embryos." Developmental Dynamics.

Yang, J., et al. (2014). "Understanding cardiac sarcomere assembly with zebrafish genetics." The Anatomical Record **297**(9): 1681-1693.

Yang, J. and X. Xu (2012). "Immunostaining of dissected zebrafish embryonic heart." Journal of visualized experiments: JoVE(59).

Yelon, D. (2001). "Cardiac patterning and morphogenesis in zebrafish." Developmental Dynamics **222**(4): 552-563.

Yelon, D., et al. (1999). "Restricted expression of cardiac myosin genes reveals regulated aspects of heart tube assembly in zebrafish." Developmental biology **214**(1): 23-37.

Zent, R., et al. (2000). "Class-and splice variant-specific association of CD98 with integrin β cytoplasmic domains." Journal of Biological Chemistry **275**(7): 5059-5064.

Zhang, M., et al. (2007). "Identification of CAP as a costameric protein that interacts with filamin C." Molecular biology of the cell **18**(12): 4731-4740.

Zhou, A.-X., et al. (2010). "Filamins in cell signaling, transcription and organ development." Trends in cell biology **20**(2): 113-123.

Zhou, X., et al. (2007). "Filamins in cardiovascular development." Trends in cardiovascular medicine **17**(7): 222-229.

Zhou, X., et al. (2007). "Filamin B deficiency in mice results in skeletal malformations and impaired microvascular development." Proceedings of the National Academy of Sciences **104**(10): 3919-3924.